Adapting Ni phyllosilicate nanotube synthesis to influence morphology and particle size

A nickel catalyst model system

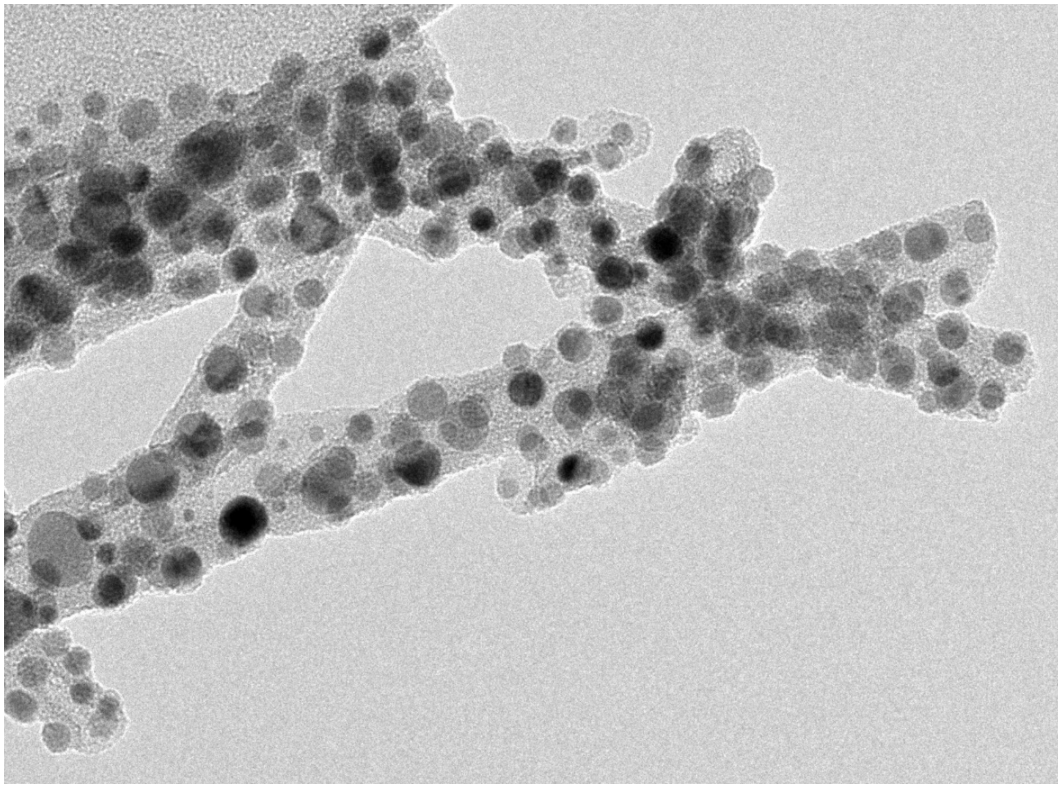

Written by: Isabell Barnhoorn, BSc

Supervised by: Savannah Turner, MSc

First examiner: Prof. dr. Petra de Jongh
Second examiner: Dr. Peter Ngene

Materials Chemistry and Catalysis
Debye Institute for Nanomaterials Science
Utrecht University
The Netherlands

November 20th, 2022

Layman abstract

Catalysts are essential for production of chemicals in industry, providing humanity with necessary tools for survival, for example medicines, food preservatives, fertilizers, fuels and packaging. A catalyst is used to facilitate reactions needed to produce essential chemicals, by lowering the energy needed for the reaction to proceed. Nickel catalysts for high temperature reactions are used to produce products from long chain hydrocarbons by hydrogenation, like waxes, resins and vegetable fats used for coatings, paints, food preservatives and other essential products. In this project the synthesis of a high temperature nickel catalyst precursor was developed in the form of nanotubes. The structure of this nickel precursor contains nickel-oxygen-silica bonds and is called nickel phyllosilicate. A nickel catalyst precursor is made in the form of nanotubes to study the particle size after reduction. The synthesis of the Ni phyllosilicate nanotubes was carried out using hydrothermal synthesis at 195 ^{o}C for 6 days. Hydrothermal synthesis is carried out in a closed steel vessel – an autoclave – which contains an aqueous reaction solution. The autoclave with aqueous solution allows a high temperatures to be reached, which allows the system to reach a high pressure and favours crystal growth. The nanotubes have been characterized with numerous techniques like electron microscopy, X-ray diffraction, Temperature Programmed Reduction and nitrogen physisorption. This has led to a full overview of the morphology and composition of synthesized Ni phyllosilicate nanotubes and the effects of synthesis time and sodium hydroxide concentration. Metal nickel particles have been formed on the nanotubes, this can be used further in catalysis and battery research.

Abstract

The use of Ni phyllosilicate precursors for Ni catalysts has led to high sintering resistance, high activity and high stability in catalysts. When this is produced in a nanotube form it is possible to study the morphology of particle formation in more detail in TEM. In this project Ni phyllosilicate nanotubes have been hydrothermally synthesized to study morphology, composition, nanotube formation and particle morphology. Nanotubes of $Ni_3Si_2O_5(OH)_4$ were synthesized utilizing nickel chloride hexahydrate, sodium hydroxide and sodium silicate solution with hydrothermal treatment at 195 ^{o}C (1.5 Ni/Si, 7 wt% NaOH). The nanotube dimensions were analysed with transmission electron microscopy. The morphology and composition were investigated with TEM, EDX, TPR, XRD, ED and N_2 physisorption. The nanotubes on average have a 235 nm length, 9.1 nm walls and 10.3 nm pores, with a crystal lattice spacing of 0.75 nm. The main nickel phases produced were a 1:1 Ni phyllosilicate ($Ni_3Si_2O_5(OH)_4$) and nickel hydroxide ($Ni(OH)_2$).

Treatment with 5 % hydrogen gas in argon at temperatures 400-750 ^{o}C produced Ni metal particles embedded in the nanotube structure, ranging from diameters of 4 to 9 nm. An increase in particle size with temperature was observed for reductions at 400, 450, 650 and 750 ^{o}C. A relationship between nanotube wall thickness and nickel metal particle size was established. The particle size increases with nanotube wall thickness until a wall thickness of 4.5 nm, after which the particle size stabilizes. Particle formation thus only originates from a depth of 4.5 nm. The particle size remains constant with increasing pore size, which implies for catalysis that the pores remain accessible to hydrogen gas and there is no issue of pore inaccessibility.

The effect of synthesis time has been studied to develop an understanding of the nanotube formation. The nanotubes are fully formed after 1 day of synthesis and start forming after 2 hours of synthesis. Flat circular plate like particles – a.k.a. discs - surround the nanotubes in the first four hours of synthesis. The appearance and disappearance of these discs has started a new understanding of the Ni phyllosilicate nanotube formation mechanism.

The findings lead to a fully characterized Ni phyllosilicate nanotube system, which is reproducible and forms a homogeneous distribution of stable nickel particles. The applications lie in heterogeneous catalysis as a model system for nickel catalysts. The Ni phyllosilicate nanotubes are also promising for battery research, where they can be used as a conducting material for electrodes.

Contents

List of abbreviations

TEM	Transmission Electron Microscopy
XRD	X-ray Diffraction
EDX	Energy Dispersive X-ray spectroscopy (also EDS or XEDS)
TPR	Temperature Programmed Reduction
ED	Electron Diffraction
TGA	Thermogravimetric Analysis
ILTEM	Identical location TEM
SEM	Scanning Electron Microscopy

List of Figures

1 Introduction

Solid catalysts are so widely used in oil refineries and chemical production that this means that almost every molecule in industry has been in contact with at least one solid catalyst.[1] The application of catalysts ranges from oil and gas refining to environmental technologies. The use of catalysts in production of fuels, chemicals and subsequent products reduces the amount of energy and raw materials needed in the production process. The market share of catalysts was 17.2 billion US$ in 2014 while it has been estimated that every 1 US$ spent on a catalyst will generate 1000 US$. The contribution of catalysts to the worldwide economy is estimated at >35 % of the world gross domestic product (GDP). In industry 80 % of catalytic processes use heterogeneous catalysts. [2] Without the use of catalysts many products cannot be made, many industries would falter, and the economy would be unrecognisable. Therefore, it is meaningful to research solid catalysts to continue their contribution to the world and improve energy efficiency.

Nickel catalysts are heavily used in the chemical industry today because of their stability at high temperatures and high catalytic activity at room temperature. They are used in hydrogenation reactions to reduce alkenes to alkanes and subsequently this is used to produce products such as waxes, resins, naphthene and margarines. Other reactions include steam reforming and methanation for the production of syngas. The wide availability, its affordable price and good catalyst stability make it a very good alternative for expensive noble metal catalysts.[3,4] This is the reason why nickel catalyst are relevant to study.

Synthesis methods to produce supported nickel catalysts include deposition precipitation (DP), co-precipitation, incipient wetness impregnation (IWI), impregnation & drying, ion adsorption, ion-exchange, sol-gel and colloidal synthesis. In industry impregnation & drying, co-precipitation and deposition precipitation are most often used because of their suitability for large scale operation. [5] Nickel catalysts for high temperature hydrogenation reactions are based on nickel phyllosilicate precursors. The catalyst derived from nickel phyllosilicate has a high stability and activity at high temperatures, as there is a strong interaction between the metal and support which reduces the sintering of nickel nanoparticles. [6] Studying the synthesis of Ni phyllosilicate prescursors is thus worthwhile for heterogeneous catalysis.

Metal silicates have been produced as precursors in catalyst manufacturing extensively. Nickel phyllosilicates can be produced using deposition precipitation, ammonia evaporation and hydrothermal synthesis. Deposition Precipitation works by precipitating a metal precursor on a suspended support material, by slowly increasing the pH of an aqueous metal salt solution. The Deposition Precipitation method was first developed in 1943 [7]. The use of urea hydrolysis in deposition precipitation further improved deposition precipitation, developed in the 1970s. [8–10] Burattin et al studied deposition precipitation and characterization of nickel phyllosilicates and their reduction mechanisms between 1993-2000. [11–16] They used the method for deposition precipitation developed by Geus et al [17–20] and Krijn de Jong [21]. During deposition precipitation a base is dissolved slowly in an aqueous metal salt solution with dissolved silica at 90 C, using hydrolysis of urea as a base to raise the pH. The phyllosilicates are formed between pH 8 and 10. [14] The advantages of DP of Ni phyllosilicates are small metal particles, a narrow particle size distribution after reduction and high metal loadings (>20 wt%). In order to attain a high metal loading however, long deposition times are necessary. [12] The Ni phyllosilicate precursors have thus historically been a successful factor in making stable Ni catalysts and are useful studying further.

Hydrothermal treatment with a base can be used effectively to produce nickel phyllosilicate nanotubes. [22–27] Nickel phyllosilicate nanotubes ($Ni_3Si_2O_5(OH)_4$) are similar to other types of serpentine silicates, like nanotubes of $Mg_3Si_2O_5(OH)_4$, $(Mg,Fe)_3Si_2O_5(OH)_4$ and $Co_3Si_2O_5(OH)_4$. [24] Hydrothermal treatment is a reaction at high temperature in a closed vessel under pressure. The container needs to be under pressure in order to reach the high temperature. Compared to DP a much shorter reaction

time under higher temperature is needed to form Ni phyllosilicates. A high pH and high temperatures during hydrothermal synthesis make sure the metal and silica species dissolve and crystallization can occur. Ni phyllosilicate nanotubes can be formed this way, depending on the reagents and concentrations used.[24,26,28]

Metal phyllosilicates bear various names in literature and appear in nature in different forms. The word 'phyllo' comes from the Greek '*φύλλο*' (fýllo) which means leaf. The 'leaves' of metal and silica are connected through oxygen, the layers of which can be seen in the TEM image in figure 1. The structure of metal phyllosilicates is built up of layers of metal and silica connected by oxygen and sometimes other anions. Nickel phyllosilicates are organized into tetrahedral and octahedral sheets where nickel and silica are bonded through oxygen atoms. The tetrahedral sheet (T in figure 2) consists of tetrahedrons with silica bonded to four oxygen atoms. The octahedral sheet (O in figure 2) consists of octahedrons with the nickel cation bonded to six anions (O, F, Cl or OH). A tetrahedral and an octahedral sheet repeating structure is called a 1:1 phyllosilicate and Kaolinite or Nepouite in nature, see figure 1. One octahedral sheet positioned between two tetrahedral sheets is called a 2:1 nickel phyllosilicate (Smectite in nature). The tetrahedron cation is Si^{4+} and the octahedron cation is Ni^{2+}. The anions in the tetrahedra and octahedra are O^{2-} and OH^-. A phenomenon that occurs which creates the continues structure involves edge-sharing of the tetrahedrons and octahedrons. The oxygen atoms connect the octahedrons and tetrahedrons. The metal octahedron and silica tetrahedron are slightly different in size, which is a reason why the sheets can curl and form a nanotube. [22] Structures of Ni phyllosilicate nanotubes are quite similar to naturally occurring chrysotile minerals. Chrysotile silica is a type of asbestos that appears in nature in the forms of $Mg_3Si_2O_5(OH)_4$, $(Mg, Fe)_3Si_2O_5(OH)_4$ and $Co_3Si_2O_5(OH)_4$. The synthetic chrysotile analogue is the nanotube form of 1:1 Ni phyllosilicate $Ni_3Si_2O_5(OH)_4$.

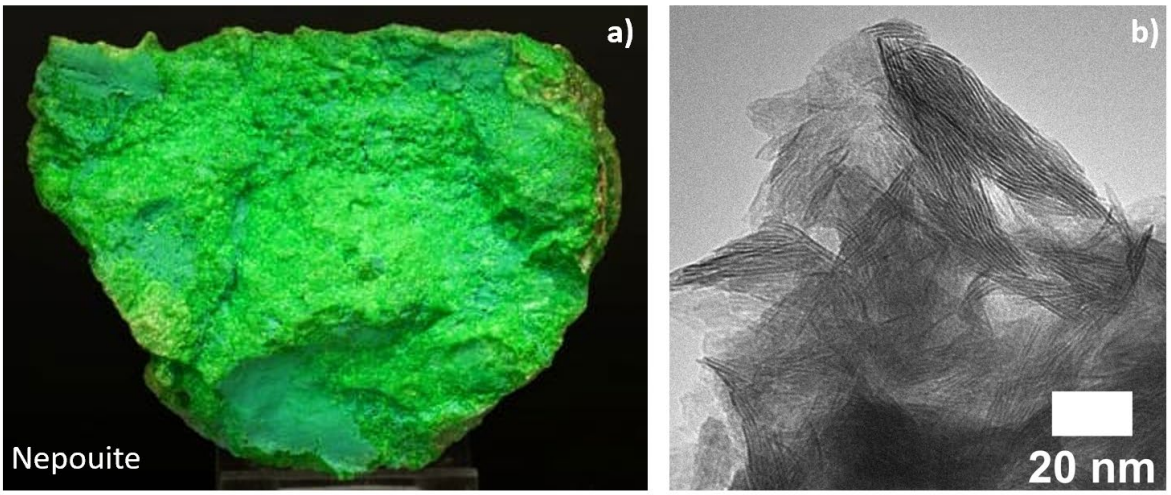

Figure 1: (a): photograph of a naturally occurring nickel silicate mineral. Trivial name: Nepouite. Chemical formula: $Ni_3Si_2O_5(OH)_4$. (b) TEM image of synthetic Ni phyllosilicate sheets synthesized with hydrothermal method.

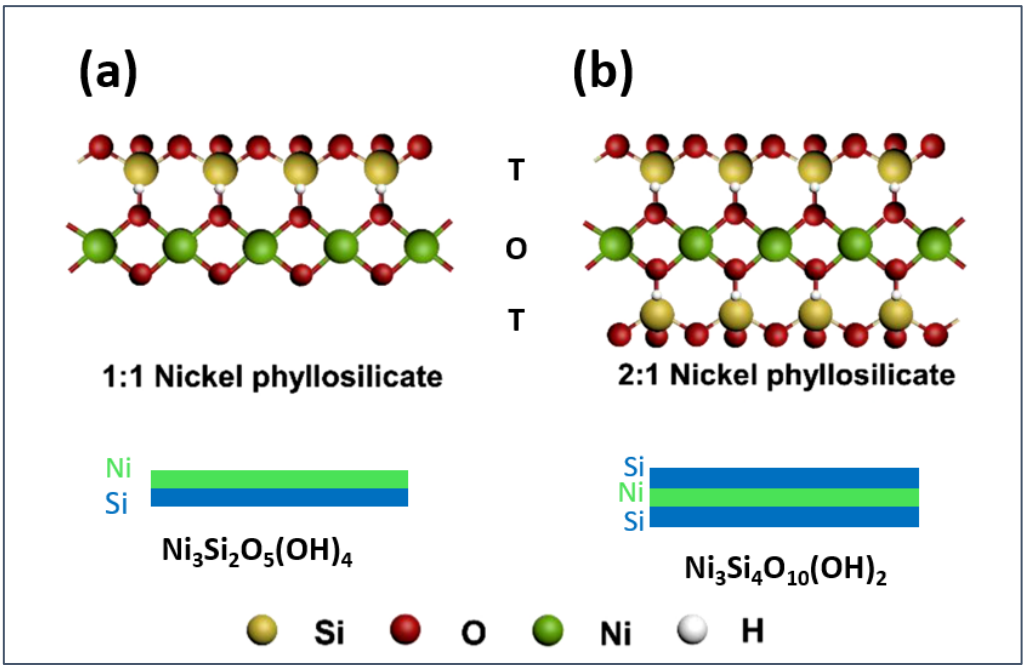

Figure 2: Structures of Ni phyllosilicate with tetrahedral metal layers (T) and octahedral silica layers (O). (a) 1:1, $Ni_3Si_2O_5(OH)_4$ (b) 2:1, $Ni_3Si_4O_{10}(OH)_2$. Top images adapted from Zhang et al [6].

The property of nickel phyllosilicates that makes it a very attractive material for catalysis applications is its homogeneous distribution of metal and silica throughout the entire material, caused by the continuous layers or sheets. After the synthesis of nickel phyllosilicates, reduction with hydrogen will lead to small nickel nanoparticles distributed on the support. In figure 3 TEM images of Ni phyllosilicate before and after reduction are shown and nickel particles on silica are clearly visible. When reducing the Ni^{2+} in this material using high temperatures and hydrogen a homogeneous distribution of nickel metal nanoparticles is created. Effectively a $Ni@SiO_2$ catalyst is produced where the silica support forms during the reduction while nickel is embedded in it. Another advantage of this precursor in catalysis is its high resistance to sintering due to the strong metal-support interaction. [6] Their intricate layered structures make them suitable for high temperature gas reactions as well as low temperature liquid reactions. [22]

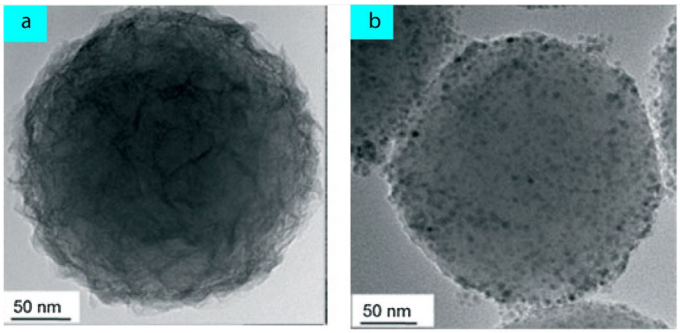

Figure 3: TEM images of (a) Ni phyllosilicate on silica support before reduction, synthesized with ammonia evaporation and (b) reduced Ni phyllosilicate supported on Stöber silica. [22]

In catalytic reactions the metal particle size is important. Depending on the specifics of the reaction the particle size needs to be adaptable. It has been shown that the nickel particle size influences the stability of the catalyst during the reaction. [29] The nickel particle size also affects carbon nanotube growth during methanation. [30] Particle growth during a catalytic reaction has been shown to lead to deactivation of a Ni catalyst because of coke formation. [31,32] Therefore it is important to understand the particle formation and growth mechanism. Through adapting parameters in the synthesis an

understanding of the influencing factors can be obtained. The reduction temperature is likely to effect the metal particle size. A higher temperature leads to bigger particles as a higher temperature leads to increased kinetic energy of particles that collide and aggregate into larger particles. [33] This is why in this study the effect of temperature on Ni particle size from phyllosilicate nanotube based precursors will be investigated.

A challenge in heterogeneous catalysis lies in the complexity of industrial heterogeneous materials in general. Generally, the goal in catalysis research is to produce materials in a more controlled way. Characterization and analysis of the material is used to achieve this goal. Often a specific size or shape is needed or wanted for an application, which is why it is useful to be able to precisely predict shape and particle size and surface area of the metal and support. The active site of the catalyst is embedded in a complicated pore structure that is sometimes difficult to characterize. The complexity of solid catalysts still limits the fruition of the applied knowledge gained with surface techniques. A solution for this problem has been found in the development of model systems for solid catalysts. Model systems can aid in studies of particle size and support effect in the catalysis research field. [34,35]

In this project a model system for nickel catalysts was developed in the shape of Ni phyllosilicate nanotubes. A representation of a sheet layer in a Ni phyllosilicate nanotube is shown before (figure 4a) and after reduction (figure 4b). The homogeneous distribution in the material before reduction causes a homogeneous particle size after treatment with hydrogen gas at high temperatures. The Ni phyllosilicate nanotubes can be a very appropriate model system due to their homogeneous distribution of nickel and silica in the material, high temperature stability and parallel sheets in a nanotube shape imageable in 3D. The Ni phyllosilicate nanotubes symmetry in 3D space make it well characterizable with microscopy techniques, which is a desired property of a catalyst model system.

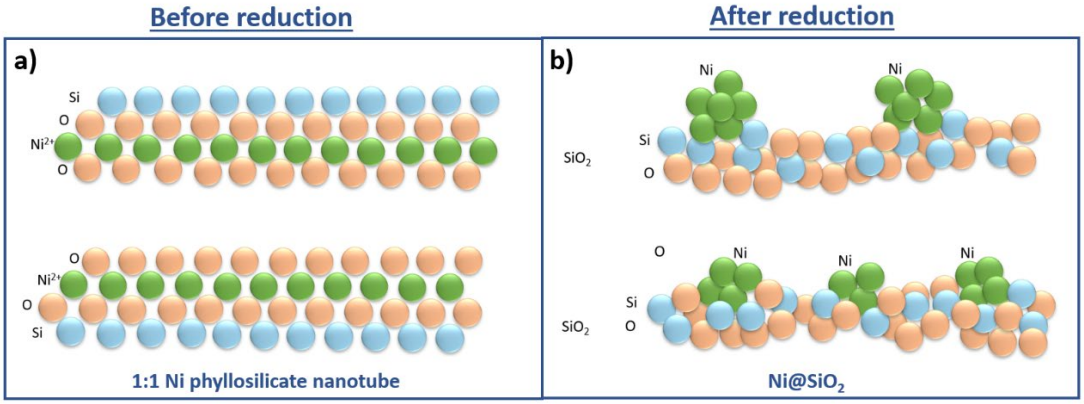

Figure 4: Representation of molecular structure of (a) Nanotube of 1:1 Ni phyllosilicate, $Ni_3Si_2O_5(OH)_4$ before reduction and (b) Ni metal particles dispersed on silica after reduction.

When Ni phyllosilicate sheets are imaged with TEM the total extent of the material cannot be measured because depth cannot be determined with electron transmissions. The possibilities of characterization expand when studying a 3D system like nanotubes, assuming a perfectly symmetric nanotube. The sheets in Ni phyllosilicate curl up into nanotubes. By synthesizing Ni phyllosilicate nanotubes, a controllable model system can be created. By imaging Ni phyllosilicate nanotubes with TEM the dimensions are clearly defined, as the nanotube is straight and a 3D object. The total volume of the sheets and the sheet thickness can be determined by analysis of TEM images. The morphology of the phyllosilicate and the metal particle size after reduction can be studied very well in this way.

The conditions that are known to affect phyllosilicate morphology are the nature of the silica precursor, the duration of the reaction, the temperature during synthesis and the concentrations of the reagents. The reagent factors that influence the Ni phyllosilicate nanotubes hydrothermal synthesis are the OH- concentration, the Ni/Si molar ratio and the addition of promoters. [13,14,22] Synthesis time has been shown to have an effect on Ni phyllosilicate morphology after deposition

precipitation. [16] The synthesis time of a hydrothermal synthesis of Ni phyllosilicate nanotubes [24,28] will likely effect the morphology in a similar way. The concentration of sodium hydroxide in hydrothermal synthesis of Ni phyllosilicate nanotubes has been varied in the study by White et al. The synthesis produces nanotubes when the NaOH concentration is kept between 2 and 10 wt%, and the Ni/Si ratio is between 1-2. [24] While the NaOH concentration and Ni/Si ratio have been studied by White et al, a study in the variation of hydrothermal synthesis time has not been undertaken. Consequently, the NaOH concentration and the synthesis time effect are explored in this thesis.

Particles formed during the reduction of Ni phyllosilicates are proposed to form through the mechanism developed by van den Berg et al for Cu phyllosilicates, as depicted in figure 5a. [36] The formation and subsequent reduction of Cu phyllosilicate was studied using time lapsed TEM images, which gave insight into the growth mechanism. The growth is based on a nucleation-and-growth scenario with autocatalytic reduction of the Cu phyllosilicate and subsequent growth of the nanoparticles governed by either diffusion-limited or reaction-limited growth. The particle size is thus determined by the concentration of metal ions surrounding the nuclei and this depends on the thickness of the phyllosilicate sheets. Therefore, it is worthwhile to study this reduction mechanism in Ni phyllosilicates as well. A nanotube form of Ni phyllosilicate allows for a more controlled study of particle formation, leading to a relationship between the wall diameter and number of sheets with particle size.

The nickel particle size after the reduction of Ni phyllosilicate is thus likely dependent on the number of sheets in the nanotube structure. When a nanotube wall is thicker it has more layers. When a nanotube wall is thinner it has fewer layers. The presence of more Ni^{2+} in the phyllosilicate structure (more layers) could lead to bigger particles after reduction. The presence of less Ni^{2+} in the phyllosilicate structure (fewer layers) could lead to smaller particles after reduction. This hypothesis has been illustrated in figure 5b: (1) Thicker nanotube walls can lead to bigger Ni particles after reduction. (2) Thinner nanotube walls can lead to smaller Ni particles after reduction. By changing the synthesis conditions the morphology of the nanotubes could be changed. In this project the variations in synthesis conditions will aim to change the Ni phyllosilicate nanotube morphologies, for example a distinction between thinner and thicker nanotube walls. The goal in this project is to change the particle size after reduction, which can depend on the sheet characteristics.

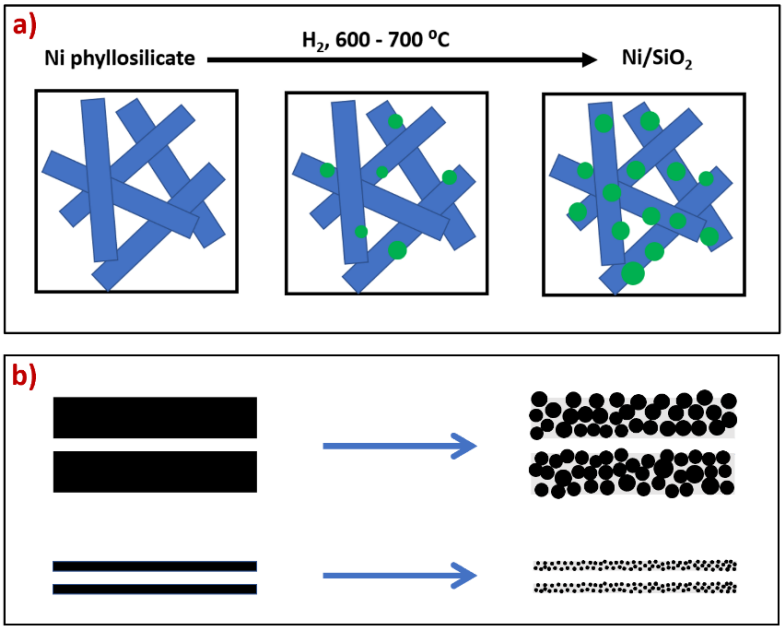

Figure 5: (a) Proposed growth mechanism of Ni nanoparticles on Ni phyllosilicate, based on the mechanism for Cu phyllosilicates by Roy van den Berg. Image inspired by [36] (b) Hypothesized mechanism of particle formation from Ni phyllosilicate nanotubes. (top) Thick sheets form big particles. (bottom) Thin sheets form small particles.

First, the aim of this project is to synthesise well-defined Ni phyllosilicate nanotubes that are pure and straight. This will be characterized using TEM, EDX, XRD, TPR and N2 physisorption. This will be used to discover the properties of the Ni phyllosilicate nanotubes and the composition and morphology of the sample. Second, control over the nanotube growth is a priority. By controlling the properties of the nanotubes, the production of a specific size of nanotube is possible. In this case the synthesis parameters that will be studied are reagent concentration, synthesis time, washing steps and ageing time. The emphasis in this study is the effect of synthesis time and NaOH wt% on the composition and morphology of the nanotube system. Finally, the reduction of Ni phyllosilicate nanotubes will be studied. The particle size effect of the reduction temperature will be determined. The nanotube wall thickness and particle size after reduction will be related to each other by use of Identical Location TEM, to answer the question whether there is a relation between wall thickness and particle size.

2 Background

2.1 Characterization of Ni phyllosilicates

The thermal stability of Ni phases influences the composition after synthesis. This has been determined by looking at E-pH diagrams with the program HSC. The stability is highest when the Gibbs energy is lowest. The thermal stability decreases as follows: 2:1 Ni Phy < 1:1 Ni Phy < $NiO + SiO_2$ < $Ni(OH)_2$ < $Ni^{2+} + OH^-$, as seen in figure 6a. The 2:1 Ni phyllosilicate phase is more stable than the 1:1 Ni phyllosilicate[25], and 2:1 will be favoured, if possible, to lower the Gibbs energy of formation. The system will strive towards the most stable phases, which determines the composition of the sample.

Characterization on Ni phyllosilicates has been carried out in the publications from Paolo Burattin, Michel Che and Catherine Louis.[13,14] A hydrothermal process of 14 days produced samples of 1:1 and 2:1 Ni phyllosilicate were prepared at 25 ^oC and 150 ^oC using sodium silicate (SiO_2 Na_2O), nickel chloride and hydrochloric acid described in the work of Decarreau [37,38]. Burattin et al used X-ray diffraction to determine the lattice spacing and XRD patterns for 2:1 and 1:1 Ni phyllosilicate phases synthesized at 25 ^oC and 150 ^oC.[14] The 2:1 Ni phyllosilicate phase has a lattice spacing of 1.6 nm at 25 °C and 1.1 nm at 150° C. The 1:1 Ni phyllosilicate phase has a lattice spacing of 1.1 nm at 25 °C and 0.8 nm at 150 °C. It seems the lattice spacing for 2:1 and 1:1 Ni phyllosilicate becomes smaller with increasing synthesis temperature. [14] A higher synthesis temperature is thus likely to lead to a lattice spacing of <0.8 nm for 1:1 or <1.1 nm for 2:1 Ni phyllosilicate. In figure 6b the XRD pattern found by Burattin et al is shown for 1:1 and 2:1 Ni phyllosilicate. The main difference between the 1:1 and 2:1 structure in XRD is that for the 2:1 there are two twin peaks at 23 and 33 2Θ while for the 1:1 there is a peak at 23 and 28 2Θ (Co-Kα). Another difference is a peak at 9 2Θ for 2:1 and a peak at 13 2Θ for 1:1 (for Co-Ka). The XRD characterization can thus be used to determine the Ni phyllosilicate presence and the phase by location of the peaks.

Temperature programmed reduction can show the Ni phases that are present in a sample, by flowing hydrogen gas through a fixed bed reactor while increasing the temperature. The thermodynamic stability increases from nickel hydroxide to nickel oxide to 1:1 Ni phyllosilicate to 2:1 Ni phyllosilicate. This means that reduction will take place at increasingly higher temperatures with increasing thermodynamic stability. In figure 6d TPR results shows this too. The reduction of 2:1 Ni phyllosilicate takes place at 650 °C. When 1:1 Ni phyllosilicate is reduced a broad peak at 500 °C and a smaller peak at 630 °C appears. When 1:1 phyllosilicate is reduced the 2:1 phyllosilicate is formed when Ni is removed from the lattice to form particles, which is why a second peak forms at 630 ^oC in figure 6d(ii). Ni precipitates form when no silica is present and shows a peak at 320 °C (figure 6d,iii). Hence TPR is a suitable technique to show the reduction temperatures of specific Ni phases in the system.

Contaminations can appear after a synthesis of Ni phyllosilicate, in the form of Ni hydroxide. Ni hydroxide exists in α-$Ni(OH)_2$ and β-$Ni(OH)_2$ form, their structure is shown in figure 6c. The beta form

has a crystal structure of Ni-OH-OH sheets parallel to each other. The alpha form has a disordered irregular turbostratic structure, where the basal planes have slipped out of alignment and other anions attach between the layers to ensure electroneutrality. The difference between the two nickel hydroxide forms can be found with IR spectroscopy and thermogravimetric analysis (TGA). The intercalated ions in the alpha form appear in IR in the shape of a strong band at 2215 cm^{-1} and a sharp band at 1287 cm^{-1} due to isocyanate NCO^- ions. This is caused by urea decomposition during deposition precipitation. [14] XRD and TPR can determine the presence of $Ni(OH)_2$, but cannot distinguish between α-$Ni(OH)_2$ and β-$Ni(OH)_2$.

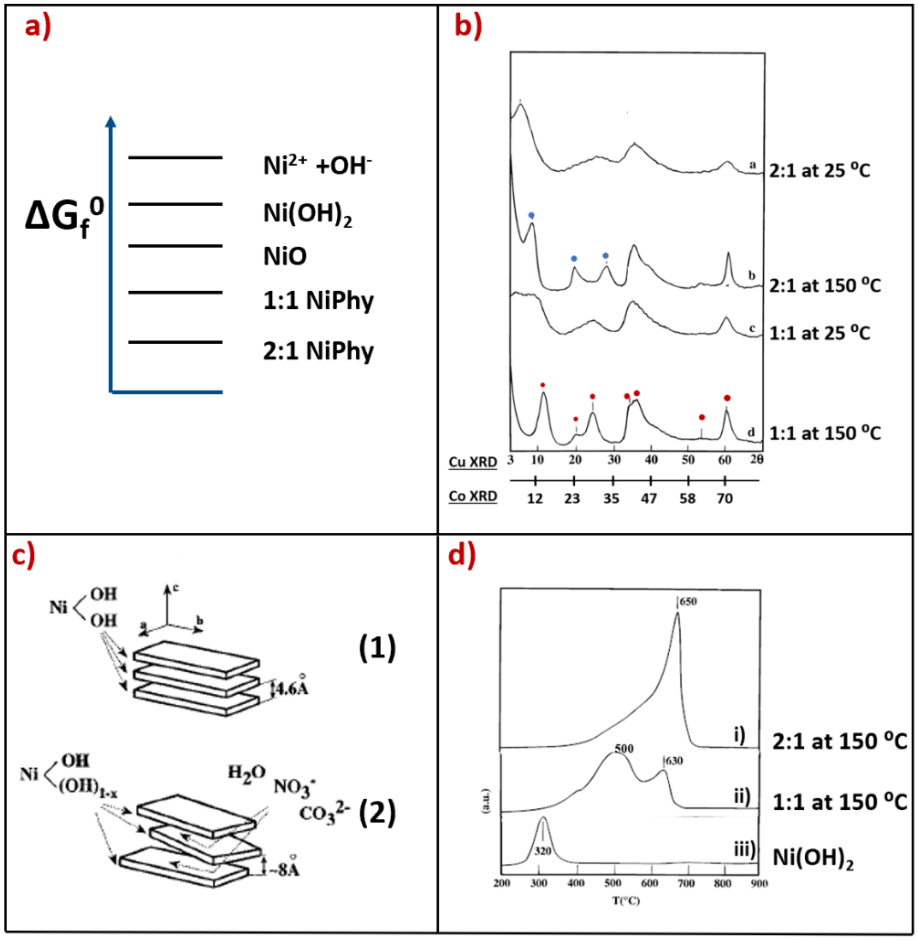

Figure 6: (a) Thermal stability of Ni phases. (b) XRD pattern of Ni phyllosilicates synthesized at 25 °C and 150 °C. The red dots indicate relevant 1:1 Ni phyllosilicate peaks, the blue dots indicate significantly different 2:1 Ni phyllosilicate peaks. (c) Ni hydroxide structures. (1) β-$Ni(OH)_2$ (2) α-Ni(OH)2 (d) TPR of Ni phyllosilicates synthesized at 150 °C, heating to 900 °C, heating rate 7.5 °C/min and 5% H_2/Ar. i) 2:1 Ni phyllosilicate synthesized at 150 °C ii) 1:1 Ni phyllosilicate synthesized at 150 C iii) synthesis at 150 °C without silica present, results in $Ni(OH)_2$. (b,d) Modified from Burattin et al, 1997. Hydrothermal treatment with sodium silicate, $NiCl_2$ and HCl at 25 or 150 °C for 14 days, from [37,38] (b-d) Figures adapted from Burattin et al [14]

The crystallinity of Ni phyllosilicate influences the reducibility: a higher crystallinity decreases the reducibility. A higher crystallinity is reached when a higher synthesis temperature is used. The 2:1 Ni phyllosilicate has a higher degree of crystallinity, which is also why it reduces at a higher temperature. There have been differences observed in short (< 4 hours) and long (>4 hours) synthesis times, during deposition precipitation. A longer deposition time increased the crystallinity of 1:1 Ni phyllosilicate. [11] Burattin et al concluded that there is a dependency on the silica surface area during deposition precipitation. When different types of silica are used, a low silica surface area caused a better crystallized 1:1 nickel phyllosilicate. [14] When no silica was used during deposition precipitation the nickel phase that was formed was α-$Ni(OH)_2$ instead of Ni phyllosilicate. The crystallinity of the α-

$Ni(OH)_2$ decreased with increasing deposition time. Variation of the synthesis time and silica source have not been investigated in Ni phyllosilicate nanotube hydrothermal synthesis yet and are worth looking into.

2.2 Ni phyllosilicate nanotubes

Nanotubes attract a lot of attention because of their promising properties. Nanotubes can be applied as very small and strong containers, in colloidal dispersions or made into fibrous bundles. They can for example be filled with electrically conductive material to produce nanowires, potentially be used for gas storage, surface coatings of electrodes or in-vitro drug delivery with a time-release mechanism.[39,40] The porous nature of nanotubes makes them suitable to adsorb gases and other fluids. The nanotubes that exist are carbon nanotubes (CNT) (1952), natural nanotubes from metal silicates, $Al_3SiO_3(OH)_4$ (imogolite), $Al_3Si_2O_5(OH)_4$ (halloysite), $Co_3Si_2O_5(OH)_4$, $Mg_3Si_2O_5(OH)_4$ (chrysotile), $(Mg, Fe)_3Si_2O_5(OH)_4$ and $Co_3Si_2O_5(OH)_4$, WS_2 (1992), titanate nanotubes, TiO_2, VO_x and others. The geological formation of chrysotile nanotubes can be mimicked with hydrothermal synthesis in a controlled way. When making $Ni_3Si_2O_5(OH)_4$ nanotubes a big advantage is the adaptability of the structure.

Nanotubes can be classified into multi-walled (MW-type), single-walled type (SW-type) and scrolled-type (S-type) nanotubes (figure 7a), which can be formed from a crystalline or polycrystalline material. Single walled nanotubes form from a rectangular sheet that connects at both ends and forms when the surface strain energy is more favourable, when the diameter exceeds a certain critical value. Examples of SW-type material include MoS_2/WS_2 nanotubes. Multi-walled nanotubes consist of multiple tubes connected through van der Waals interaction. Scrolled nanotubes form through the rolling up of a sheet, through a spontaneous rearrangement of atoms in a 2D crystal structure. The driving force for the scrolled-type nanotube also has its basis in the limitation of surface and edge energies, involving van der Waals forces. [41] Ni phyllosilicate nanotube likely fall into the S-type category.

Nanotubes can be further classified based on synthesis pathways (figure 7b). The tubular structure is either a self-organization type or a template-assisted type. The synthesis needed depends on the materials chosen for nanotube formation. Insoluble materials like carbon nanotubes (CNT) and boron nitride nanotubes can be synthesized using Chemical Vapor Deposition (CVD) on a catalyst particle. Materials which are electrolyte soluble can be formed into nanotubes by use of electrodeposition on a nanoporous template. Soluble materials that can recrystallize in a solution can be formed into nanotubes by a hydrothermal treatment or a sol-gel method, involving either a template or a spontaneous nanotube formation. [39,41]

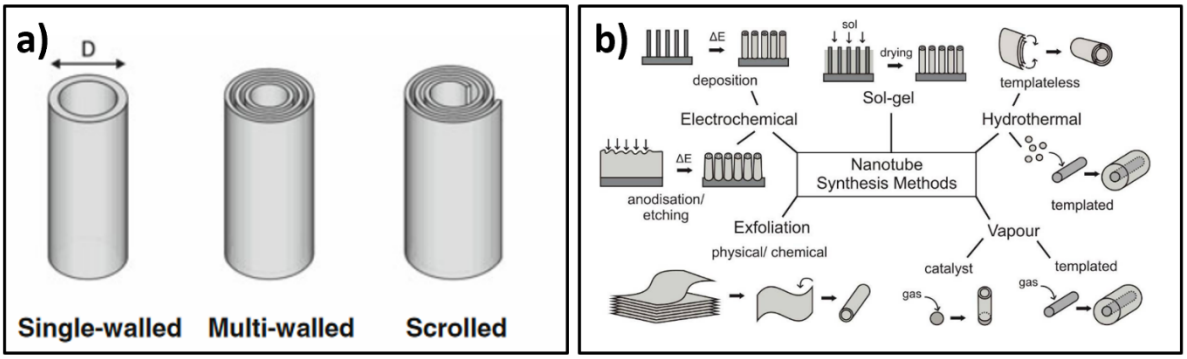

Figure 7: (a) Structural types of nanotubes. [41] (b) *Existing nanotube synthesis methods. Reproduced from* [39].

The hydrothermal treatment requires only simple equipment (an autoclave), no templates are needed, easily scalable to gram quantities and involves a one-step procedure. Template based synthesis

requires first the synthesis of the template and require after nanotube formation the removal of the template from the nanotubes. Self-organization type nanotubes are formed from materials with a strong covalent bonding character in a 2D layered structure. Only poor covalent materials require a template. [41] The thermodynamic driving force for the scrolling mechanism is likely the formation of new covalent bonds between the material, to limit surface energy. In the case of Ni phyllosilicate nanotubes, the scrolling creates new bonds between the Ni octahedral layer and Si tetrahedral layer through oxygen. The driving force of Ni phyllosilicate and chrysotile nanotube formation has been studied by Krasilin and Gusarov[42–44]. The difference in size between metal octahedra and silica tetrahedra in the 2D sheet creates stress on the crystal lattice. This and the opposite surface energies on the silica and metal side of the sheet contribute to the scrolling of the 2D sheet into a 3D tube. The size mismatch between the sheets is shown in figure 8a and the scrolling mechanism is shown in figure 8b, which controls the Ni phyllosilicate nanotube formation.

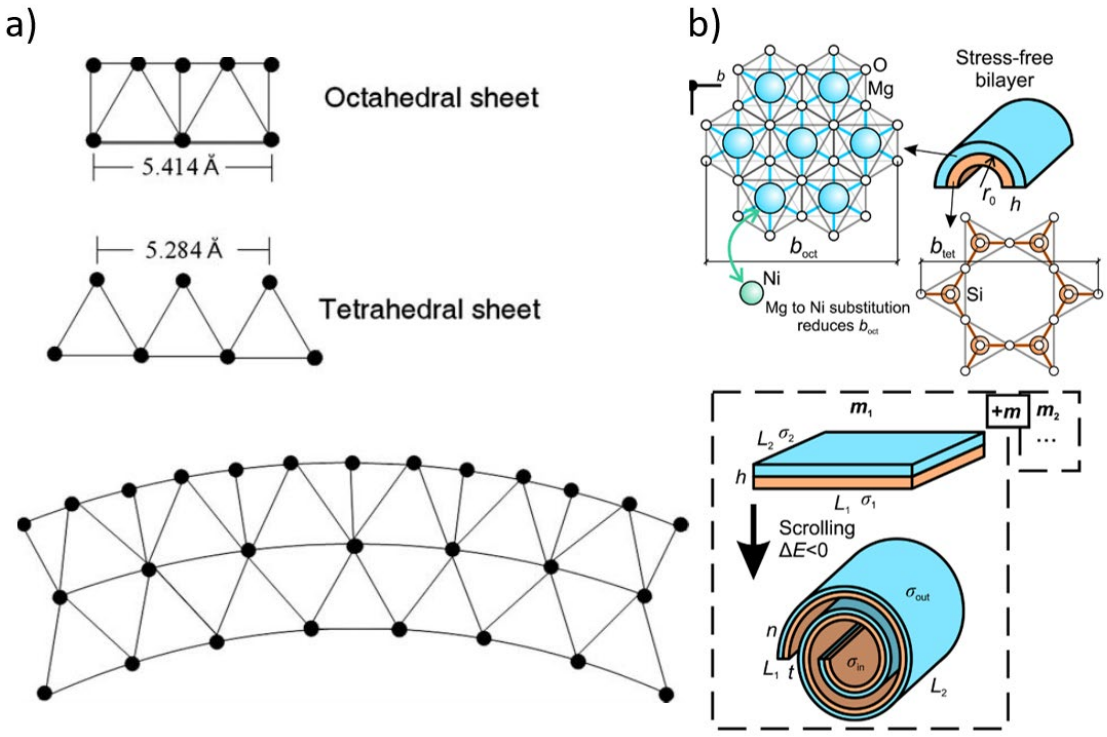

Figure 8: Mechanical structure and scrolling origin. a) size mismatch in octahedra and tetrahedra. [26] *b) Bending of sheets lead to scrolling into a multiwalled nanotube with metal octahedral sheet facing outwards. Phyllosilicate nanotube modelling and growth.*[44]

Korytkova et al [45] did a lot of previous work on phyllosilicate type nanotubular structures, chrysotile nanotubes and formation mechanisms. The synthesis used by them to produce Ni phyllosilicate nanotubes required very high temperatures (400 ^{o}C), non-aqueous solvents and an inert atmosphere. A simpler method was developed by Yang et al [46] , which uses lower temperatures (190-210 ^{o}C) in an aqueous highly alkaline medium and does not require a glovebox. White et al [24] used this method and studied variations in Ni/Si ratio and NaOH concentrations. They found that at lower temperatures only sheets are formed. The hydrothermal treatment mimics the natural environment underground where chrysotile type nanotubes are formed. A base is required for the dissolution and recrystallization of the material. The basic environment is needed to partially dissolve silica. The dissolved silicate anions react with metal cations and hydroxide anions to form a phyllosilicate structure. The metal/silica ratio, temperature, NaOH wt%, synthesis time and silica source thus affect the morphology, structure and dimensions of phyllosilicates. [22]

In the study by White et al [24] nanotubes were formed while the NaOH concentration was between 2-

10 wt% and the molar Ni/Si ratio above 1.5, as shown in figure 9. A Ni/Si ratio of 1.5 and 7 wt% NaOH was found to be the most ideal, forming nanotubes that were straight and crystalline with an inner diameter of 10 nm and an average length of 90-300 nm. Below a Ni/Si ratio of 1.5 (Ni/Si=1.0 with 4 wt% NaOH) nickel deficient nanosheets are formed and above a Ni/Si ratio a higher amount of β-$Ni(OH)_2$ is formed besides nanotubes. This leads to the conclusion a Ni/Si ratio above 1.5 creates an excess of nickel which produces more or bigger β-$Ni(OH)_2$ crystals. At a Ni/Si ratio below 1.5 a deficit in nickel takes place, causing no Ni phyllosilicate nanotubes to be formed. [24] The amount of β-$Ni(OH)_2$ has been studied with TGA by White et al, using a 4 wt% NaOH concentration while varying the Ni/Si ratio. The $Ni(OH)_2$ quantity increased with increasing Ni/Si ratio, a 1.5 Ni/Si sample containing 1 wt% $Ni(OH)_2$, a 2.0 Ni/Si sample containing 29 wt% $Ni(OH)_2$ and a 3.0 Ni/Si sample containing 15 wt% $Ni(OH)_2$. Therefore, the synthesis conditions according to White et al need to be between 2-10 wt% NaOH and 1.5 Ni/Si ratio.

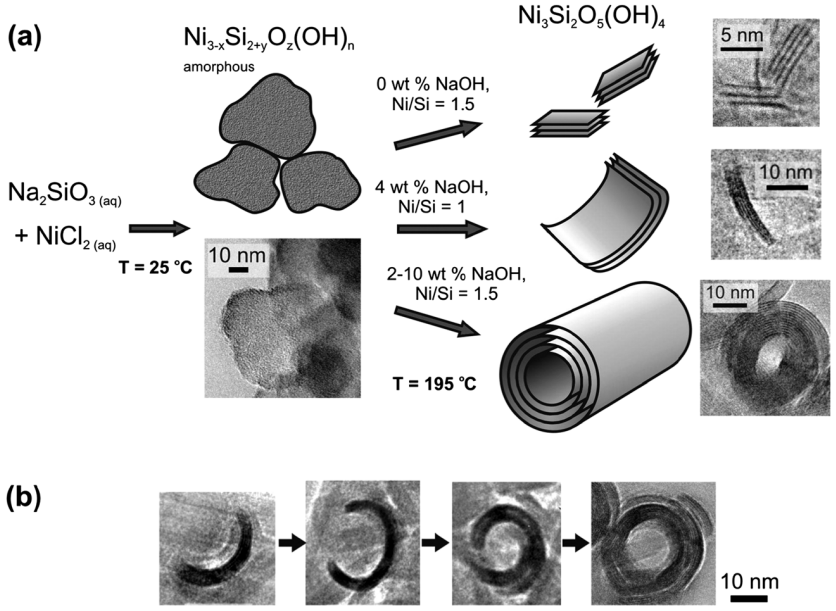

Figure 9: (a) Reaction mechanism where amorphous material $Ni_{3-x}Si_{1+y}O_z(OH)_n$ recrystallises as $Ni_3Si_2O_5(OH)_4$ under hydrothermal treatment at 195 °C. When no NaOH is added, the crystals do not grow much beyond the nucleation stage, and when the molar Ni/Si ratio is equal to 1 crystal growth does not proceed beyond nanosheets 15-20 nm long. It is only when Ni/Si = 1.5 and C_{NaOH} = 2-10 wt% the extent of recrystallisation allows the formation of complete tubes within 48 hours. (b) HRTEM images of $Ni_3Si_2O_5(OH)_4$ nanosheets at different stages of scrolling, found in the sample obtained at Ni/Si = 1.5 and C_{NaOH} = 4 wt%. [24]

$$3Ni_{(aq)}^{2+} + 2SiO_{3(aq)}^{2-} + 2H_2O + 2OH_{(aq)}^{-} = Ni_3Si_2O_5(OH)_{4(s)} \quad (1)$$

$$3Ni_{(aq)}^{2+} + 6OH_{(aq)}^{-} = 3\beta\text{-}Ni(OH)_{2(s)} \quad (2)$$

$$2SiO_{3(aq)}^{2-} + 2H_2O = 2SiO_{2(s)} + 4OH_{(aq)}^{-} \quad (3)$$

During the synthesis there appear to be three reactions that take place less or more depending on the NaOH wt% and the Ni/Si ratio. The formation of $Ni_3Si_2O_5(OH)_4$ (1:1 Ni phyllosilicate) depends on the OH^-, Ni^{2+} and SiO_3^{2-} concentration (reaction 1). As OH- is consumed in reaction (1) the pH decreases. If the pH drops below 7 that will cause dissolved SiO_3^{2-} to precipitate to solid SiO_2 (reaction 3), which reduces the amount of dissolved Si(IV) required for reaction (1). This will only happen for very low

sodium hydroxide concentrations. When the sodium hydroxide concentration is very high with a 15 wt% NaOH this creates an excess of OH- ions, which will cause more precipitation of β-$Ni(OH)_2$ (reaction 2) to dominate instead of $Ni_3Si_2O_5(OH)_4$, and no phyllosilicate nanotubes will be formed. [24] It is important to find a balance in nanotube formation (reaction 1) while limiting nickel hydroxide formation (reaction 2) and a presence of the right amount of silica dissolved (reaction 3).

Analysis of TEM images in White et al saw an increase in nanotube length and a small increase in width with increasing NaOH concentration. Physisorption showed an increase in pore size with increasing NaOH concentration. TEM and SEM images revealed a wider length distribution with increasing NaOH concentrations. [24] The synthesis used by Yang et al using $NiCl_2.6H_2O$ and Na_2SiO_3 as starting materials produced Ni phyllosilicate nanotubes of > 100 nm length and 8-15 nm pores. [46]

The formation of phyllosilicate nanotubes has been shown to be dependent on OH- concentration, temperature, molar ratio of metal cations, the charge of the metal compared to the silicates and the presence of seed crystals. [40,45,47] In magnesium based phyllosilicates crystallization was based on seeds of $Mg(OH)_2$, $Mg_3Si_4O_{10}(OH)_2$ and $Mg_3Si_2O_5(OH)_4$, which are flat lamellar crystals. These three seed molecules contain a octahedral $Mg(II)O_6$ sheet of the brucite structure ($Mg(OH)_2$). From these seeds of the brucite structure, crystals grow from solution to form nanosheet structures of $Mg_3Si_2O_5(OH)_4$.[45] A similar mechanism takes place in the formation of Ni phyllosilicate nanotubes, where $Ni(OH)_2$, $Ni_3Si_4O_{10}(OH)_2$ and $Ni_3Si_2O_5(OH)_4$ seed crystals are formed. [40] The SiO_4 tetrahedra form on one side while the $Ni(II)O_6$ octahedra attach to the other side to form a hexagonal crystal structure. Due to the difference in size of the tetrahedral silica and the octahedral metal the sheets start curling up into nanotubes when the temperature increases. Factors that influence the solubility of Si(IV) and Ni(II) species have an influence on the formation of the nanotubes. Both the pH, the temperature and the synthesis time effect the solubility of Si(IV) and Ni(II), so they play a role in the crystallization of nickel silicate during hydrothermal synthesis.

The appearance of $Ni(OH)_2$ after Ni phyllosilicate nanotube structures is something that happens during the synthesis used by White et al.[24] A pure sample would contain only Ni phyllosilicate nanotubes. For applications of Ni phyllosilicate nanotubes in catalysis and electrochemistry a sample without $Ni(OH)_2$ would be advantageous. Formation of Ni phyllosilicate nanotubes has been shown to use seed crystals of the brucite structure to form octahedral sheets. Nickel hydroxide has such a brucite structure and is used as a seed crystal. The prevention of the nickel hydroxide formation is something that is desired, but since it is also involved in the nanotube formation this might not be possible. The fact that nickel hydroxide can be detected by XRD could mean that an excess of seed crystals forms during hydrothermal treatment. Finding a way to remove the nickel hydroxide post synthesis could be a possible solution to investigate further. The synthesis used by White et al [24] was based on a method used by Yang et al[46], but produced different results. The divergence lies in the $Ni(OH)_2$ content: Yang et al appears to have formed pure Ni phyllosilicate nanotubes and no $Ni(OH)_2$, while White et al only formed β-$Ni(OH)_2$ at a 15 wt% NaOH and 1.0 Ni/Si. The only difference in the synthesis between the two is the drying step (Yang et al: 80 °C in air, White: 24 hours in vacuum at RT) and the synthesis time (Yang: 24 hours 190-210 °C, White: 48 hours 195 °C). The XRD pattern shown by Yang et al contains only Ni phyllosilicate peaks while White et al showed only $Ni(OH)_2$ peaks. The synthesis time and drying step could thus be important in the formation of Ni phyllosilicate nanotubes and $Ni(OH)_2$. By changing this, the formation of $Ni(OH)_2$ could possibly be prevented.

A solution to $Ni(OH)_2$ presence might also be found by changing the synthesis completely, but it would mean a more complicated and expensive procedure. McDonald et al have used a hydrothermal synthesis under glovebox conditions. [26] The preparation of the synthesis was carried out under a nitrogen atmosphere, where $NiCl_2.6H_2O$, silicic acid and distilled water were mixed, a 1.0 M NaOH solution was added dropwise (Molar Ni/Si = 1.5 and OH-/Ni = 5). After stirring under nitrogen for 3 days the solution was added to a Parr autoclave and purged with argon. The synthesis was carried out at 250 ^oC and 10MPa for 18 hours with a 500 psi argon. TEM images showed only Ni phyllosilicate nanotubes of maximal 200 nm in length, 25-30 nm outer diameter and pores of 10 nm. A broad pore size distribution around 17 nm was found with N_2 physisorption, with a peak between 5 and 10 nm and a BET area of 110 m^2/g. XRD showed only Ni phyllosilicate peaks at 11, 20, 24, 34, 36 and 61 degrees 2Θ and no sign of nickel hydroxide peaks. The difference between the two syntheses is the absence of oxygen from the reaction environment. The presence of oxygen could thus be the factor that causes extra nickel hydroxide to form, as a hydrothermal treatment without air results in no nickel hydroxide formation.

Another synthesis procedure that did not produce nickel hydroxide was carried out by Korytkova et al,[40,45,48] using $NiSiO_3$, $Ni(OH)_2$ and NaOH to perform hydrothermal synthesis under high temperatures (250-400 °C) and high pressures (30-100 MPa) for 12-48 hours. The $NiO:SiO_2$ ratio is 3:2 and the NaOH mass % varied between 1-3. Nanotubes of lengths 113-300 nm, widths 10-15 nm and pore sizes of 2-3 nm were produced. The total surface area was 110-115 m^2/g. No presence of $Ni(OH)_2$ was observed by them in XRD.

The structure of the Ni phyllosilicate nanotubes can possibly be slightly altered post synthesis. Korytkova et al observed in TEM that the lattice spacing in the nanotubes increased slightly with increasing atomic number of metal chlorides (untreated: 0.72 nm, NaCl treated: 0.726 nm, KCl treated: 0.731 nm, CsCl treated: 0.730 nm; treatment: 10 h, 80 ^oC). [48] This means that other metals could be incorporated in the Ni phyllosilicate nanotube structure post synthesis. With increasing ionic radius (Na^+: 102 pm, K^+: 138 pm, Cs^+: 167 pm) [49] Korytkova [48] observed an increasing lattice spacing. The treatment of the Ni phyllosilicate nanotubes with metal chloride (NaCl, KCl and CsCl) solutions at 80 °C caused nanotube broadening. Nanotube treatment with metal hydroxide solutions (Na, K and Cs hydroxides) at 80 °C created a structural-morphological change where K_2SiO_3 particles formed inside the sheets when treated with 1 M KOH solution. [48] The pore size of the nanotubes increased when the hydroxide treatment duration increased. The Ni phyllosilicate nanotubes remained completely intact and suffered no destruction under these treatments, unlike Mg phyllosilicate nanotubes, which were damaged from this treatment. Therefore, the Ni phyllosilicate nanotubes can be used as a storage material. The metal ion composition inside the sheets can possibly be altered by design to explore different properties of the nanotubes.

2.3 Reduction of Ni phyllosilicates

Ni phyllosilicate sheets

Carbon build-up is often a problem in Ni catalysts supported on silica during catalytic reactions. Since it causes the catalyst to deactivate while the reactor becomes overloaded with coke. It has been shown that a strong metal-support interaction and a high dispersion over the support can decrease coke formation during catalysis. Phyllosilicates have a very good metal-support interaction, so they offer a solution to heavy coke formation in nickel catalysts during a catalytic reaction. [25]

The reduction of Ni phyllosilicate sheets is discussed in the next section. Sivaiah et al proposed a mechanism for the reduction of 1:1 Ni phyllosilicate sheets, which is shown in figure 10b. When a 1:1 Ni phyllosilicate is reduced with hydrogen below 700 degrees ^oC a partially reduced Ni phyllosilicate forms as an intermediate that resembles 2:1 Ni phyllosilicate. Nickel N^0 particle form while the

remaining phyllosilicate structure acts as a support, which now has vacancies because of the expelled Ni^{2+} from the structure. The intermediate has the structure of a 2:1 Ni phyllosilicate. The reduction above 700 °C will fully reduce the intermediate 1:1 Ni phyllosilicate phase and form Ni particles on SiO_2.

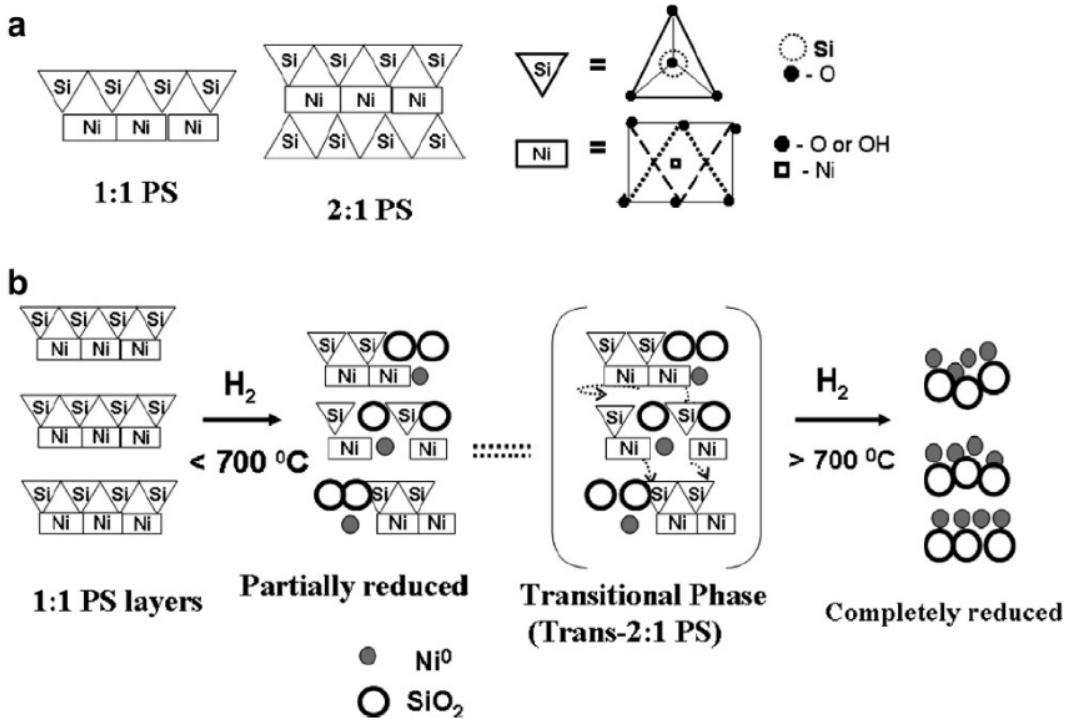

Figure 10: Structure of 1:1 and 2:1 Ni phyllosilicate (a) and mechanism of Ni phyllosilicate reduction (b) [25]

The intermediate 1:1 Ni phyllosilicate phase can be proven with in-situ XRD. In situ XRD reduction was performed by Sivaiah et al[25] on 1:1 and 2:1 Ni phyllosilicate by heating from room temperature to 800 °C with a heating rate of 10 °C/min (3%H_2 in He, flow rate of 50 mL/min), shown in figure 11. Reduction of 1:1 Ni phyllosilicate shows a peak at 7° 2Θ (Cu-Ka) in in-situ XRD that appears at 600 °C, this is the peak that signifies the transition state between 1:1 Ni phyllosilicate and the completely reduced phase. At the same time Ni particles form on the remaining structure of 1:1 Ni phyllosilicate, which is visible in the in-situ XRD spectrum from 500 °C and higher at 44.5 and 51.8° 2Θ. In 2:1 Ni phyllosilicate in-situ XRD reduction Ni^0 peaks only start appearing from 700 °C. A reorganization of the tetrahedral and octahedral sheets take place when the transition state forms, while Ni particles are embedded in the remaining structure. The XRD peak of 7° 2Θ signifying the transition state also formed during calcination in air at 700 °C in a previous study by Sivaiah et al [50], where NiO peaks also appeared at 37.2, 43.3 and 62.9 ° 2Θ. The formation of a transition 2:1 Ni phyllosilicate like state thus takes place at 600 – 700 °C both in air and in a hydrogen environment.

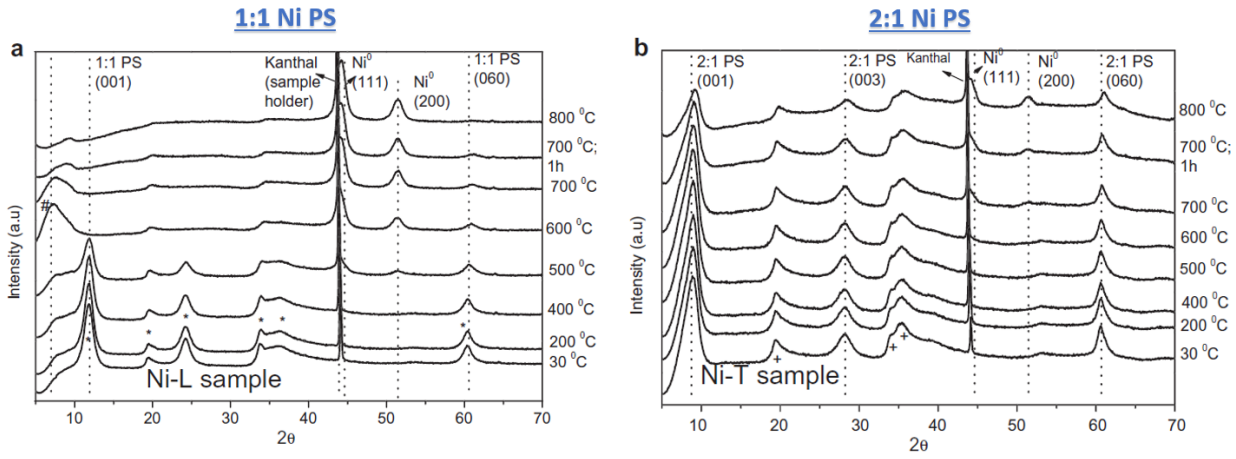

*Figure 11: In-situ XRD during reduction of 1:1 Ni phyllosilicate (a) and 2:1 Ni phyllosilicate (b) under 3% H_2/He. (Cu-Kα) PS: phyllosilicate. *: 1:1 Ni phyllosilicate. +: 2:1 Ni phyllosilicate.* [25]

The thermodynamic stability of the 1:1 and 2:1 Ni phyllosilicates are different. The 2:1 phase is thermodynamically more stable than the 1:1 phase, as can be seen in the in-situ XRD spectrum. The 2:1 Ni phyllosilicate signifying peaks remain constant from low to high temperatures. The appearance of Ni^0 peaks signifies particle formation on the 2:1 Ni phyllosilicate structure. A TPR under 5% H_2/Ar of both types of Ni phyllosilicate (pre-treated at 500 °C under argon) by Sivaiah et al [50] shows a broad peak at 550 °C and a lower one at 700 °C. The 2:1 Ni phyllosilicate has one broad peak at 790 °C with a range from 700 °C to 820 °C. This also signifies the higher thermal stability of 2:1 Ni phyllosilicate because the reduction occurs at a higher temperature. The fact that two peaks appears in the TPR of 1:1 Ni phyllosilicate points to the fact that 1:1 is transformed to the 2:1 transition state.

The catalytic activity of a Ni phyllosilicate derived catalyst has been studied with CO_2 reforming of CH_4 [50]. The catalyst was reduced by treating the 1:1 and 2:1 Ni phyllosilicate at 700 °C under a pure H_2 gas flow (35 mL/min). The 2:1 Ni phyllosilicate derived catalyst has a higher catalytic activity than the 1:1 Ni phyllosilicate-based catalyst. The CO_2 conversion rate for the 1:1 is 35 % and the 2:1 has a constant CO_2 conversion of 50 % over a period of 0 to 12 hours. The CH_4 conversion rate is 17 % and 37 % respectively for 1:1 and 2:1 Ni phyllosilicate. This means that the 2:1 based phyllosilicate catalyst is more thermally stable and has a higher catalytic activity but requires more energy to form Ni particles (more than 700 °C).

To evaluate particle size formation in sheets and nanotube Ni phyllosilicate the studies of Louis et al [16]and Yang et al [46]can be compared. Ni phyllosilicate sheets gave a constant average Ni particle size of 6.5 nm when reduced at 700 °C with TPR (5% H_2/Ar and 7.5 C°/min), using deposition precipitation as synthesis.[16] The average Ni particle size of reduced Ni phyllosilicate nanotubes synthesized by Li et al with a hydrothermal method was 11.2 nm when nanotubes had a 11.6 nm wall thickness and 37.3 nm nanotube width [28], Yang et al used $NaBH_4$ hydrothermal reduction. Since the synthesis and reductions of sheets and nanotubes are so vastly different in this case, it is difficult to compare the two particle sizes.

2.4 Applications of Ni phyllosilicate nanotubes

The applications of Ni phyllosilicate nanotubes range from catalysis to battery materials. The high porosity, straight dimensions and sorption properties make the Ni phyllosilicate nanotubes an attractive new material for hydrogen gas storage. Nanowires, drug delivery, nanoelectronics, photocatalysis and nanolithography are other likely fields of applications. [39] The non-tubular Ni phyllosilicate is already applied to study CO_2 methanation reactions.[6,51–53] A CO_2 to CH_4 catalytic test on

Ni phyllosilicate derived catalysts showed a high activity and stability for CO_2 reforming. Sivaiah et al found a constant CH_4 conversion between 20 and 35 % and a CO_2 conversion between 35 and 50 % for Ni phyllosilicate derived catalysts [25]. Core-shell particles of Ni inside a SiO_2 shell produced from Ni phyllosilicate nanotubes showed a high sintering resistance, high CO_2 and CH_4 conversion rates (70-80%) and high H_2/CO ratio (0.8) [28] The same kind of studies can be performed on Ni phyllosilicate nanotubes to study catalytic activity and stability. The 3D symmetry properties of the nanotubes make for an easily characterized catalyst model system. The partial reduction of Ni phyllosilicate nanotubes gives the nanotubes variable magnetic properties and a certain conductivity. The use of the $Ni_3Si_2O_5(OH)_4$ nanotubes as an anode in lithium ion batteries is promising, with the discharge capacity amounting to 226.7 $mA.h.h^{-1}$ after 21 cycles with a 20 $mA.g^{-1}$ rate in the study by Yang et al. [46] Hence, Ni phyllosilicate nanotubes have applications in catalysis and battery material research.

The properties of the Ni phyllosilicate nanotubes can be adapted as needed for use, also allowing for incorporation of other metals or ions into the structure, as explained in the previous section. [48] The natural occurrence of Co phyllosilicate nanotubes means it is also possible to combine Ni and Co into phyllosilicate nanotubes, potentially leading to $NiCo@SiO_2$ core-shell particles. [54] A similar synthesis could produce Co phyllosilicate nanotubes, which could have the same range of applications and more as Ni phyllosilicate nanotubes, as a stabilizing agent in Li batteries.[55]

3 Experimental methods

3.1 Chemicals & Instruments

The chemicals that were used for the Ni phyllosilicate nanotube synthesis include nickel chloride hexahydrate (Sigma-Aldrich), sodium silicate solution, sodium hydroxide pellets and Millipore water:

$NiCl_2(H_2O)_6$ – 99.9 % trace metals, 1.92 g/ cm^3 , Sigma-Aldrich
Na_2SiO_3 - reagent concentration, 1.39 g/mL , Sigma-Aldrich
NaOH pellets - 2.13 g/cm^3 , Emsure, Sigma-Aldrich
Millipore water from a Milli-Q apparatus.

For the hydrothermal synthesis a PTFE Teflon liner of 250 mL and a matching DAB-3 autoclave were used, produced by Berghof and supplied by Sysmex Europe (figure 12). For this system the maximum temperature is 250 ˚C and the maximum pressure is 300 bar. An Heraeus UT6P Oven (old autoclave 1) is used. A temperature of 195 ˚C is reached for a period of 1 hour to 6 days. The temperature ramp was 30 minutes from room temperature, which is about 5.7 ºC/min and the vent is set at 40 %. The pressure at 195 ºC was approximately 15 bar, based on steam tables for water vapour pressure.

Figure 12: Picture of the DAB-3 autoclave and teflon liner used for hydrothermal synthesis of Ni phyllosilicate nanotubes. [56] *Maximum pressure: 300 bar. Maximum temperature: 250 °C.*

3.2 Synthesis of Ni phyllosilicate nanotubes

The Ni phyllosilicate nanotubes were synthesized using a hydrothermal synthesis method, adapted from White and Yang et al [24,46]. At room temperature, 2.84 gram of nickel chloride hexahydrate and 120 mL Millipore water were added to a 250 mL Teflon liner and stirred with a stirrer bar until dissolved. Following this, 0.7 mL sodium silicate solution was added dropwise with a Finn pipet while stirring, to achieve a 1.5 Ni/Si molar ratio. After 10 minutes of stirring the required amount of NaOH pellets was added to reach a 5, 7, 10 or 13 wt% NaOH concentration; 6.5, 9.2 or 13.5 gram of NaOH pellets were added. The solution is aged for 20 minutes, by stirring with a stirrer bar. The Teflon liner with the solution was then secured into the DAB-3 autoclave reactor. The autoclave reactor was afterwards placed in the autoclave oven and heated to 195 ˚C for a certain time, varying between 1 hour and 6 days. The reaction equation if 1:1 Ni phyllosilicate forms would be the following: 3 $NiCl_2$. $6H_2O + 2Na_2SiO_3 + 2NaOH \rightarrow Ni_3Si_2O_5(OH)_4 + 6NaCl + 5H_2O$

After hydrothermal synthesis in the autoclave, the reactor was left to cool down naturally to improve crystallization. Then washing and centrifugation steps were carried out. The sediment was resuspended by stirring and shaking. Washing is performed with Millipore water until the pH is 6. Centrifugation is carried out between 1200 – 1600 rcf, 14-16 G for 3 – 15 minutes per washing step, depending on the sample. The centrifuge used was an Eppendorf Centrifuge 5804. After each centrifugation step the pH was measured with pH strips. When the desired pH was reached, pH=6, the final washing step was carried out with ethanol to improve the drying step. Drying took place in vacuum at room temperature for 24 hours.

The way centrifugation is performed is important to prevent gel formation of the sample, depending on the NaOH concentration. A high NaOH concentration formed a gel more easily, this is likely because nanotubes become longer with higher NaOH wt% used in the synthesis. Longer nanotubes have a larger aspect ratio of length/diameter and have different sedimentation properties. The reader is referred to chapter 7.2 “Gel formation” for more details.

3.3 Reduction Ni phyllosilicate nanotubes

TPR

The Ni phyllosilicate nanotubes were reduced using Temperature Programmed Reduction to gain insight in the Ni phases present and determine suitable temperatures for dedicated reductions. A Micromeritics AutoChem II Chemisorption Analyzer was used. The TPR sample is dried for 30 minutes at 120 ˚C, subsequently heated to 900 ˚C with a 10 ˚C/min temperature ramp under a 5 % H_2/Ar gas stream. The amount of sample used lay between 50 and 60 mg. The samples were crushed with a mortar and sieved to obtain a fraction of 38-425 µm to prevent clogging of the TPR machinery.

Tube oven reduction

When relevant reduction temperatures were found with TPR, the Ni phyllosilicate nanotube sample synthesized for 6 days was reduced at various temperatures using a Thermolyne tubular oven with a 5% H_2/Ar gas stream. The gas flow was set by turning the hydrogen flow at 2 and the argon flow at 40. Reduction temperatures used were 350 ˚C, 400 ˚C, 450 ˚C, 650 ˚C and 750 ˚C. The temperature ramp was set at 10 C˚/min. The temperature was maintained for 2 hours, after which the oven switched itself off. The Identical Location TEM grid sample was reduced using the same conditions in the tube oven, at 650 ˚C.

3.4 Characterization techniques

3.4.1 Transmission Electron Microscopy (TEM)

Electron Microscopy techniques were utilized in this project to study the properties and structure of Ni phyllosilicate nanotubes and resulting particle size. The nanotube dimensions in the nanoscale warranted the necessity of TEM techniques. TEM images were taken on a Technai T20 operated at 200 kV and a Talos L120C operated at 120 kV with a single tilt holder. For EDX and STEM images the Talos F200X was used, operating at 200 kV. Sample preparation was executed with 300 mesh Au grids were used with a holey carbon film, produced by Agar Scientific. A tiny pinch of the sample powder was mixed with ethanol in a 5 mL Eppendorf tube and sonicated for 2-4 hours in a sonication bath. The nanotubes were deposited on the TEM grid by dropping one drop of the mixture on top and dried in air for 1 minute. If the reader is interested, more knowledge on TEM can be found in Williams & Carter and here [57,58].

EDX/STEM

Energy Dispersive X-ray Spectroscopy was performed in Scanning Transmission Electron Microscopy (STEM) mode to determine the Ni, Si and O elemental distribution of unreduced and reduced Ni phyllosilicate nanotubes. The specific elements can be mapped with EDX because of the following principle: (1) a high energy electron generated in the STEM collides with an electron from the core shell of the atom, (2) the electron in the atom moves out of the shell by scattering and (3) an electron from a higher energy shell takes its place, resulting in the emission of an element specific X-ray. For more information on EDX helpful videos can be found here [59] and here [60].

ED

Electron diffractograms were taken on the Technai T20, Talos F120C and Talos F200X. The Selected Area aperture was used to focus on an area of interest that only contained nanotubes. The Selected Area aperture blocks a part of the beam to reduce the area under the beam. In this way diffraction patterns come only from the objects in the Selected area. This technique is useful to determine the Ni phases present in the nanotube. Peaks from XRD and ED can be matched with one another. The two types of phyllosilicate can be distinguished with this.

Electron diffraction can give information about the composition in a similar way as XRD, as it also gives a diffraction pattern, a Selected Area Electron Diffraction (SAED) pattern. The electrons from the transmission electron microscope beam diffract on the crystal lattice of the material inserted in the electron microscope. The interaction of the electrons with the positively charged core of the atom makes the electrons scatter. The bending of the beam of electrons (particle-wave duality) creates a scattered pattern on the back focal plane of the camera. The diffraction pattern appears in the shape of rings or of dots. A dot pattern indicates high crystallinity when looking at a single crystal under the microscope. A circle pattern forms when looking at a group of crystals, so an average diffraction pattern will form in this case. The information from electron diffraction is different to X ray diffraction as it is performed on a specific location of a sample on a TEM grid. This is accomplished by using a selected area on the fluorescent screen in the microscope, which is why this technique is called Selected Area electron Diffraction (SAED). The object of interest for diffraction can be measured, like a nanotube or a cluster of nanotubes on its own, without side-products from the reaction in the field of view, that would be present in a powder XRD pattern. The combination of XRD and ED is useful to get a clearer picture of the sample composition.

ILTEM

Identical Location TEM was applied to study the relation between nanotube wall diameter and particle size. The grids used are composed of silicon nitride (SiN) windows (SiMPore TEM grids SN100-A50Q33). Each grid has 9 square windows and 1 rectangular window. It is much easier to find the same location

again on these grids (see figure 13). A nanotube sample synthesized with 7 wt% NaOH for 6 days, suspended in ethanol was deposited on the SiN grid. TEM images were taken with the Talos F200X before and after the reduction of the same grid areas. The SiN grid with sample was heated in the tube oven under a 5 wt% H_2/Ar stream, resulting in Ni particles in a nanotube pattern. Plenty of nanotubes could be matched with before and after images. Analysis was performed on 24 nanotubes with image J, Excel, and Origin.

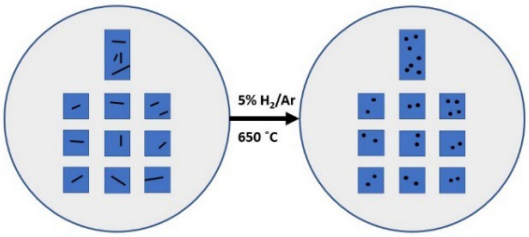

Figure 13: Representation of a SiN ILTEM grid. Nanotube sample was deposited on the grid suspended in ethanol, sonicated for 2-3 hours. The grid with sample was then heated in the tube oven at 650 ˚C with 5%H_2/Ar gas flow for 2 hours, with a heating rate of 10 ˚C/min.

3.4.2 Powder X-ray diffraction

X-ray diffractograms were taken on a 2nd G_{en} Bruker D2 Phaser XRD with a cobalt filament (Co-Kα = 1.7891 Å). Measurements were performed between 5˚ and 90˚ 2θ with increments of 0.02-0.03˚ 2θ and 1.000 – 1.500 s/step. The sample was prepared by grinding the dried sample in a mortar and distributing the powder on a flat specimen holder. XRD is used in order to determine the composition of the sample, i.e. to determine purity, crystallization and presence of Ni phyllosilicate and to distinguish 1:1 and 2:1 Ni phyllosilicate. For more information on crystallography and diffraction the reader is referred to Hammond [61].

3.4.3 N_2-Physisorption

The N_2 physisorption measurements were carried out at -196 °C on a Micromeritics TriStar II Plus Surface Area and Porosity Analyzer. The sample was prepared in an airtight physisorption tube. The pore volume was evaluated with a single point adsorption at p/p^o = 0.995. The desorption volume is used to determine the Barret, Joyner and Halenda (BJH) pore size distribution of the nanotube sample. The t-plot method is used to determine the micropore volume. The Brunauer-Emmet-Teller (BET) method is applied to calculate the total surface area. The drying before physisorption is performed at 120 ^oC in vacuum. Nitrogen physisorption is performed on several samples. A surface area of ± 114 m_2/g was expected from literature [24]. More information on physisorption can be found in Thommes et al. [62]

4 Results and discussion

First, the Ni phyllosilicate nanotube system is fully characterized with TEM, XRD, EDX, ED, TPR and N_2 physisorption. Second, the effect of synthesis variations of sodium hydroxide and synthesis time are shown using the same techniques. Third, the reduction of Ni phyllosilicate nanotubes is studied by looking at the effect of temperature on particle size and the relation of wall thickness with particle size, using TEM.

4.1 Ni phyllosilicate nanotubes

The properties, composition and morphology of the Ni phyllosilicate nanotubes will be described in detail in this section. The nanotubes were synthesized with 7 wt% NaOH for 6 days at 195 °C. The composition of the nanotube samples was studied with XRD, Electron Diffraction, TPR, EDX and lattice space determination using HRTEM images. The synthesis is expected to create mostly 1:1 Ni phyllosilicate nanotubes. It is necessary to distinguish between 1:1 (≈46 % Ni) and 2:1 (≈36% Ni) [50] Ni phyllosilicate because it determines the amount of Ni/Si in the nanotubes, which is constant over the whole sheet of the nanotube. It is also useful to know what other by-products might have been formed during nanotube synthesis, in order to find ways to make the sample purer.

The XRD measurement of the Ni phyllosilicate nanotube sample is shown in figure 14. The phase of Ni phyllosilicate corresponds to is 1:1 ($Ni_3Si_2O_5(OH)_4$), since peaks are present at 13 (001), 28 (002), 39.5 (200), 42(202) and 72 (030) degrees 2Θ. It is impossible to determine whether the Ni phyllosilicate peak at 23 degrees 2Θ is present, as this position overlaps with a sharp peak that corresponds with $Ni(OH)_2$. The crystalline peaks in the XRD spectrum at 22.4, 40.6, 55.0, 61.3, 69.7, 74.3, 82.6, 84.0 and 87.0 correspond to $Ni(OH)_2$. Minute peaks at 34.8 and 45.0 also correspond to $Ni(OH)_2$. Small peaks at 45.7 and 47.9 correspond to $NiCl_2.6H_2O$, the starting material. The peak at 50.9 corresponds to NiO. The $Ni(OH)_2$ peaks are higher and smaller than the 1:1 Ni phyllosilicate peaks, this means that $Ni(OH)_2$ appears more crystalline than Ni phyllosilicate. The XRD result shows that the sample mainly consists of 1:1 Ni phyllosilicate, in addition to crystalline $Ni(OH)_2$.

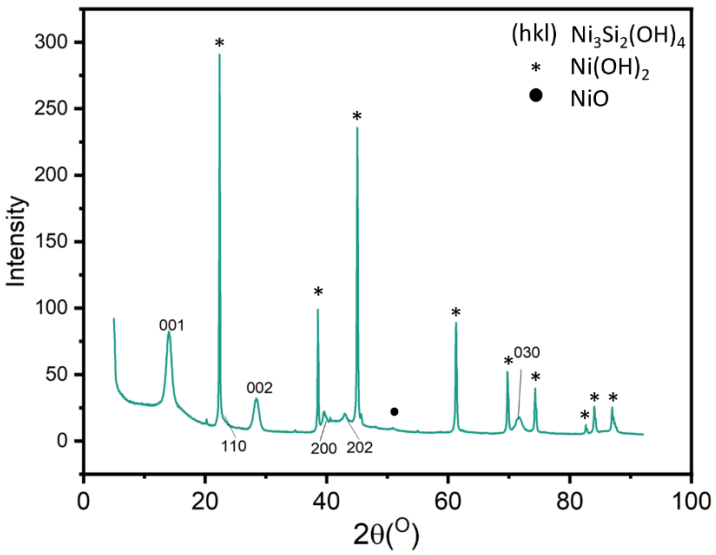

Figure 14: Powder-XRD pattern of Ni phyllosilicate nanotubes.

Electron diffraction of Ni phyllosilicate was carried out on a cluster of nanotubes. The SAED pattern, nanotube cluster and diffractogram are shown in figure 15. The peaks of ED have been matched by using the relation principles to the last XRD Ni phyllosilicate peak at 72 degrees 2Θ, assuming the outer ring of the SAED pattern corresponds with it. The presence of Ni phyllosilicate can be confirmed with

ED, by the 001, 202 (1:1), 110 and 030 (general Ni phyllosilicate) peaks. The blue dots in figure 15A indicate a match with 2:1 Ni phyllosilicate. The presence of 2:1 Ni phyllosilicate can be explained by one of the following: 1) it is possible that part of the Ni^{2+} in the 1:1 structure is converted to 2:1 Ni phyllosilicate under the electron beam, depleting Ni from the lattice and forming a 2:1 transition state 2) In the cluster of nanotubes normal phyllosilicate sheets are present too, containing also differently ordered Ni/Si sheets, thus possibly 2:1 Ni phyllosilicate. Two peaks in figure 15A correspond to Ni hydroxide. It indicates that $Ni(OH)_2$ might be present in the cluster of nanotubes. The small unlabelled peak next to the 030 peak has not been matched to any compound (both NiO, Cu, Au, and Ni have been checked) and is likely a forbidden reflection within the lattice. Electron diffraction on Ni phyllosilicate nanotubes can thus conclude that mainly 1:1 Ni phyllosilicate, an amount of $Ni(OH)_2$ and some 2:1 Ni phyllosilicate are present in the cluster displayed in figure 15.

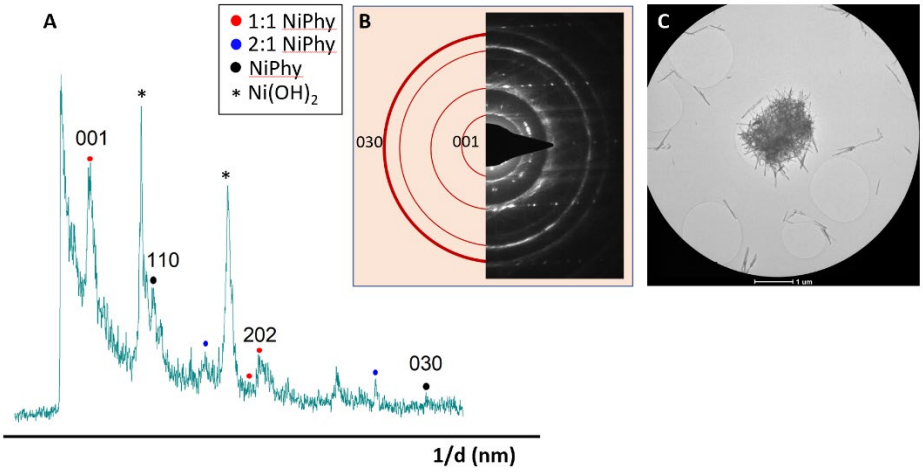

Figure 15: Electron diffraction of a Ni phyllosilicate nanotube cluster. (A) Plot profile drawn from the SAED ring pattern. (B) SAED pattern of a nanotube cluster. (C) Nanotube cluster TEM image using a Selected Area aperture.

The Ni phyllosilicate nanotubes highly regular pore structure is visible in the high-resolution TEM image in figure 16. The wall of the nanotube shows the homogeneous structure of the material in its regular straight lattice. The lattice spacing is visible, showing the nickel octahedral sheet in the darker line and the silica tetrahedral sheet in the lighter lines. The hollow core is apparent from the TEM image, as well as in a SEM image in figure 43 in the supplementary information. The lattice spacing of the nanotube walls of several high-resolution images were measured, using the FFT/Inverse FFT/Plot Profile method in ImageJ. The average lattice spacing of the Ni phyllosilicate nanotubes is 0.754 nm, which matches the lattice of a 1:1 type Ni phyllosilicate. (Lattice 1:1 Ni PS: 0.8-1.1 nm) [14] When the average lattice spacing is known it is possible to calculate the average number of sheets in the wall, using the average wall thickness. The average wall size is 9.1 nm and contains on average 12 sheets of Ni phyllosilicate (see figure 16d), which is useful information when one wants to match the number of layers with the particle size after reduction. The information from XRD, ED and HRTEM lattice spacing all point to a 1:1 type Ni phyllosilicate nanotube.

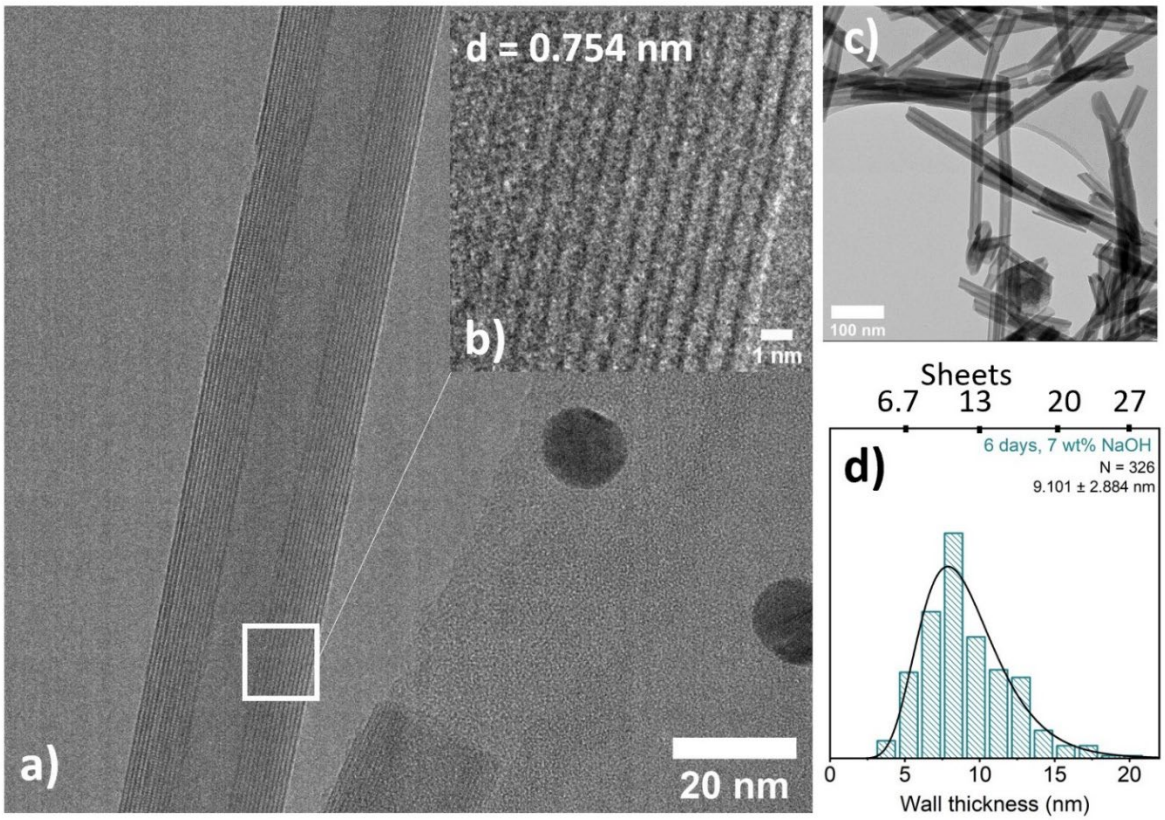

Figure 16: (a) High resolution TEM image of Ni phyllosilicate nanotubes synthesized for 6 days at 195 ˚C with 7wt% NaOH. (b) Close up image shows the lattice. A lattice spacing of 0.754 nm has been found. (c) Low magnification image of Ni phyllosilicate nanotubes. (d) Wall thickness PSD of Ni phyllosilicate nanotubes, with corresponding number of sheets indicated.

Temperature programmed reduction is used to determine the nickel phases in the sample, to determine purity, contaminants and type of Ni phyllosilicate. In figure 17 the TPR profile of the Ni phyllosilicate nanotube sample is shown, identifying nickel hydroxide, nickel oxide, 1:1 Ni phyllosilicate and 2:1 Ni phyllosilicate. Nickel hydroxide decomposes to NiO between 200 °C and 320 °C, showing peaks at 230 °C and 317 °C, releasing H_2O. NiO reduces to Ni metal around 350 °C, shown in the asymmetric peak. The 1:1 Ni phyllosilicate reduces between 450 °C and 620 °C. The peak between 620 °C and 710 °C seems to be an indication of a 2:1 Ni phyllosilicate phase. The two peaks at 544 and 710 °C indicate a 1:1 Ni phyllosilicate. The intermediate 2:1 Ni phyllosilicate phase can form when 1:1 Ni phyllosilicate reduces (see chapter 2, figure 11). The 1:1 Ni phyllosilicate lattice loses Ni^{2+} during the reduction, draining the lattice of nickel and forming a 2:1 type structure with more silica layers and less nickel layers. This leads to the conclusion that the intermediate 2:1 Ni phyllosilicate phase only forms during the TPR process and was not formed during the synthesis. The formation of an intermediate 2:1 Ni phyllosilicate phase can be proven by performing in-situ XRD from room temperature to 800 °C, as carried out by Sivaiah et al on non-tubular Ni phyllosilicate [25,50]. An alternative possibility is a 500 ^{o}C tube oven reduction and doing HRTEM on the sample to determine whether the lattice spacing has changed. The information of relevance from TPR is that the Ni phases include $Ni(OH)_2$ and 1:1 Ni phyllosilicate.

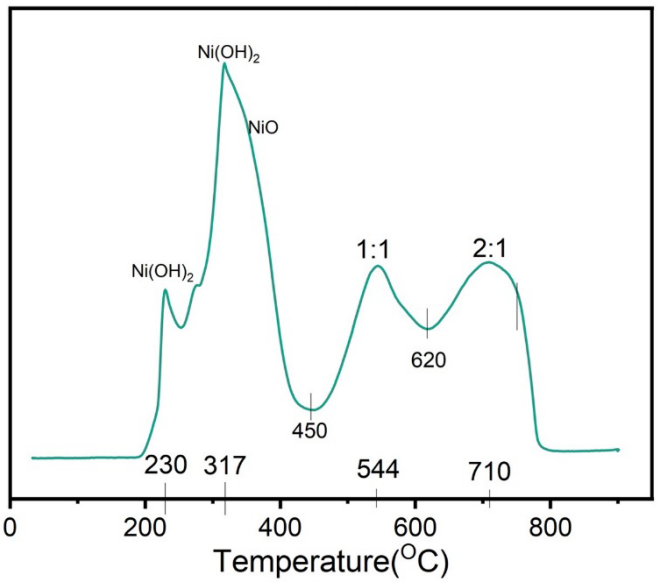

Figure 17: Temperature Programmed Reduction graph of the Ni phyllosilicate nanotube sample. Heating rate is 10 C˚/min to 900 ˚C with 5% H_2/Ar with a drying temperature of 120 ˚C for 30 minutes.

Combining XRD, ED, lattice spacing and TPR results lead to the conclusion that a 1:1 Ni phyllosilicate and crystalline $Ni(OH)_2$ are present. The amount or type of $Ni(OH)_2$ cannot be determined without doing TGA measurements (Thermogravimetric Analysis). The formation of $Ni(OH)_2$ during synthesis is problematic for applications in catalysis and battery research, because $Ni(OH)_2$ has electrochemical activity and is used on positive electrodes.[63–65] If these nanotubes would be tested with electrochemical techniques, the presence of $Ni(OH)_2$ makes it impossible to separate Ni phyllosilicate nanotube influence from $Ni(OH)_2$ effects. In the synthesis used in this study it seems impossible to stop the $Ni(OH)_2$ formation, but perhaps the $Ni(OH)_2$ can be removed post-synthesis by the dissolution of $Ni(OH)_2$ using HNO_3 titration, as lower pH will change the Ni phase, as can be seen on a EpH diagram (See chapter 7.5: figure 78). White et al determined the solubility of β-$Ni(OH)_2$ steeply increases below pH 7.[24,66] A calcination step in air around 400 °C before reduction with hydrogen gas can also remove the $Ni(OH)_2$ but will create Ni outside the lattice from $Ni(OH)_2$ reduction.[50] A change in the drying step is also worth exploring, concerning the differences $Ni(OH)_2$ content of Yang et al[6] and White et al[24], as discussed in chapter 2. A glovebox hydrothermal synthesis is also a solution, seeing as the study by McDonald et al produced Ni phyllosilicate nanotubes without $Ni(OH)_2$ present. This would indicate that the presence of oxygen increases $Ni(OH)_2$ formation. Thus there are options to prevent or remove $Ni(OH)_2$ in the Ni phyllosilicate nanotubes.

This synthesis was successful in the formation of nanotubes, as can be seen in figure 18. The nanotubes synthesized are straight with a regular pore distribution (figure 18B). The nanotubes appear pure, with no platelets or other objects directly around them. At a larger scale the appearance of large black objects becomes visible (figure 18A). Particles of $Ni(OH)_2$ reduce under the electron beam to Ni. The black objects would have been crystalline Ni hydroxide particles. The nanotubes are hollow inside, providing a tubular structure (figure 18 DEF). The end of a nanotube is visible in figure 18F, showing a hollow core and resembling the result of the scrolling mechanism described in literature. The length, wall thickness, pore size and width were measured in at least 10 images with ImageJ to get a representative distribution. The nanotubes have on average a 263 nm length, 28.9 nm width, 9.1 nm walls and 10.3 nm pores (see figure 19). The pore size of 10.3 nm is confirmed with a desorption N_2 physisorption measurement (figure 19). The physisorption measurement shows a peak around 10 nm, which falls within the pore size range measured with TEM images. The broad peak in the desorption graph around 50 nm (from 25 to 100 nm) signifies the intratubular space between the nanotubes. The small peak at 2 nm is a physisorption artifact where the pore gets blocked, so the opening becomes

very small. The surface area of the nanotubes according to N_2 physisorption BET analysis is 48.23 m^2/g (see figure 44b in SI), quite a lot lower than the expected 114 m^2/g from White et al.[24] A reason for this could be that the presence of bulky by-products can increase the BET surface area during physisorption. The analysis of TEM images can thus conclude that straight nanotubes with regular pore structure were formed successfully, but the formation of by-products also took place.

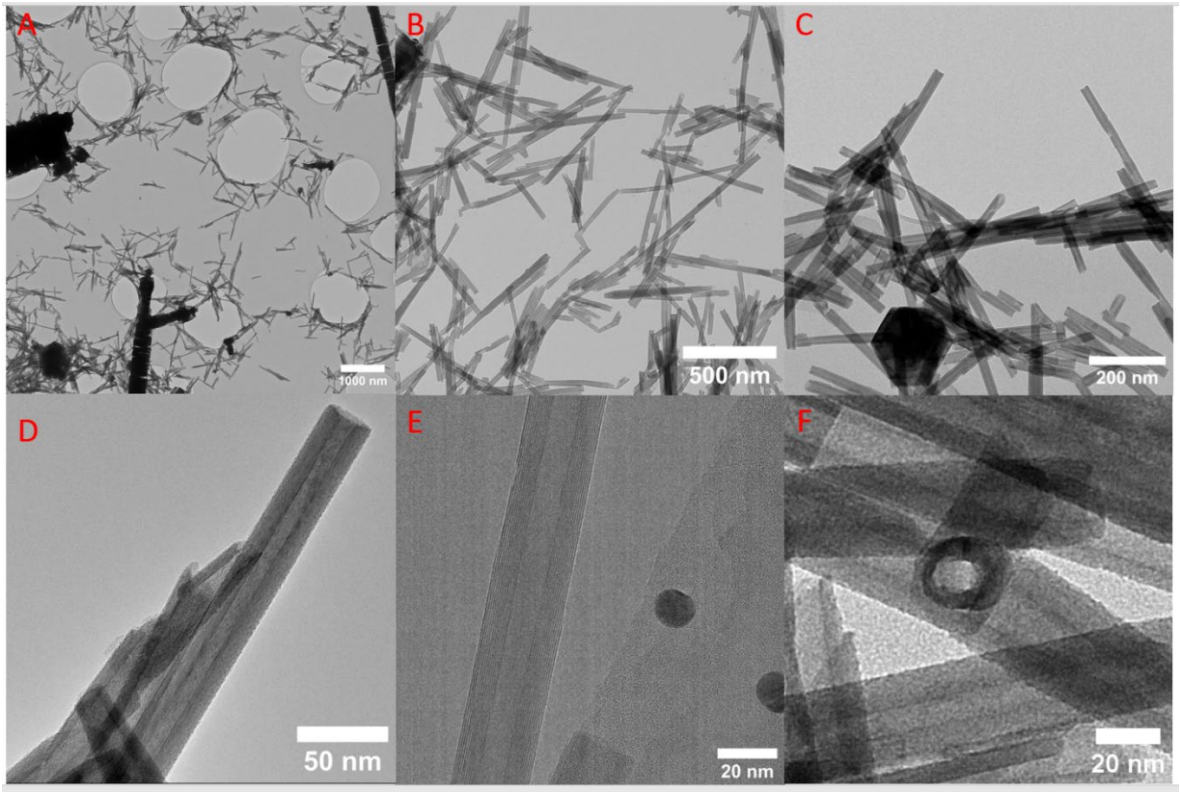

Figure 18: TEM images of Ni phyllosilicate nanotubes. Synthesis: 6 days and 7 wt% NaOH. (A) General overview (B) Big scale nanotubes. (C) Middle scale (D) Side view nanotube (E) HRTEM image showing lattice spacing. (F) Nanotube end on view.

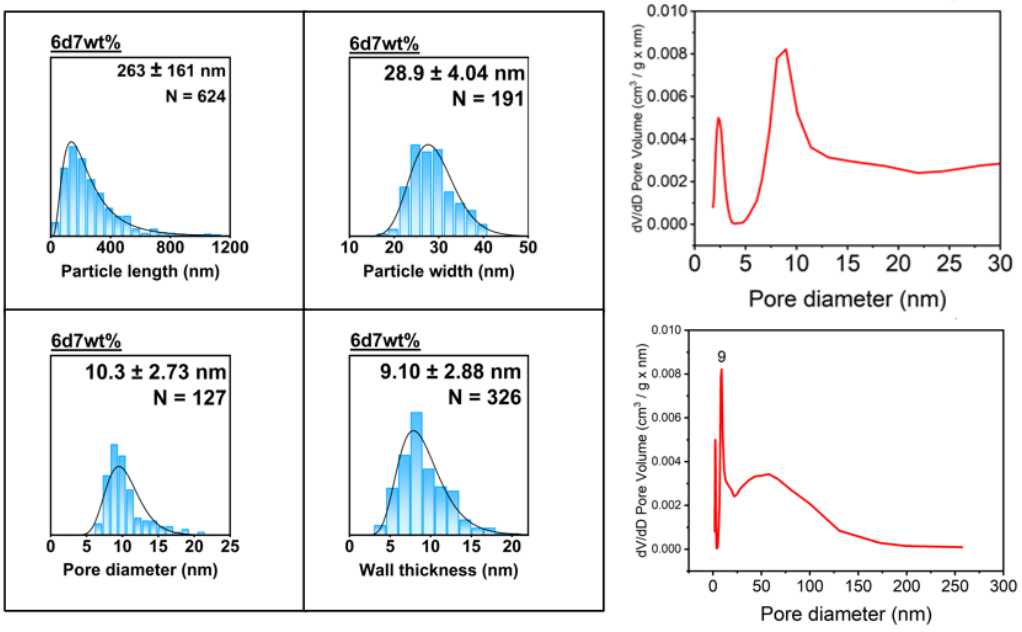

Figure 19: (Left) Ni phyllosilicate nanotube dimensional size distributions of length, width, wall thickness and pore diameter. (Right) BJH pore size distribution of Ni phyllosilicate nanotubes from N_2 desorption.

4.2 Synthesis variation: NaOH effect

The variation of NaOH concentration creates a different composition and morphology of a Ni phyllosilicate nanotube sample. Characterizations of nanotube samples synthesized with 10, 7 and 5 wt% NaOH for 6 days at 195 °C are described in this section. The pH is initially 14.45, 14.28 or 14.13 for 10, 7 or 5 wt% NaOH , based on calculations. First, the composition of the samples is compared with XRD and TPR. Second, the change in nanotube morphology is discussed using TEM images and nanotube dimension analysis (PSD's).

The number of compounds observed in XRD is the same in all samples synthesized, both 5, 7 and 10 wt% NaOH. All samples contain the 1:1 Ni phyllosilicate peaks at 13, 28, 39, 42 and 72 2Θ. The presence of $Ni(OH)_2$ is apparent in all NaOH wt% variations as well. Nickel oxide has a small peak in all samples, indicated at 50 2theta. The expectation is for the $Ni(OH)_2$ quantity to increase with increasing NaOH wt%. The ratio of 1:1 Ni phyllosilicate peaks to Ni hydroxide peaks changes with NaOH wt% when observing XRD patterns of samples from 10, 7 and 5 wt% NaOH (figure 20abc). The 1:1 Ni phyllosilicate peaks retain almost the same intensity while changing NaOH concentration. The $Ni(OH)_2$ peaks in the XRD pattern become sharper and more intense with decreasing NaOH wt%, this signifies an increase in crystallinity of $Ni(OH)_2$ with decreasing NaOH wt%. The XRD of the 10 wt% NaOH sample is significantly different from 7 and 5 wt% NaOH, as the 10 wt% NaOH (figure 20a) shows more amorphous peaks than 5 and 7 wt% NaOH (figure 20bc). The base of the $Ni(OH)_2$ XRD peaks indicate crystal size. A broadening is observed for the $Ni(OH)_2$ peaks in the 10 wt% sample, indicating larger $Ni(OH)_2$ nanocrystals. The NiO peak is slightly broader relative to the other peaks in the 10 wt% NaOH sample, indicating relatively more NiO present compared to NiO in the 5 and 7 wt% samples. Essentially, we can conclude from XRD patterns that the 10 wt% sample contains a different form of Ni(OH)2 than the 7 and 5 wt% NaOH samples, one that is more amorphous. The amount and phase of $Ni(OH)_2$ present can be determined with TGA, but that is outside the scope of this project. The structure of $Ni(OH)_2$ becomes less crystalline with increasing NaOH, relative to the 1:1 Ni phyllosilicate.

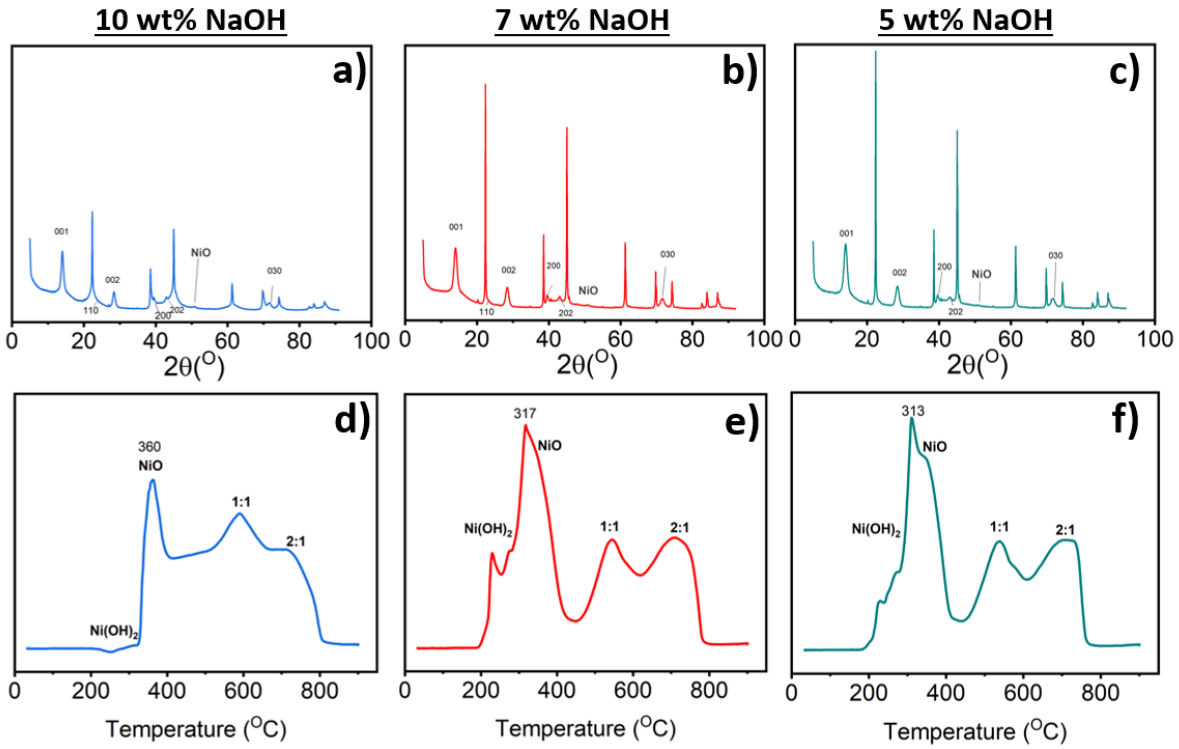

Figure 20: XRD and TPR of 5, 7 and 10 wt% NaOH nanotube samples. (a-c) XRD of 10, 7, 5 wt% NaOH. (d-f) TPR of 10, 7, 5 wt% NaOH.

The Ni phases have been investigated with TPR under 5 %H_2/Ar to 900 °C. The phases present are $Ni(OH)_2$, NiO and Ni phyllosilicate. Like the XRD result, the composition of the samples changes with changing NaOH wt%. The Ni phyllosilicate present shows two peaks in 5 and 7 wt% NaOH (figure 20ef) and a broader combined peak in the 10wt% NaOH peak (figure 20d). The presence of less of the 2:1 transition state for the 10 wt% NaOH sample could be the explanation for this. The difference in the NiO and $Ni(OH)_2$ composition in the high NaOH wt% (figure 20d) and the low NaOH wt% (figure 20ef) is evident in TPR. The $Ni(OH)_2$ appearance in TPR is similar in the 5 and 7 wt% NaOH samples, but vastly different in the 10 wt% NaOH sample. While the 5 and 7 wt% NaOH samples show positive $Ni(OH)_2$ peaks at 250 °C and 300 °C, the 10 wt% NaOH sample shows only a negative peak at 250 °C. The dehydration mechanism for $Ni(OH)_2$ during heat treatment is **$Ni(OH)_2 \rightarrow NiO + H_2O$**. The $Ni(OH)_2$ could be in a different phase or shape in the 10 wt% NaOH sample, or a larger quantity of $Ni(OH)_2$ could be present in the 10 wt% NaOH sample. The dehydration of $Ni(OH)_2$ releases water, and the water can increase the conductivity of the gas stream. (water: 0.606 $W.m^{-1}.K^{-1}$, water vapour, 125 °C: 0.0267 $W.m^{-1}.K^{-1}$, water vapour, 225 °C: 0.0359 $W.m^{-1}.K^{-1}$, Ar: 0.016 $W.m^{-1}.K^{-1}$, H_2: 0.168 $W.m^{-1}.K^{-1}$). The higher quantity of $Ni(OH)_2$ could release more water. If the water released from $Ni(OH)_2$ at 250 °C increases the gas thermal conductivity, a negative peak can be formed. The result from XRD and TPR need to be supplemented with other techniques to determine the $Ni(OH)_2$ type and quantity. Thermogravimetric Analysis (TGA) can help determine the wt% of $Ni(OH)_2$.

The reason for the different XRD and TPR result for the 10 wt% NaOH sample might be due to the different morphology that is visible in the nanotubes themselves. Figure 21c shows the HRTEM image for 10 wt% nanotubes. The nanotube structure is covered in small crystal particles, possibly $Ni(OH)_2$ or a mix of $Ni(OH)_2$ and NiO. The fact that the Ni phyllosilicate and $Ni(OH)_2$ particles are attached to each other might change the reduction mechanism. A more thorough investigation with HRTEM on the $Ni(OH)_2$ crystal morphology is needed to understand these developments. The usage of TEM to study the $Ni(OH)_2$ crystal structure and morphology changes with changing NaOH wt% while using TGA to determine the quantity can help solve this mystery further.

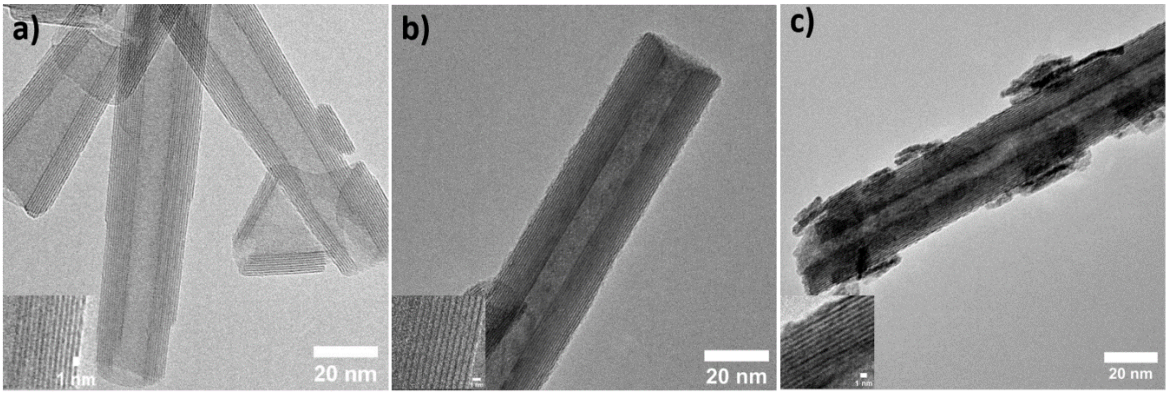

Figure 21: High resolution TEM images of 5, 7 and 10 wt% NaOH samples. a) 5 wt% NaOH (lattice spacing: …) (b) 7 wt% NaOH, lattice spacing: 0.754 nm (average over multiple images) (c) 10 wt% NaOH, lattice spacing: 0.6719 nm (one image)

The morphological changes that have been studied include pore size, wall thickness and length. An increase in length, a decrease in pore size and an increase in wall thickness is expected with increasing NaOH wt% from literature. [24] The changes in pore size are visible in figure 21, the pore size visibly becomes smaller from 5 wt% (figure 21a) to 7 wt% (figure 21b) to 10 wt% (figure 21c), while not much change is seen in the wall thickness. The distribution of the pore sizes of Ni phyllosilicate nanotubes is shown in figure 22abc for the 5, 7 and 10 wt% NaOH synthesis. The average pore size remains stable from 5 to 7 wt% NaOH and decreases at 10 wt% NaOH (figure 22A). The pore sizes show a slight binomial distribution in figure 22abc, becoming stronger as the NaOH wt% increases, while the distribution broadens to smaller and bigger pore sizes. The distribution of wall thicknesses is shown in figure 22def for 5, 7 and 10 wt% NaOH synthesis. The wall thickness is stable with 5 and 7 wt% NaOH

and increases with 10 wt% NaOH (figure 22B). The distribution of wall thickness is broadening with an increase in NaOH wt%, as seen in figure 22f. The particle size analysis of wall thickness and pore size indicates that the growth of the wall is dependent on NaOH concentration. It is thus likely that the walls grow from the outside inwards as the NaOH concentrations increases, because the pore size decreases, and the wall size increases.

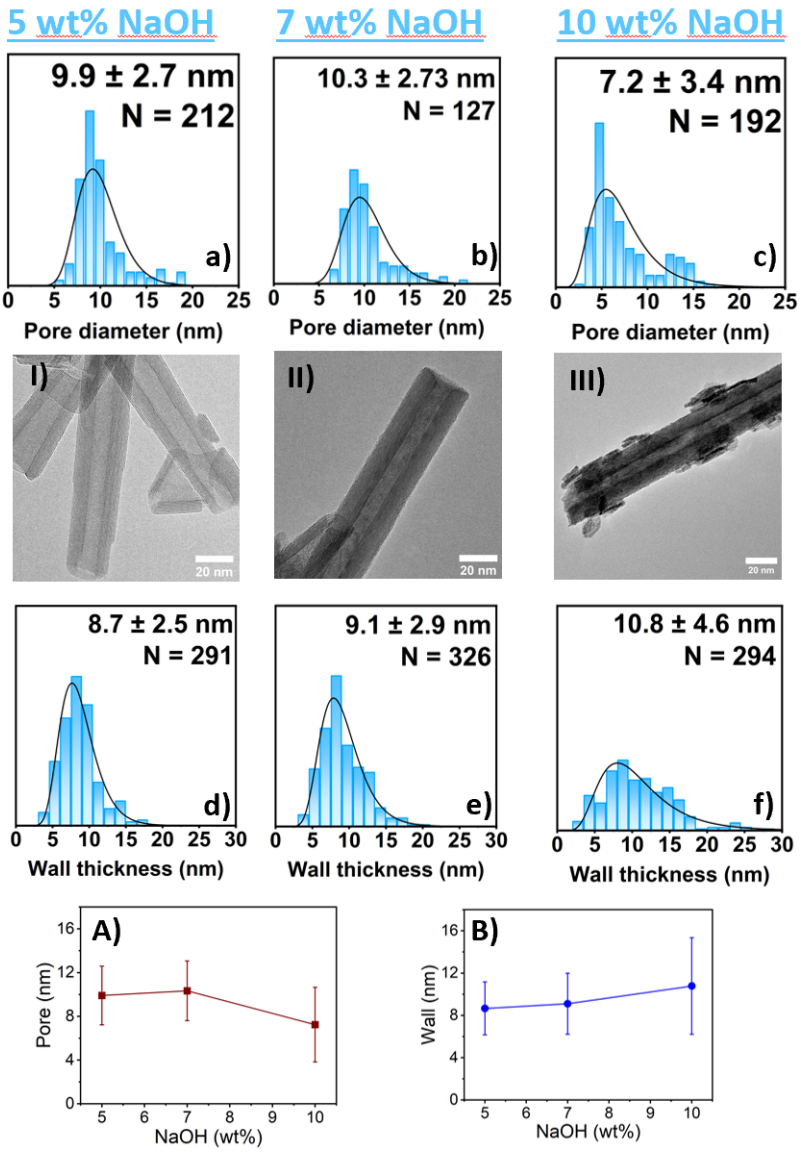

Figure 22: Comparing wall and pore diameter of 5, 7 and 10 wt% NaOH. (a-b) Pore PSD 5-10 wt% NaOH (I-III) TEM images 5-10 wt% NaOH. (d-f) Wall PSD 5-10 wt% NaOH. (A) Pore vs NaOH wt% (B) Length vs NaOH wt% (C) Wall size vs NaOH wt%

The length distribution becomes broader as the NaOH concentration increases. The Ni phyllosilicate nanotubes increase in length with increasing NaOH concentration, as can be seen in figure 23abc. The distribution of the length becomes broader as the NaOH concentration increases, see figure 23def. The average length increases from 149.5 nm to 263.3 nm to 554.4 nm, for 5, 7 and 10 wt% respectively. The trend for the length increase is shown in figure 24, with differences in standard deviations being large enough to conclude that the length increases with increasing NaOH wt%. For application in a model system this means that the nanotubes can be adjusted in length.

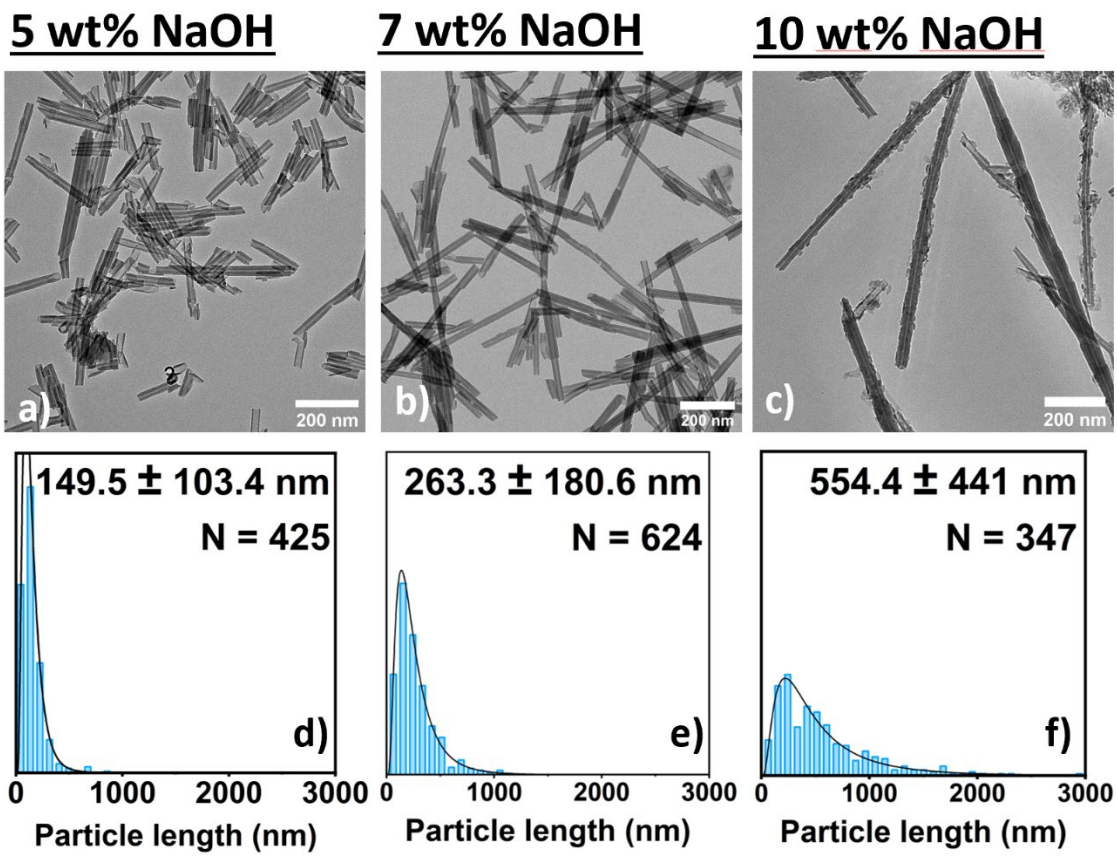

Figure 23: Comparing lengths of 5, 7 and 10 wt% NaOH (a) TEM 5 wt% NaOH (b) TEM 7 wt% NaOH (c) TEM 10 wt% NaOH (d) Length PSD 5 wt% NaOH (e) Length PSD 7 wt% NaOH (f) Length PSD 10 wt% NaOH.

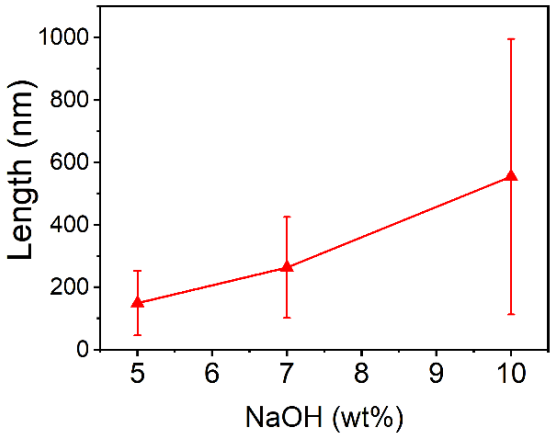

Figure 24: Nanotube length vs NaOH wt%.

The conclusion to be drawn from this section is that the morphology and composition changes when the NaOH concentration increases. The dimensions of length and wall thickness increase while the pore size decreases with increasing NaOH. The composition is different at a high NaOH concentration, especially the $Ni(OH)_2$ component, which can be studied further with TEM and TGA. The dissolution of SiO_2 increases as the pH increases from pH 9, as determined by White et al.[24] The presence of Si(IV) species in solution is essential for the nanotube formation during synthesis (reaction 3 on page 17).[24] If there is not enough silica dissolved, the reaction that forms Ni phyllosilicate nanotubes (reaction 1 on page 17) will not proceed, instead the excess nickel ions will react with hydroxide ions to form nickel hydroxide (reaction 2 on page 17). At the same time, a higher NaOH concentration would also increase the Ni(OH)2 formation (reaction 2 on page 17). The different morphologies of a high and low NaOH

wt% produced nanotubes might thus be due to the fact that a higher NaOH concentration causes the silica species to dissolve better, which increases the crystallization of nanotubes that contributes to a length increase but also produce by-products because of an excess of OH^- ions.

4.3 Synthesis variation: Reaction time effect

The amount of time the sample is treated at 195 ^oC during hydrothermal synthesis influences the nanotube properties and formation. The synthesis was performed at 1 day, 2 days, 4 days and 6 days initially. To further study the inception of the Ni phyllosilicate nanotubes, shorter reaction times were completed of 1, 2, 3 and 4 hours. The Ni phyllosilicate nanotubes start forming after two hours and develop further with increasing synthesis time. The evidence for this can be found in XRD spectra and TEM images. In figure 25 the XRD spectra of 1 to 4 hours synthesis are displayed. The peaks of Ni phyllosilicate are indicated with lines, at 13, 28, 39.5, 44 and 72 2Θ. The peaks with asterixis at 13 and 28 2Θ show the most prominent change over time, which start to appear at a reaction time of 2 hours. Ni hydroxide is already present at 1 hour synthesis and increases in crystallinity according to XRD. The development of the Ni phyllosilicate peaks in the XRD stays almost constant after 1 day of synthesis, as can be seen in figure 26.

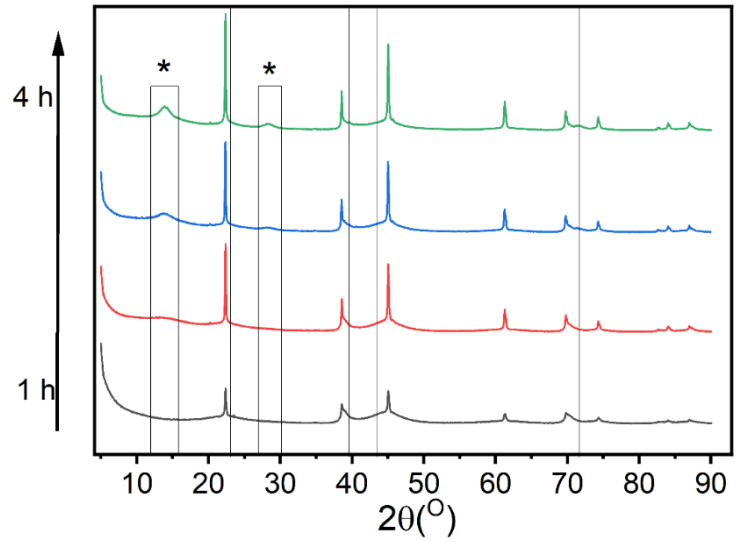

Figure 25: XRD spectrum of samples synthesized for 1, 2, 3 and 4 hours. Samples used 7 wt% NaOH. Ni phyllosilicate peaks are indicated with a line.

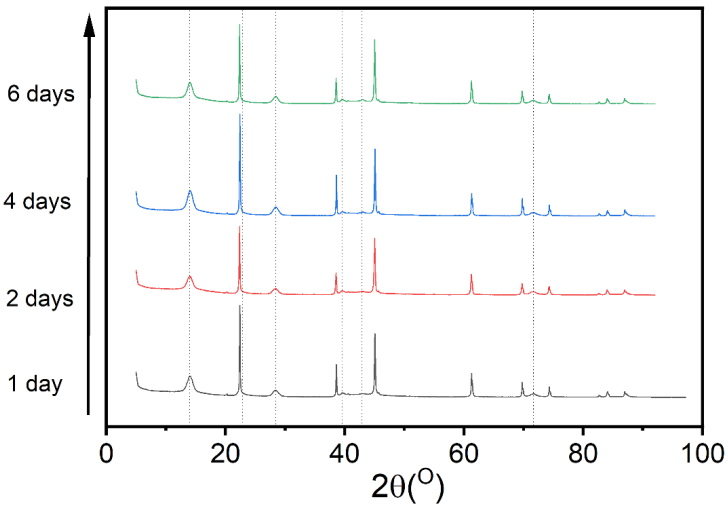

Figure 26: XRD spectrum of Ni nanotube samples synthesized for 1 day, 2 days, 4 days and 6 days. Samples used 7 wt% NaOH.

The constant trend observed in XRD in figure 26 is also visible in TPR of samples of 1 to 6 days, see figure 44a in the supplementary information. The composition of Ni phases in TPR remain constant, except for an increase in the 250 ^{o}C $Ni(OH)_2$ peak. The conclusion to draw from XRD is that 1:1 Ni phyllosilicate peaks form at 2 hour synthesis and remain stable from 1 day of synthesis.

The development over time of nanotubes is shown with TEM images in figure 27. The nanotubes are visible after 2 hours of synthesis (figure 27b) and start growing when the synthesis time increases. The nanotubes are fully formed at 1 day of synthesis (figure 27e). Before nanotube formation only other objects can be seen in TEM images (1 hour synthesis, figure 27a). The objects visible look like platelets or grey circles (figure 28). They could be the same object (=a disc), appearing as a grey circle when perpendicular to the electron beam and as a platelet when parallel to the electron beam. The grey circles and dark platelets that are visible in the beginning and start decreasing in number as the nanotubes form (see figure 27abcd). The time when nanotubes are fully formed at 1 day (figure 27d), only a few objects are left surrounding the nanotubes. This phenomenon indicates that discs are involved in the nanotube formation.

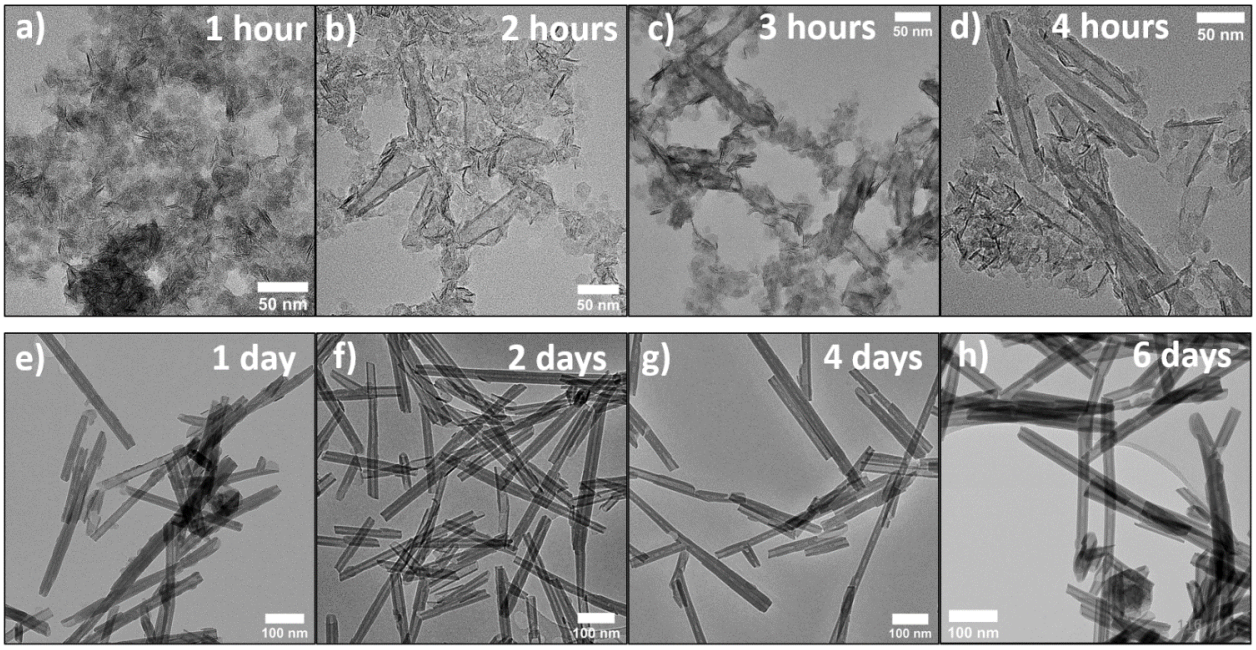

Figure 27: TEM images of samples synthesized for 1, 2, 3 and 4 hours (a-d); 1, 2, 4 and 6 days at 195 °C. (e-h). All samples used 7 wt% NaOH.

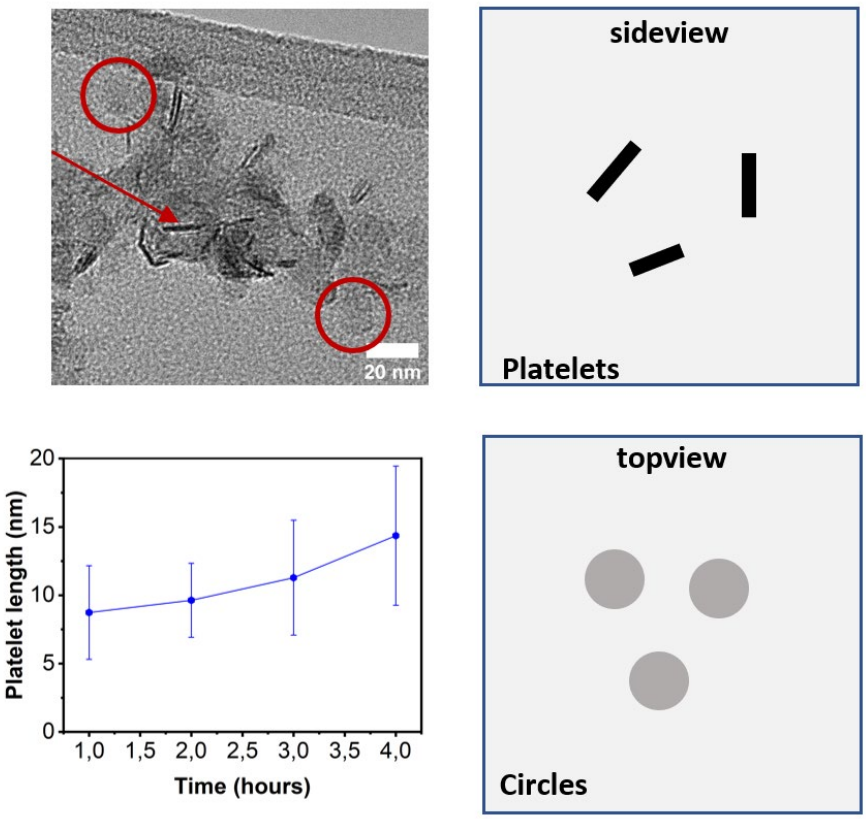

Figure 28: Building blocks of nanotubes are discs, displayed as platelets or circles in TEM images (Top, left). Diameter of platelets were measured and plotted versus time, for 1, 2, 3 and 4 hour syntheses (bottom, left). sideview and topview of platelets (right)

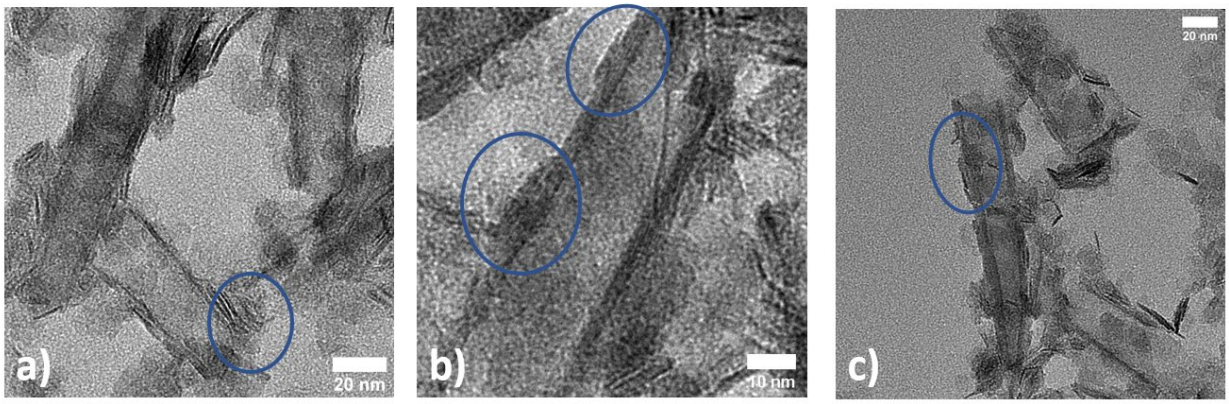

Figure 29: TEM images illuminating direction of platelet attachment. (a,b) Growing from inside to outside (c) Growing from outside to inside

Analysing the disc objects parallel to the beam in TEM images from 1 to 4 hours showed growth in diameter from 1 to 4 hours synthesis, potentially contributing to longer nanotubes with increasing synthesis time. The discs seem to attach to the nanotube and contribute to the growth of the sheets (figure 29). The TEM images show a growing trend from inside to outside (figure 29ab), while others show a growth from outside inwards (figure 29c).

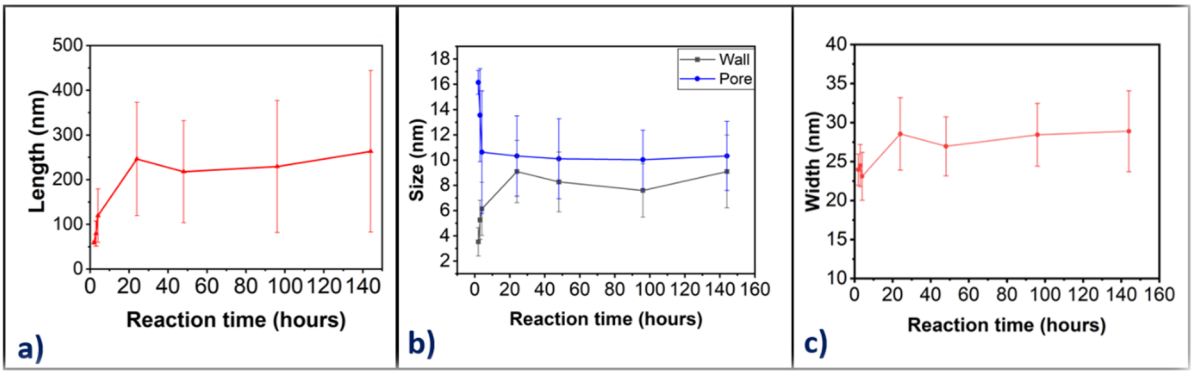

Figure 30: Average length, wall diameter, pore size and width of nanotubes plotted against reaction time, 1, 2, 3, 4, 24, 48, 96 and 144 hours. Averages were obtained by measuring TEM images with ImageJ. (a) Average nanotube length plotted. (b) Wall and pore size of nanotubes plotted. (c) Nanotube width plotted.

The growth of the nanotubes themselves is shown in figure 30, where length, wall thickness, pore size and width have been shown as a function of time. The nanotube length increases fast with increasing reaction time initially, until 1 day, after which the length keeps increasing a little bit, as seen in figure 30a. Pore sizes start big and decrease with increasing synthesis time, but wall diameters increase with increasing synthesis time (figure 30b). The nanotube width is stable at low reaction times, then increases at 1 day and stays stable with increasing reaction times (figure 30c). In terms of nanotube formation this result means that the walls grow from the outside inward, since the width remains constant. This contradicts the growth from the inside outward, which was seen in figure 29ab. Most likely, the growth happens mostly from the outside inward but also slightly from the inside outward.

In figure 31 the particle size distributions of the length, pore and wall size are displayed for every synthesis time with 7 wt% NaOH. The distributions of the length are right-skewed and remain constant, while broadening a little at 6 days. The pore size distributions have a bell and bimodal like distribution at day 1, 2, 4 and 6 and remain constant. The wall size distributions are bell shaped and slightly right-skewed and remain constant from 1 to 6 days synthesis. The length distribution becomes slightly broader with increasing synthesis time, while the distribution for pore and wall thickness remains constant, as shown in figure 31.

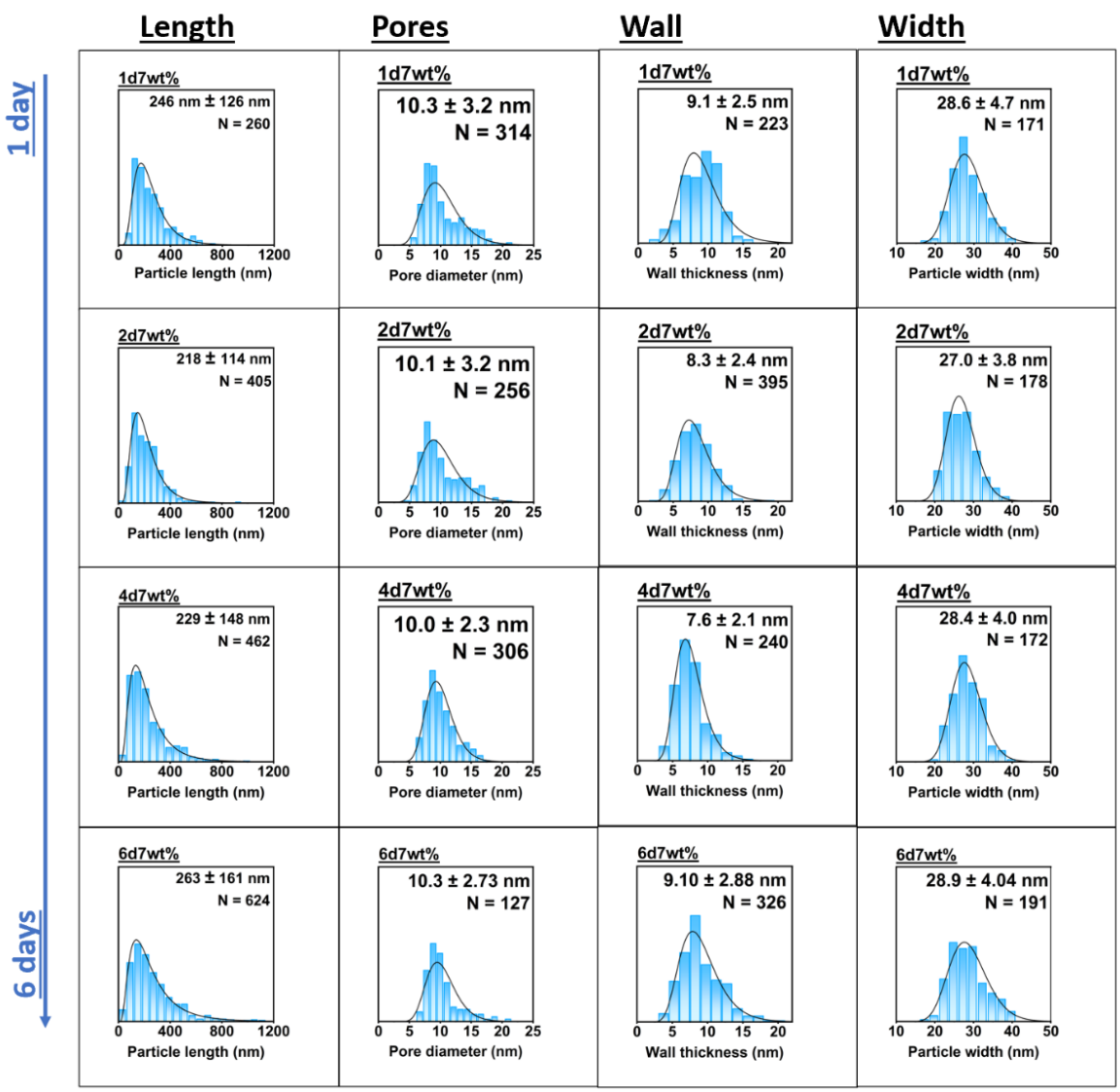

Figure 31: Particle Size Distributions of length, pore and wall sizes for 1 day to 6 day synthesis at 7 wt% NaOH.

The Ni phyllosilicate nanotubes made in this project sometimes appear in an end-on-view orientation. Studying the TEM images has led to details on different stages of nanotube formation, as can be seen in figure 32. A scrolling mechanism is involved in the formation, described in chapter 2 for chrysotile and Ni phyllosilicate nanotubes. The scrolling mechanism thus seems also applicable to Ni phyllosilicate nanotubes. The role of the discs in the scrolling mechanism needs to be studied further. The synthesis time does not seem to have a further effect on nanotube morphology and composition after a synthesis time of 24 hours. To gain more information on the nanotube development in the early stages, it is necessary to conduct more experiments between 4 hours and 24 hours and analyse the dimensions with TEM images.

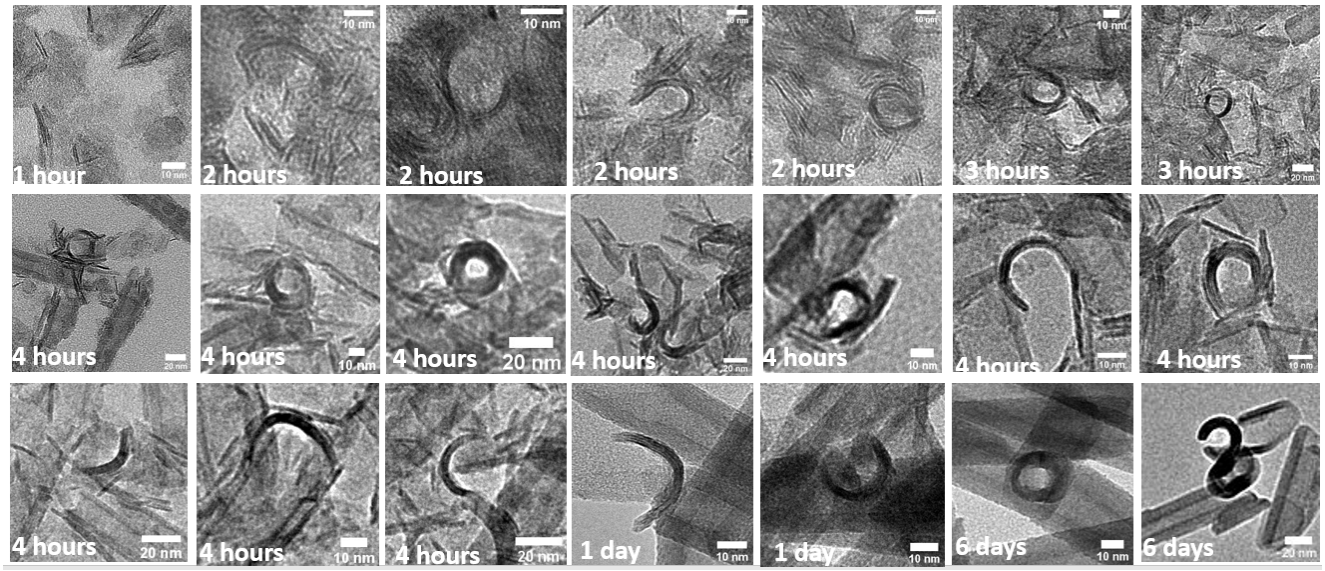

Figure 32: TEM images of formation stages of Ni phyllosilicate nanotubes with side views of scrolling mechanism.

4.4 Reduction Ni phyllosilicate nanotubes

The composition and distribution of the nanotubes can be studied further using Energy Dispersive X-ray spectroscopy (EDX). The atomic distribution of nickel, silica and oxygen in the Ni phyllosilicate nanotubes is constant over the whole length of the tube. It is further evidence that the material is a nickel – oxygen - silica material like Ni phyllosilicate. In the middle of the tube the Ni, Si and O distributions are less dense, indicating a hollow core of a nanotube. Figure 33bcd shows evidence of the properties of Ni phyllosilicate to be a homogeneous precursor for Ni catalysts. The Ni phyllosilicate nanotubes were reduced at 650 °C with a 5 % H_2/Ar gas stream for 2 hours and imaged with TEM, STEM and EDX.

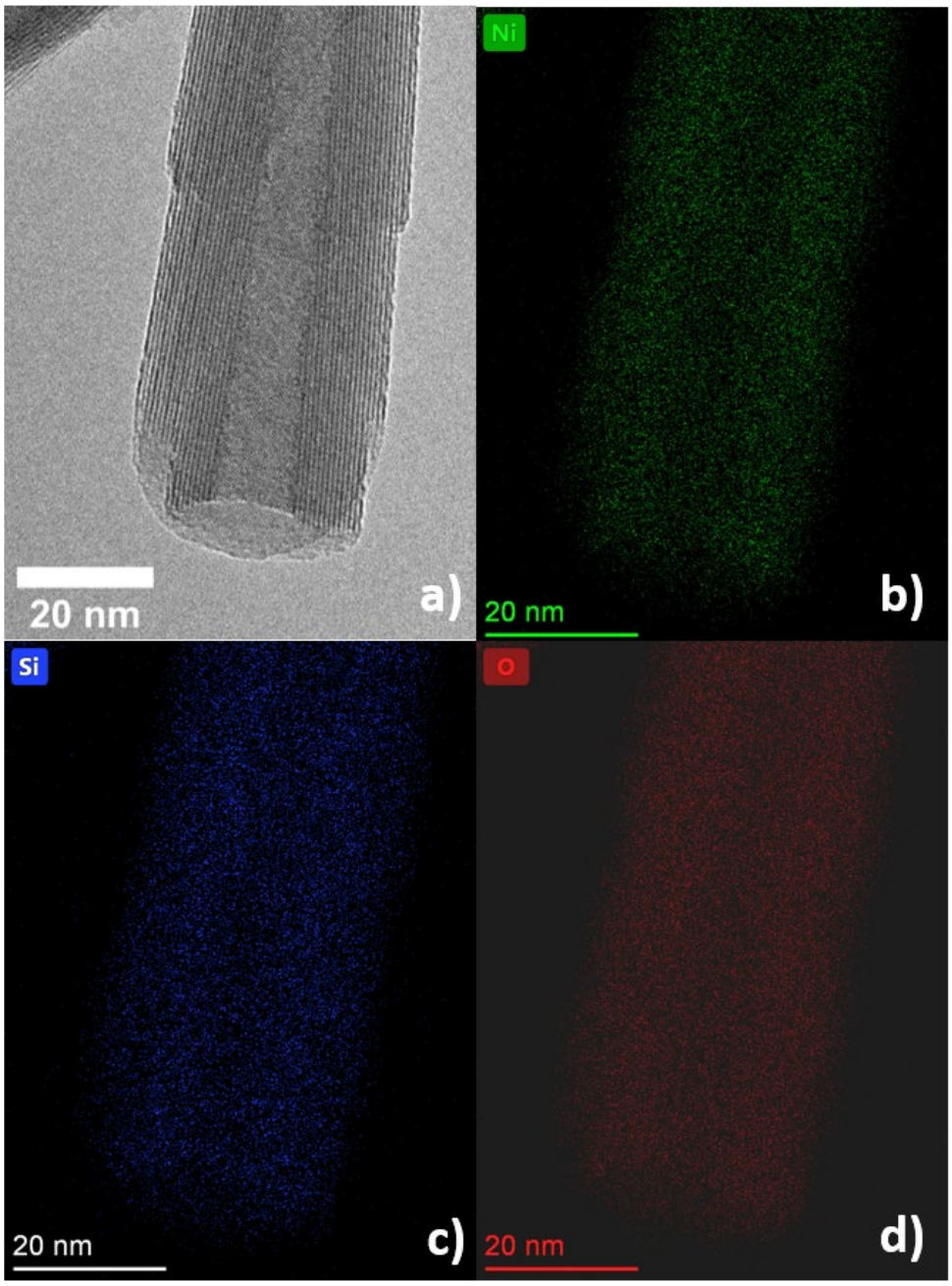

Figure 33: TEM image and EDX maps of Ni, Si and O of Ni phyllosilicate nanotube before reduction. (a) high resolution TEM image nanotube (b) nickel EDX map nanotube (c) silica EDX map nanotube (d) oxygen EDX map nanotube

The homogeneous distribution in the Ni phyllosilicate nanotube leads to a homogeneous particle size distribution after reduction under hydrogen has taken place. The weight % of Ni and Si in the nanotubes was explored with quantitative EDX using a low background holder, the result of which can be seen in table 1 in the supplementary information. The reduction produced nickel particles that are still embedded in the nanotube structure and well dispersed. The STEM image in figure 34a show a homogeneous particle distribution and figure 34c show these are Ni particles. The EDX elemental mapping shows the redistribution of Ni and Si atoms from the Ni phyllosilicate structure into Ni particles on silica (figure 34b). The Ni particles are embedded into silica, as holes in the silica elemental map (figure 34d) appear at the locations where Ni particles are present. This means that Ni particles are successfully incorporated into the silica support.

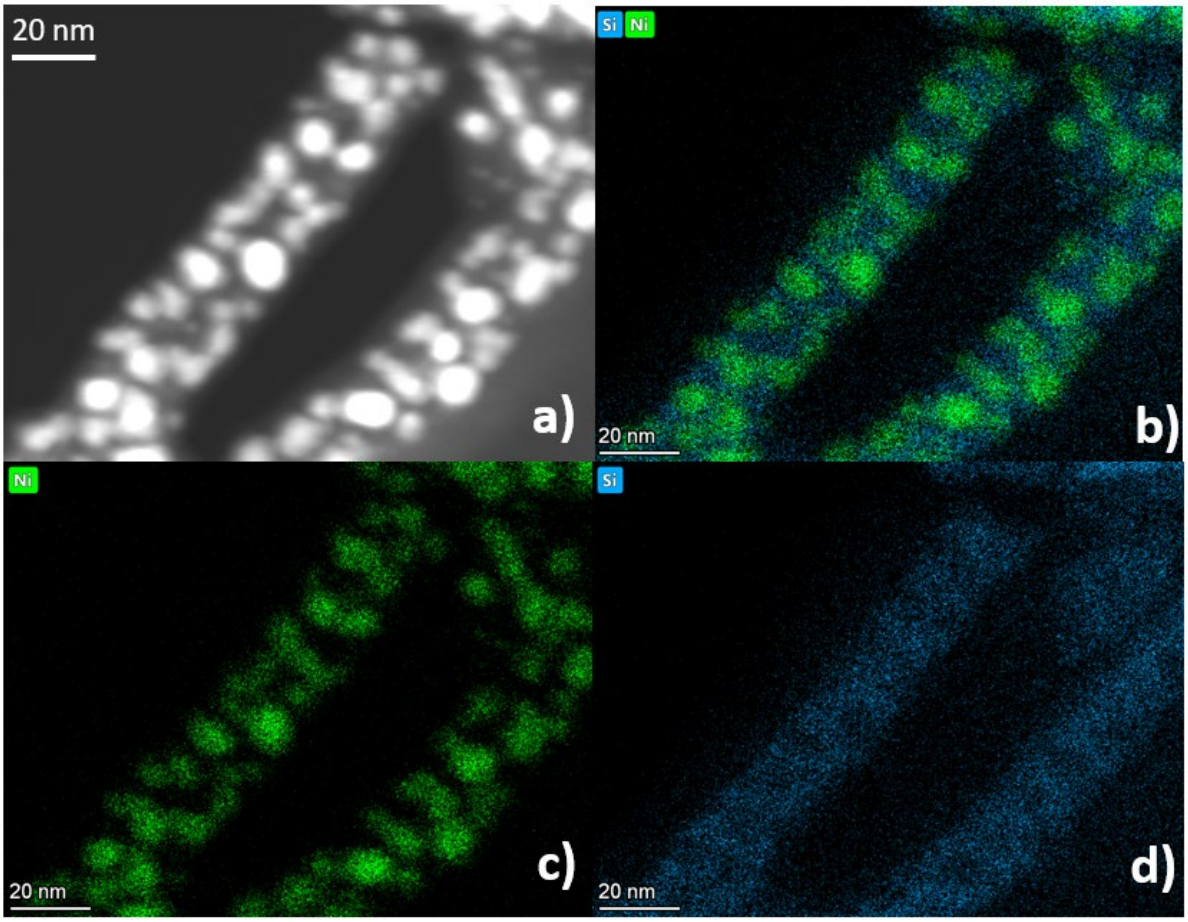

Figure 34: STEM and EDX images of reduced nanotube, Ni@SiO_2 particles are shown with STEM and EDX after Ni phyllosilicate has been reduced at 650 ˚C under 5% H_2/Ar for 2 hours, with a 10 ˚C/min heating rate. (a) STEM image Ni/SiO_2 (b) Ni/Si elemental map after reduction, (c) Ni elemental map after reduction (d) Si elemental map after reduction

A detailed overview of the 650 °C reduced Ni phyllosilicate nanotubes is shown in TEM images in figure 35 and STEM images in figure 36. At large scale dark pieces of nickel can be seen (figure 35a), which can be fully reduced $Ni(OH)_2$. At larger magnification the particles in the nanotube shape become better visible (figure 35bcd). The individual particles inside the nanotubes are best visible at a 20 nm scale (figure 35f). To better distinguish particles, some STEM images are shown in figure 36.

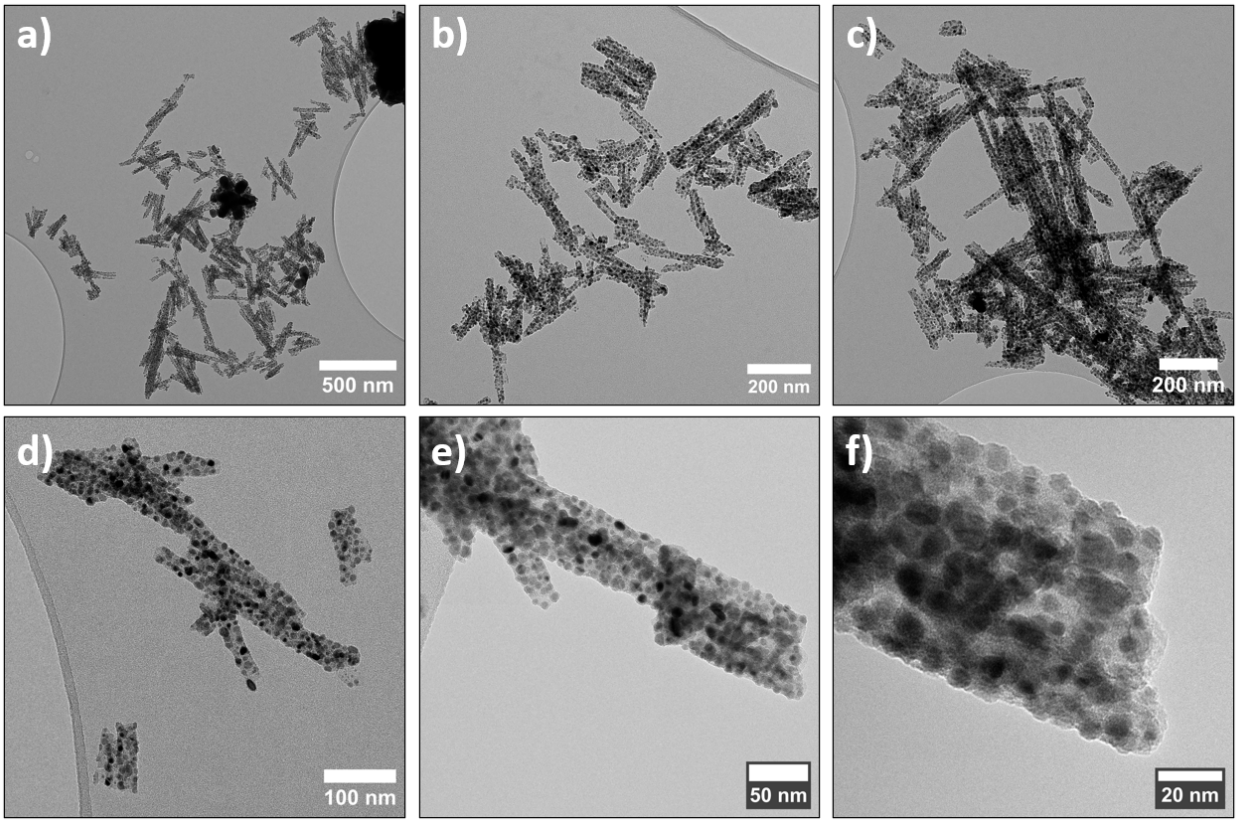

Figure 35: Bright field TEM images of reduced Ni phyllosilicate nanotubes at 650 °C under 5% H_2/Ar for 2 hours.

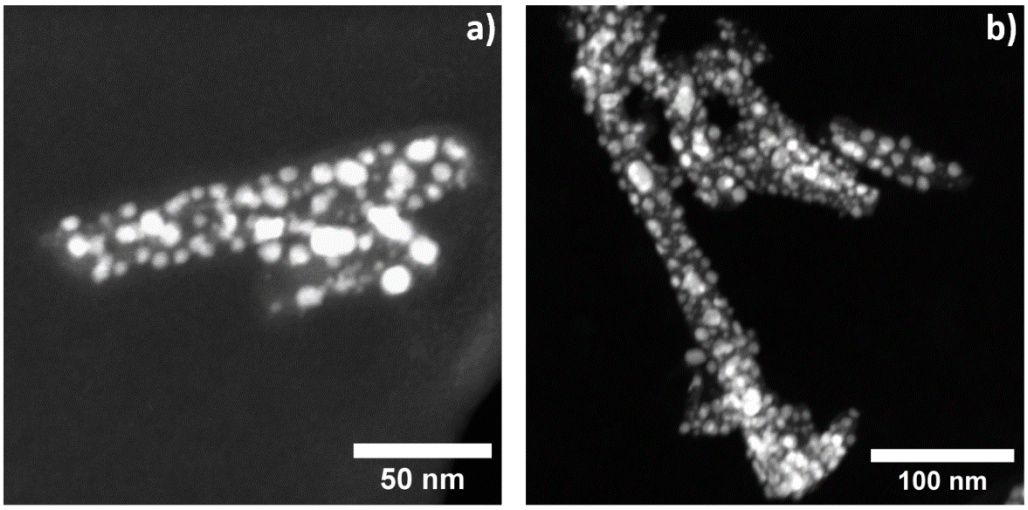

Figure 36: Dark field STEM images of reduced Ni phyllosilicate nanotubes (650 °C, 5 % H_2/Ar)

4.4.1 Effect of temperature on particle size

The effect of temperature on the particle size has been investigated by the reduction of Ni phyllosilicate nanotubes, because catalyst particle size has been shown to influence stability and activity during reactions.[11,29,30,33] Reductions have been carried out under a 5% H_2/Ar gas stream at temperatures of 350, 400, 450, 650 and 750 ^oC, using a Ni phyllosilicate nanotube sample synthesized with 7 wt% NaOH for 6 days. A fresh batch of Ni phyllosilicate powder was reduced each time. This sample was chosen because it has an average nanotube length interesting for battery and catalysis applications [46] and has straight nanotubes with minimal contamination. An increase of particle size with increasing temperature is observed.

The particle formation mechanism can be seen in figure 5 in the introduction. A higher temperature increases particle kinetics and will cause more particles to seam together into bigger particles. A 1:1 phyllosilicate is expected to be fully reduced around 650 °C and 2:1 Ni phyllosilicate is fully reduced around 750 °C (figure 17, TPR graph). The nickel hydroxide in the sample could be around the nanotubes, inside the nanotubes or separated from the nanotubes. Nickel hydroxide is expected from TPR to fully reduce before 450 °C (figure 17: TPR of sample & figure 77a: TPR of Blanco $Ni(OH)_2$).

Particles originating from the Ni phyllosilicate lattice structure in the nanotubes have formed during reductions at 650 °C and 750 °C (figure 37de). These are the temperatures where reduction of 1:1 Ni phyllosilicate occurs in TPR. Average particle sizes of 7.4 ± 2.4 nm for 650 °C and 9.2 ± 3.1 nm for 750 °C reductions were found (figure 37hi). Reductions at lower temperatures were carried out to investigate whether particles still form. Surprisingly, particles still formed inside the tubes at 400 °C and 450 °C reductions (figure 37bc). Average particle sizes of 4.1 ± 1.5 nm for 400 °C and 5.4 ± 1.8 nm for 450 °C reductions were found (figure 37fg). No particles were found inside the tube after reduction treatment at 350 °C (figure 37a), but sporadically something was found adhered to the outside. This is shown by tilting the stage during TEM measurements, to image a nanotube under different angles to get more 3D information (figure 38). Tilting between 0 and 60 degrees showed that particles present around nanotubes after 350 °C reduction are only adhered to the outside, as particles visible inside the tube in the left image in figure 38 move away to the side after tilting 60 degrees. The particles measured after 400 °C and 450 °C reductions could form from reduced $Ni(OH)_2$ adhered to the nanotube walls and likely do not originate from the Ni phyllosilicate lattice, as there is an inhomogeneous spread in the particle size distributions of 400-450 °C and 650-750 °C that indicates a difference. Particle size distributions of 400 °C and 450 °C (figure 37fg) are more bell shaped and distributions of 650 °C and 750 °C are more tilted to the right (figure 37hi). The particle sizes from 400 °C to 750 °C do show an increasing trend, as can be seen in figure 37A. However, the contribution to particle size formation from the Ni phyllosilicate structure is mainly present in reductions at 650 °C and 750 °C.

To gain more understanding of the particle formation more steps can be taken. The reduction of the Ni phyllosilicate nanotubes at 500 °C is needed to conclude with TEM images whether the 1:1 Ni phyllosilicate lattice is still intact. This will confirm whether particles formed at 400 °C and 450 °C were formed from the Ni phyllosilicate lattice or from $Ni(OH)_2$ adhered to the walls. A N_2 physisorption measurement of a 750 °C reduced sample can confirm whether the pores are completely disappeared or not. These steps will hopefully give more insight into the temperature effect on the particle size in Ni phyllosilicate nanotube catalyst precursors.

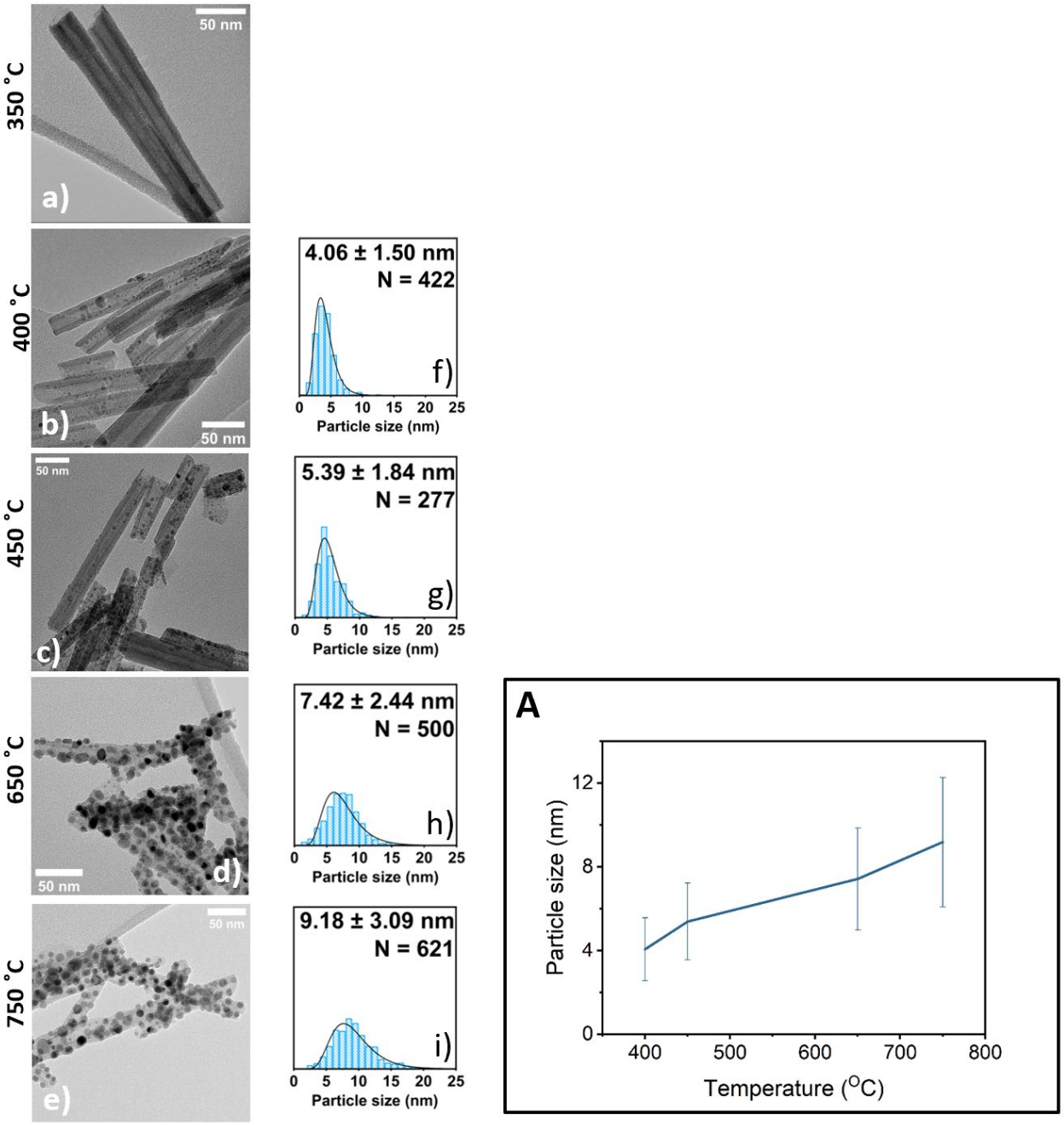

Figure 37: Ni phyllosilicate nanotubes synthesized with 7 wt% NaOH for 6 days at 195 °C are treated under a 5% H_2/Ar gas stream. Reductions at 350 °C, 400 °C, 450 °C, 650 °C and 750 °C were carried out. Multiple TEM images of the reduced nanotubes were analysed in ImageJ to attain average and standard deviations in the particle size. (a-e): TEM images of particle formation from low to high temperature. (f-i): Corresponding particle size distributions. (A): Average diameter of Ni particles in reduced Ni phyllosilicate nanotubes is set against reduction temperatures.

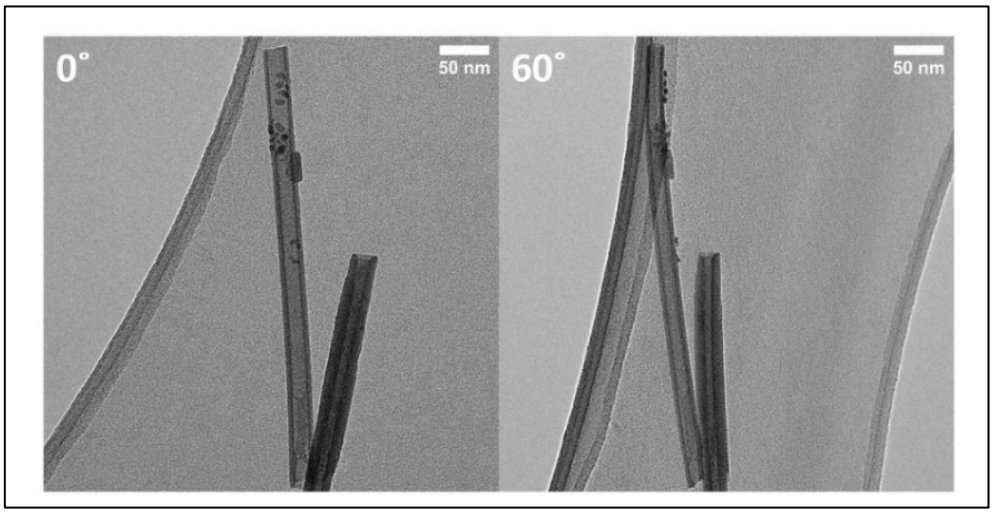

Figure 38: 350 °C reduction at 5% H_2/Ar for 2 hours, heating rate 10 °C/min. Left: Nanotube with apparent particles in the middle, at 0 degree angle. Right: Same nanotube at 60 degree angle, particles that appeared in the middle before have moved to the side.

4.4.2 The relation of nanotube morphology to particle size

The hypothesis of the relation between the wall thickness and resulting particle size was mentioned in the introduction. What it involves is that a thicker nanotube wall will lead to bigger particles and a thinner nanotube wall will lead to smaller particle after reduction. The relationship between nanotube wall diameter and particle size after reduction has been studied with Identical Location TEM. The sample synthesized for 6 days with 7 wt% NaOH was deposited on a ILTEM grid and reduced at 650 °C in a tube oven (see Methods), this sample was chosen because the nanotubes appear homogeneous, of appropriate length and to be able to compare with the regular reductions. TEM images were taken before and after the reduction. The analysis was carried out by matching the unreduced and reduced particles and measuring the particle size. The unreduced-reduced matches are shown in the supplementary information in 7.4. The particle size, nanotube wall thickness, the length of the nanotube section and the pore size of 24 nanotube matches were measured. An example of a thin walled nanotube and its reduced counterpart is shown in figure 39. An example of a thick walled nanotube is shown in figure 40. The relation of wall thickness and pore size is shown in figure 41ab. The relation of wall volume to particle size is shown in the supplementary information in figure 52. The comparison of all 24 matches in wall thickness, pore sizes and total wall volume has led to the acquisition of information to test this hypothesis.

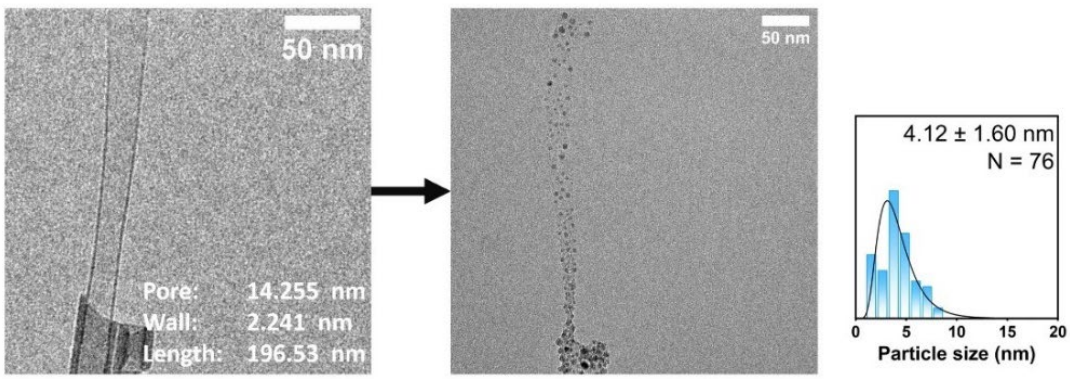

Figure 39: Example of an unreduced and reduced Ni phyllosilicate nanotube with thin walls.

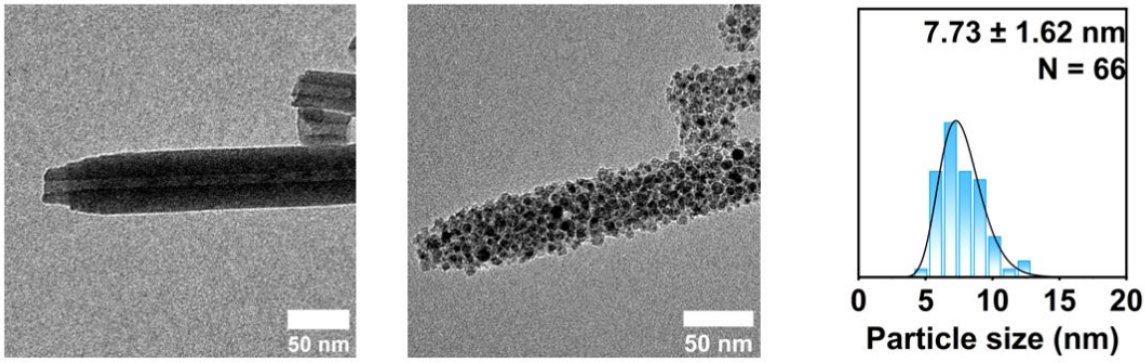

Figure 40: Example of an unreduced and reduced Ni phyllosilicate nanotube with thick walls.

The relationship of the wall thickness and particle size is displayed in figure 41a. There appears to be an increase in particle size until a wall thickness of 4.5 nm, after which the particle size stabilizes with increasing wall thickness between particle sizes of 5 to 8 nm. An implication of this for catalysis is that the particles only form from a depth of 4.5 nm into the wall. This means that with Ni phyllosilicate nanotube walls wider than 4 nm there is no correlation anymore between particle size and depth of the sheets. This can be applied to non-nanotube Ni phyllosilicates, which is used as a precursor in industrial catalysts.

The relation of Ni phyllosilicate nanotube pore sizes and resulting particle size has to an understanding of pore accessibility. The correlation between nanotube pore size and particle size is displayed in figure 41b. The particle size is constant with increasing pore diameter, with a slight dip in particle size around 14.5 nm. The significance of this is that the nanotube pores stay open to hydrogen gas during reduction and that there is not an issue of inaccessibility of the pores. This is important when planning catalytic tests on this system.

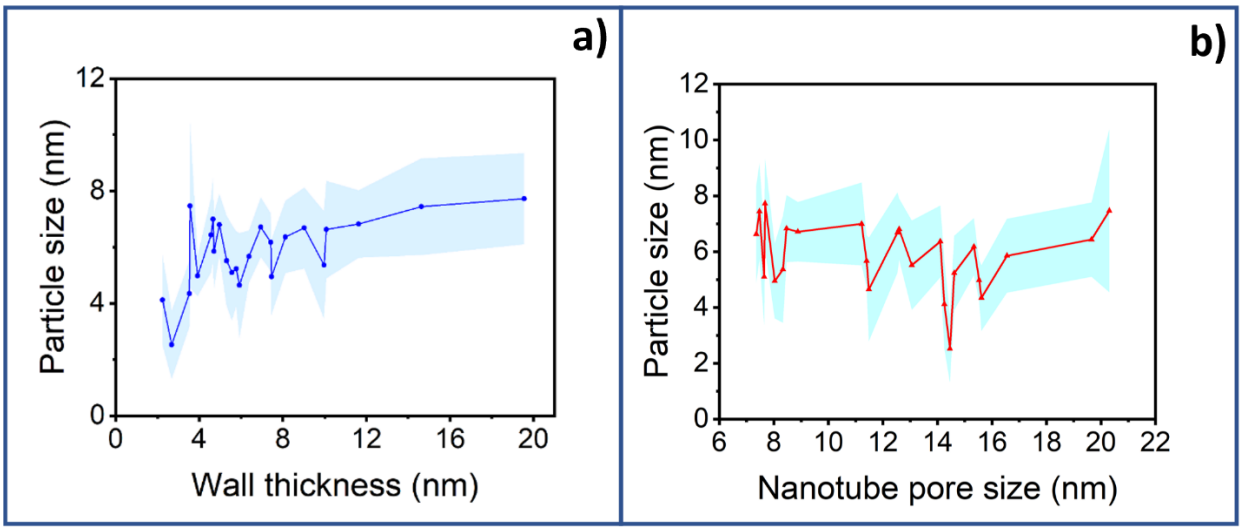

Figure 41: (a) Relation of particle size vs nanotube wall thickness. (b) Relation of particle size vs nanotube pore size.

5 Conclusion

The Ni phyllosilicate nanotubes were synthesized using a nickel chloride hexahydrate, NaOH and sodium silicate with 1.5 Ni/Si and 7 wt% NaOH. The dimensions were determined with transmission electron microscopy. The nanotubes on average have 235 nm lengths, 9.1 nm walls and 10.3 nm pores. A crystal lattice spacing of 0.75 nm was determined with HRTEM images. Other nickel phases produced as by-products are nickel hydroxide and nickel oxide. Lattice spacing, XRD, ED and TPR results indicate a 1:1 Ni phyllosilicate as main phase.
Treatment with 5 % hydrogen gas in argon at temperatures 400-750 °C produced Ni metal particles embedded in the nanotube structure, ranging from diameters of 4 to 9 nm. A linear increase of particle size with temperature was observed for temperatures 400, 450, 650 and 750 ^{o}C. A relationship between nanotube wall thickness and nickel metal particle size was established. The particle size increases with increasing wall thickness up to a wall thickness of 4.5 nm, after which the particle size remains stable with increasing wall thickness. The particle growth thus sources its material from a depth of 4.5 nm into the sheet. The particle size remains stable with increasing pore sizes and indicates that pores remain accessible to hydrogen in a range of 8 to 20 nm pore diameter.
Variation of the NaOH concentration between 5 and 10 wt% has led to insights into composition and morphology changes. An increase in nanotube length and nanotube wall thickness is observed with increasing NaOH concentration. A decrease in nanotube pore size is observed with increasing NaOH concentration. A broadening of the length distributions occurs with increasing NaOH wt%.
The effect of synthesis time has been studied to develop an understanding of the nanotube formation. The nanotubes are fully formed after 1 day of synthesis and start forming after 2 hours of synthesis. The presence of discs in the first 4 hours of synthesis has been established and has started a new understanding of the formation mechanism. The nanotube walls grow both from the outside inwards and from the inside outwards.
The findings lead to a fully characterized Ni phyllosilicate nanotube system, that is reproducible and forms a homogeneous distribution of stable nickel particles. The applications lie in heterogeneous catalysis, where it can be used as a model system for nickel catalysts. The Ni phyllosilicate nanotubes are also promising for battery research, where it can be used as a conducting material for electrodes.

6 Outlook

Ni phyllosilicate nanotubes can be treated with hydrogen to produce particles embedded on a tubular silica support. The desired particle size can be obtained by varying the temperature. Several catalytic tests for hydrogenation reactions can be carried out with these reduced nanotubes. By forming Ni particles inside the nanotubes, the tubes become electrically conductive. The conductivity of the nanotubes could be varied by reduction treatment to be applied in a study on anode battery materials.
A similar study could be performed on cobalt phyllosilicate nanotubes. The removal of $Ni(OH)_2$ from the sample is necessary in order for future applications to be fruitful. The formation of $Ni(OH)_2$ can possibly be prevented by performing a synthesis in a glovebox, under a nitrogen and argon atmosphere. Another possibility lies in taking a different approach in the drying step. Alternatively, the dissolution of $Ni(OH)_2$ from the nanotube sample can be accomplished with nitric acid titrations.

The obtained results on NaOH variation in this thesis can be improved by performing TGA on the samples. This can show the difference between high and low NaOH wt% nanotube samples. The $Ni(OH)_2$ formation in this system is interesting to study further, possibly in a bachelor thesis. The $Ni(OH)_2$ particles could be characterized by TEM and TGA. The nanotube lattice spacing can be analysed at different NaOH concentrations to see if a decrease or increase is observed. To study the effect of synthesis variations on the final particle size, nanotube samples of 5, 7 and 10 wt% NaOH can be

reduced. The effect of NaOH concentrations on the final particle size can then be seen.
The formation of Ni particles on the nanotube support can be studied further with electron tomography before and after reduction. After 3D images have been generated it will be clear whether particles form on the outside or on the inside of the tube. A study with in-situ TEM will also provide more clarity on the kinetics of the particle formation.
To provide more insight on the first stages of nanotube growth, more syntheses between 4 and 24 hours can be carried out. Analysing the dimensions will lead to conclusions on the direction of growth of the walls and when growth stabilizes.

Acknowledgements

My first and big appreciation goes to my supervisor, Savannah Turner, for her marvelous supervision, guidance, constructive feedback, kind support and encouragement. Her joy for science, education and electron microscopy have been very inspiring and it has been wonderful working together. The positivity, humor and teamwork have been amazing. Learning from you has been very enjoyable. Thank you very much!

Also, I greatly appreciate prof. Dr. Ir. Krijn de Jong for his encouragement and advice during my master thesis. And thank you, Krijn and Jovana Zecevic, for hiring Savannah because that was an excellent choice.

Thank you, Luc Smulders, for discussing my research plans with me while Savannah was on pregnancy leave and being her replacement. The organization of Savvie's maternity presents from MCC was a lot of fun. I would like to thank Yuang Piao, for taking HRTEM/STEM/EDX images together and his TEM support. Special thanks go out to Ing. Hans Meeldijk for training me on the Technai T20 and Talos L120C.

Many thanks to all the members of the Material Chemistry & Catalysis group for their kind welcome and nice conversations. My thanks to all technicians for their practical support. I would like to thank Remco Dalebout for the TPR training, Dannie Wezendonk for the XRD training and Ad van der Eerden for the autoclave safety training. Additionally, I would like to thank Jan Willem de Rijk and Chris Schneijdenberg for their technical support. My appreciations go out to Suzan Schoemaker and Claudia Keijzer for the physisorption measurements and SEM images. I thank Kyra van Nieuwkerk for proofreading a version of this thesis. My thanks to Ben Erné and Albert Philipse from the Physical & Colloidal Chemistry group for answering my questions on gel formation, analytical centrifugation and sedimentation. Furthermore, I want to thank my family, especially Ria, Lidwien and Paul for supporting me.

7 Supplementary Information

7.1 Extra Characterizations nanotubes

This section outlines SEM, XRD, TEM, EDX and TPR results of 5, 7 and 10 wt% nanotube samples not included in chapter 4.

7.1.1 NaOH effect

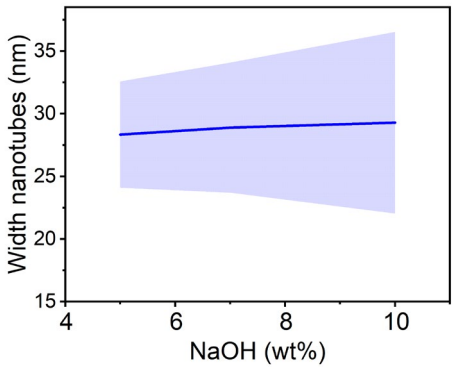

Figure 42: Width nanotubes with increasing NaOH wt%

7.1.2 Nanotubes with 5 wt% NaOH

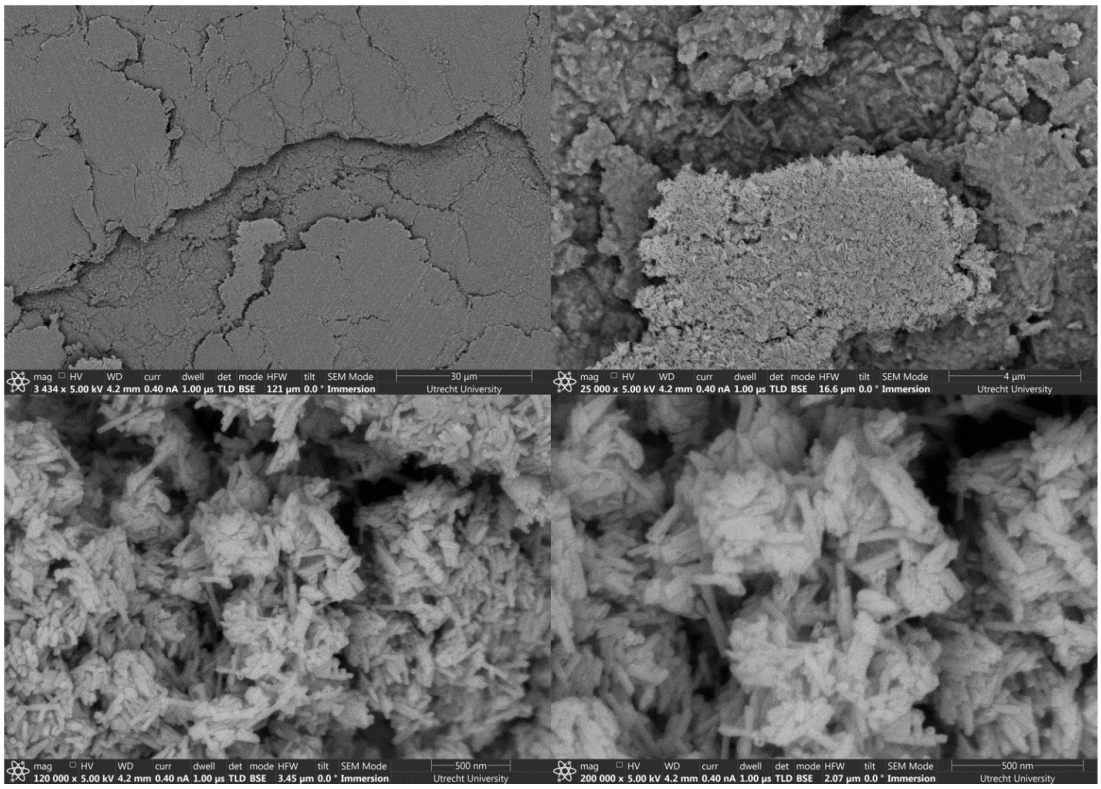

Figure 43: SEM images of Ni phyllosilicate nanotubes, 2 day synthesis with 5 wt% NaOH

7.1.2 Extra characterizations of 7 wt% NaOH samples

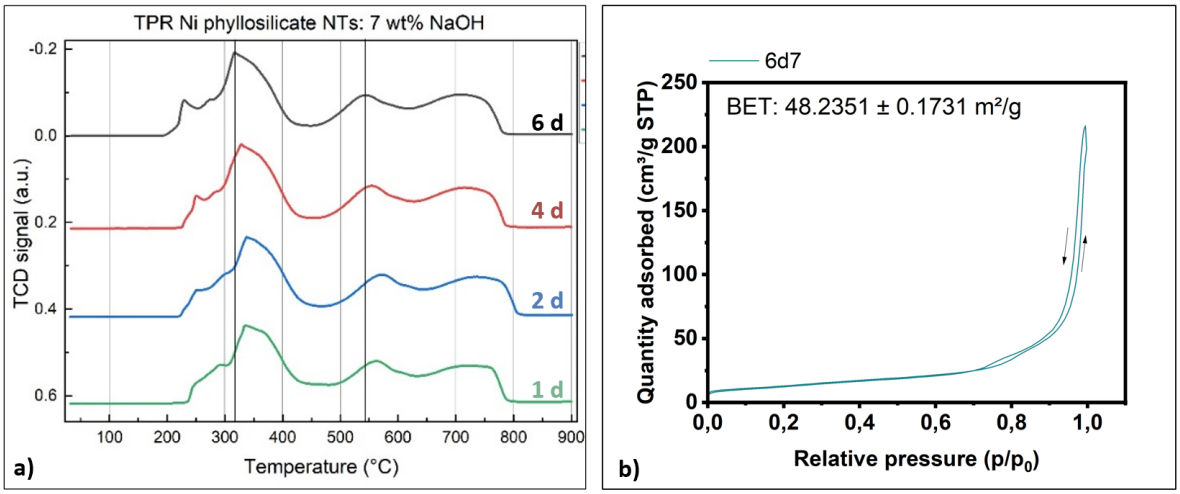

Figure 44: (a) TPR graphs of samples synthesized for 1, 2, 4 and 6 days. All samples used 7 wt% NaOH. (b) Adsorption isotherm N2 physisorption of Ni phyllosilicate nanotube sample.

Table 1: EDX analysis of Ni and Si content in Ni phyllosilicate nanotubes. EDX was performed with a Au Holey carbon grid in a Beryllium low background holder.

EDX	**Element**	**Weight %**	**Atomic %**
Multiple tubes	Si	37.34	55.47
	Ni	62.65	44.52
Single nanotube	Si	72.63	84.72
	Ni	27.36	15.27
Single nanotube	Si	56.53	73.10
	Ni	43.46	26.89

7.1.4 Ageing time effect

The effect of ageing time was studied. The solution of Ni chloride hexahydrate, sodium silicate and NaOH was stirred for 24 hours instead of 20 minutes before synthesis at 195 °C for 2 days. No significant difference was observed in XRD and TPR. A difference was seen in N_2 physisorption.

7.1.5 Extra images reduced nanotubes

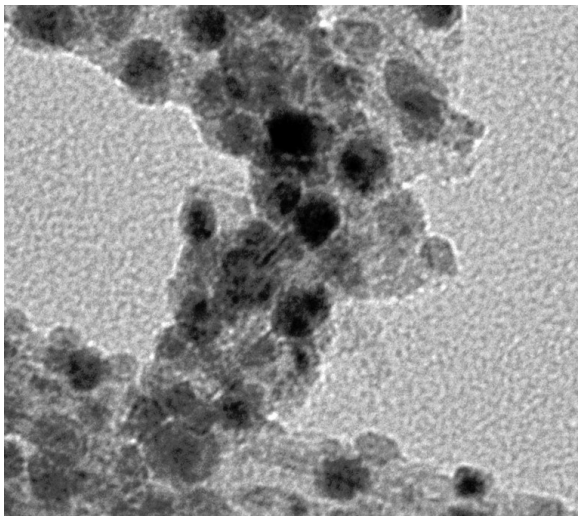

Figure 45: Moiré pattern or Ni phyllosilicate lattice left over.

7.1.6 XRD grain sizes

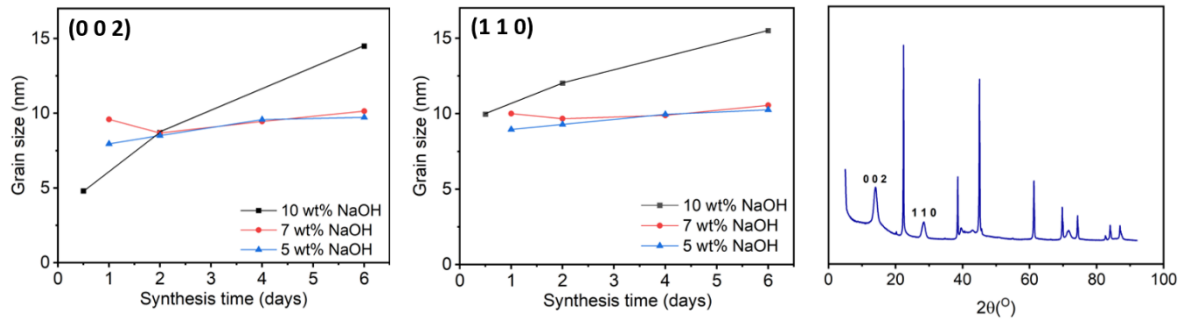

Figure 46: Grain sizes from XRD calculated with the Scherrer equation. K=1.

Grain sizes of the 100 and 200 peak of Ni phyllosilicate were determined using the software on the XRD PC, using K=1,0 and the Scherrer equation. The constant K=1.0 in the Scherrer equations assumes cubical particles. It is an approximation for the disc-like platelets which could be the building blocks for the nanotubes. The grain sizes correspond roughly with the sizes found for the platelet shaped objects in TEM images in 1 hour to 4 hour synthesis.

7.2 Gel formation & extra characterizations 10 wt% NaOH

The samples synthesized with 10 wt% NaOH took a longer time to wash and centrifuge than the lower NaOH wt% samples. The sedimentation went very slowly for 10 wt% samples, which meant a long centrifugation until a clear supernatant was produced. The supernatant remained green initially and slowly became more translucent as centrifugation time increased. The little sediment that was present initially looked clay like, but as centrifugation time increased a gel-like consistency appeared. Analysis

of TEM images showed longer nanotubes with higher NaOH wt%, which thus have a higher aspect ratio of Length/Diameter (L/D).

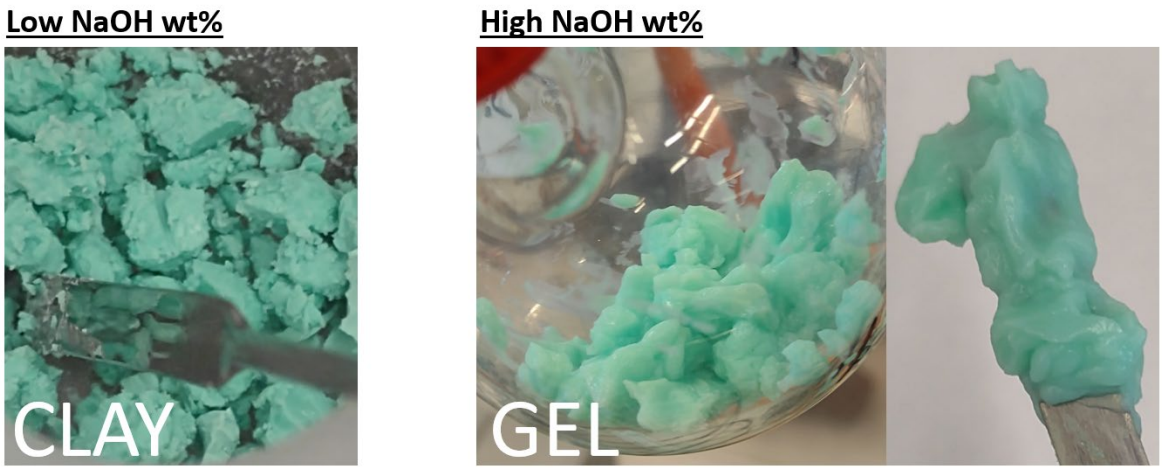

Figure 47: Appearance of synthesis product after washing & centrifugation. Left: clay appearance at low NaOH wt% (5-7). Right: gel appearance at high NaOH wt% (10)

The gel formation can be explained with the higher aspect ratio. A higher aspect ratio creates a higher friction factor in a solution, which slows down the sedimentation rate. The packing of longer tubes with a higher aspect ratio is also different from shorter tubes. This can be demonstrated using short and long wooden sticks ('saté prikkers'). Put the long wooden sticks parallel to each other in a glass jar, then shake the jar, the result will be that the wooden sticks take up a larger volume than before. When short sticks or balls are used (representing spherical particles or short tubes) the result will be the same before and after shaking. This relates to the longer sedimentation rate of long nanotubes. Philipse et al studied the packing of spheres and rods and concluded that 'long thin rods always randomly pack into entangled isotropic networks.' [67]

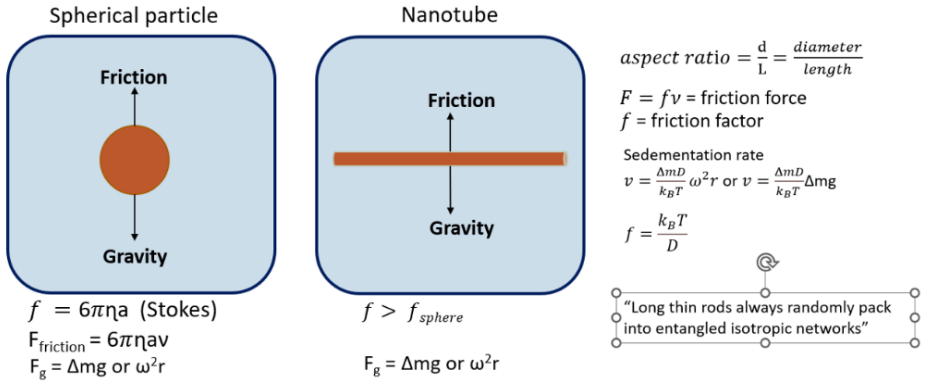

Figure 48: Sedimentation rates are dependent on particle shape.

To attempt to prevent gel formation, ethanol was used in the washing in the early stages of this research. This sped up the sedimentation and prevented gel formation. However, the results of TPR, XRD and TEM showed unsatisfactory results. The nanotubes were badly visible in TEM images because of contamination with by products and posed a problem for statistical analysis. To solve this problem the washing and centrifugation step was changed. The old washing step included washing with MQ water and ethanol from early stages. The new washing step only used ethanol when pH 6 was reached. The centrifugation was carried out very carefully in the new washing procedure: only very slow speeds were used to try to prevent entangling and gel formation. The new washing procedure created better visible nanotubes, but a cream like gel was still often formed. When centrifugation of supernatant is

continued through to try to get more product, a more translucent gel is formed. A comparison of dried gel and clay samples under TEM showed the clay sample contained more visible nanotubes.

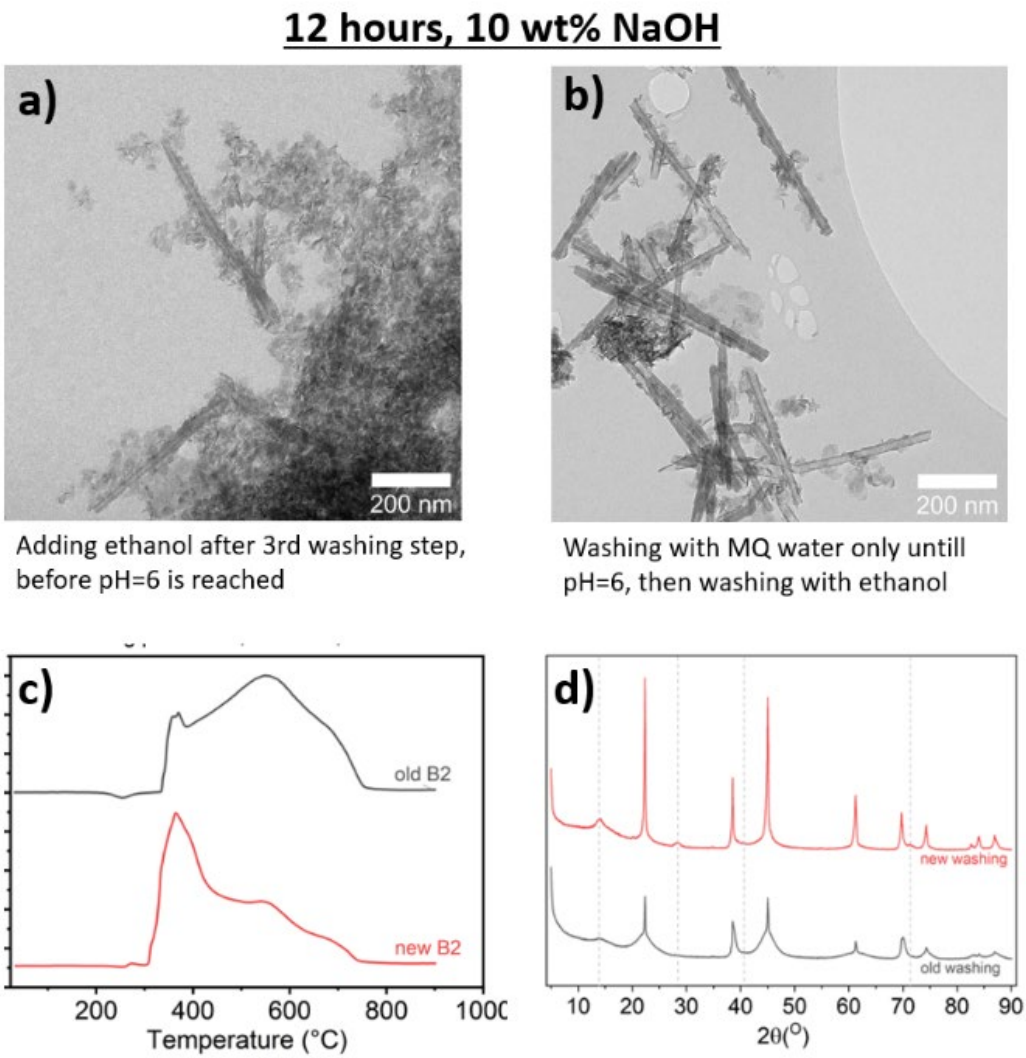

Figure 49: Washing procedure change. a) TEM image old washing b) TEM image of new washing c) TPR of old and new washing d) XRD of old and new washing

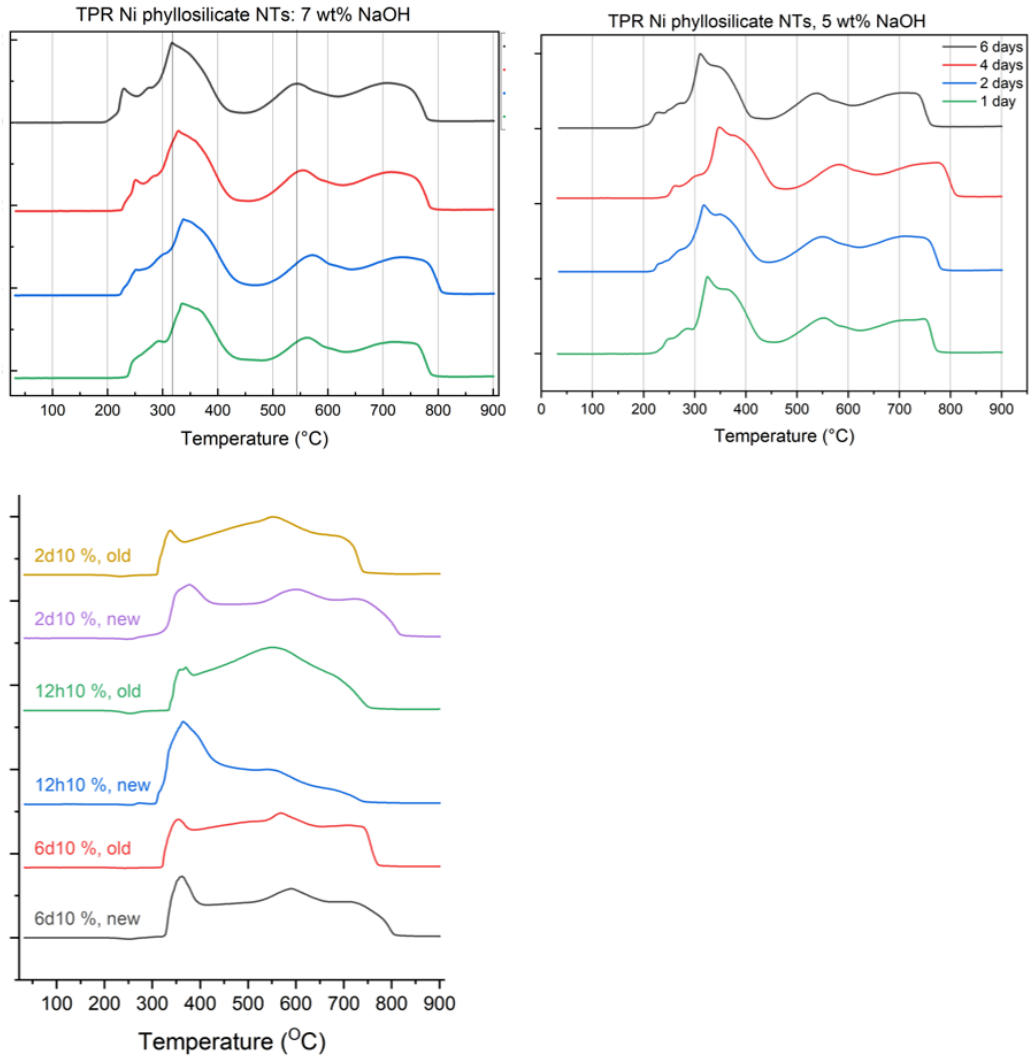

Figure 50: TPR results of 10, 7 and 5 wt% NaOH nanotube samples.

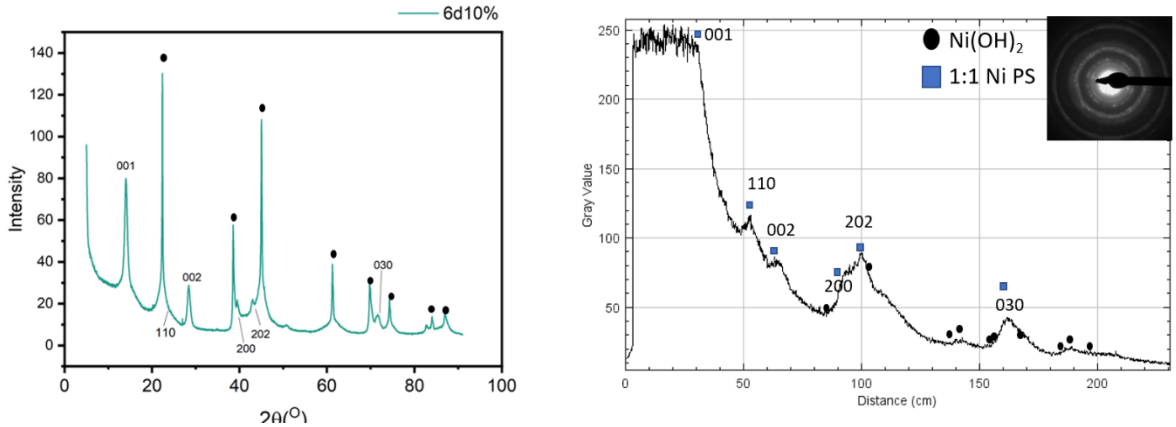

Figure 51: XRD and ED of 6d10 sample.

7.3 List of samples

Table 2: Samples with 1.5 Ni/Si ratio

Name		NaOH wt%	Synthesis time
6d10		10	6 days
4d10		10	4 days
2d10		10	2 days
1d10		10	1 day
12h10		10	12 hours
6d7		7	6 days
4d7		7	4 days
2d7		7	2 days
1d7		7	1 day
4h7		7	4 hours
3h7		7	3 hours
2h7		7	2 hours
1h7		7	1 hour
6d5		5	6 days
4d5		5	4 days
2d5		5	2 days
1d5		5	1 day
1h5		5	1 hour

7.4 Reduction: ILTEM images

The analysis of the nanotube images before and after reduction were performed using Excel and ImageJ. The TEM images used per data point will be shown in this section, including the particle size distributions of the reduced nanotubes. The image sets are ordered according to wall thickness, from small to large wall diameters, as depicted in Table 3.

Table 3*: Data used for figure... of ILTEM. Wall thickness of nanotubes and average particle size of reduced nanotubes.*

ID	Wall thickness (nm)	Average particle size (nm)	st dev particle size (nm)	N	Pore size	Length
NT 6	2.241	4.1211	1.5998	76	14.255	196.53
NT 20	2.684	2.5269	1.2101	30	14.458	53.154
NT 24	3.532	4.3457	1.1767	6	15.615	84.896
NT 3	3.564	7.4651	2.9169	5	20.306	40.91
NT 23	3.924	4.9822	0.7225	8	15.528	45.878
NT 12	4.566	6.4336	1.3314	30	19.654	90.047
NT 10	4.657	6.9959	1.4816	37	11.221	257.889
NT 8	4.704	5.8553	1.3232	63	16.554	454.185
NT 17	4.962	6.8033	1.0963	29	12.597	124.312
NT 21	5.312	5.5167	1.6019	28	13.061	141.382

NT 19	5.561	5.0963	1.7058	125	7.647	438.744
NT 1	5.767	5.2343	1.3336	16	14.614	96.726
NT 11	5.924	4.6497	1.8532	64	11.487	126.922
NT 7	6.382	5.6720	0.9271	67	11.404	497.259
NT 2	6.947	6.7140	1.0641	43	8.882	310.861
NT 14	7.421	6.1807	1.0235	47	15.339	204.666
NT 22	7.459	4.9503	1.3384	28	8.03	114.496
NT 9	8.122	6.3672	1.2873	36	14.105	160.592
NT 4	9.028	6.6849	1.4401	17	12.534	43.983
NT 18	9.968	5.3670	1.9119	22	8.334	37.098
NT 16	10.085	6.6279	1.7335	98	7.354	311.828
NT 13	11.627	6.8275	1.1994	86	8.468	85.036
NT 5	14.626	7.4428	1.7172	28	7.471	207.357
NT 15	19.546	7.7251	1.6205	66	7.677	390.236

The relation between total wall volume and particle size is displayed in figure 52. The result resembles the wall thickness and particle size relation. The volume was calculated using the length of a section or whole nanotube, the pore size and the wall diameter. Since the length is often the length of a section and not always a whole tube, the result is included in the supplementary information here.

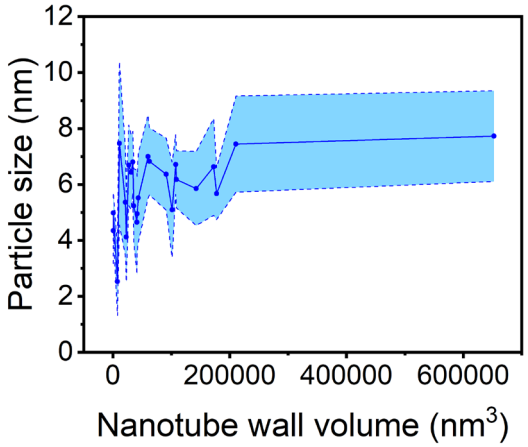

Figure 52: Relation between particle size and nanotube wall volume.

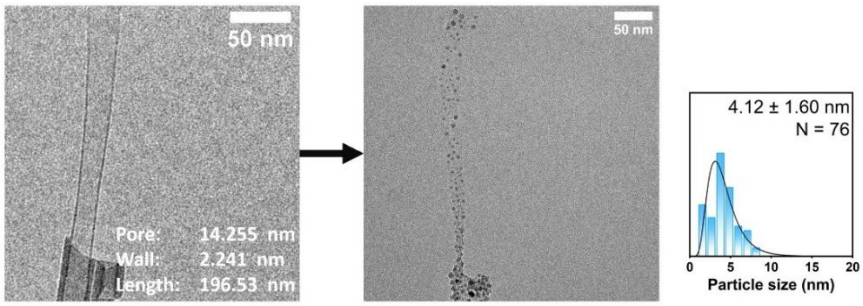

Figure 53: ILTEM NT 6

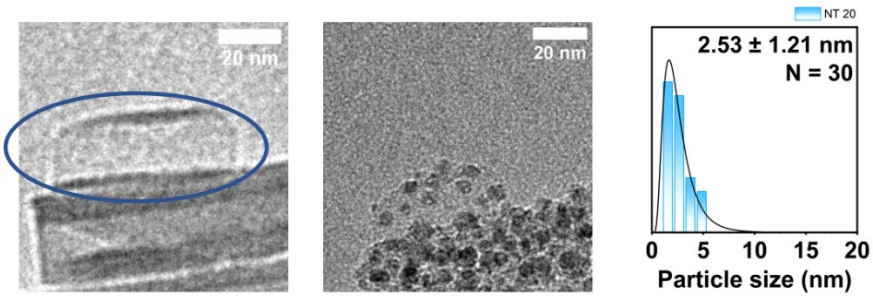

Figure 54: ILTEM NT 20

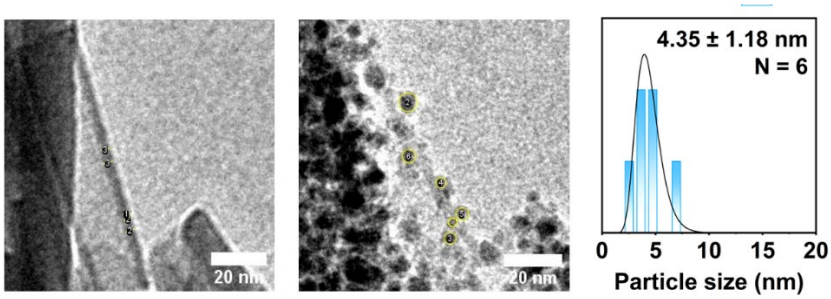

Figure 55: ILTEM NT 24

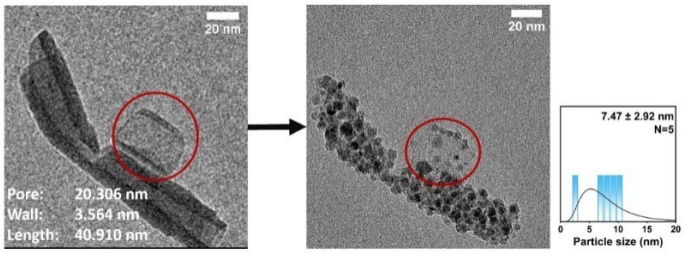

Figure 56: ILTEM NT 3

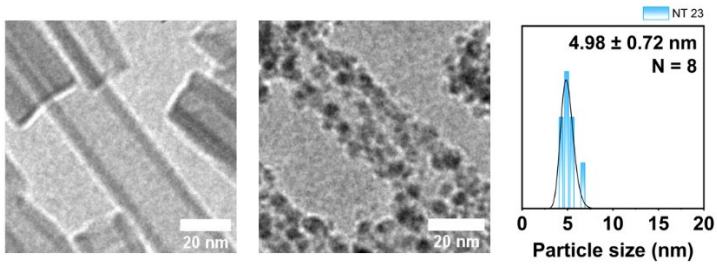

Figure 57: ILTEM NT 23

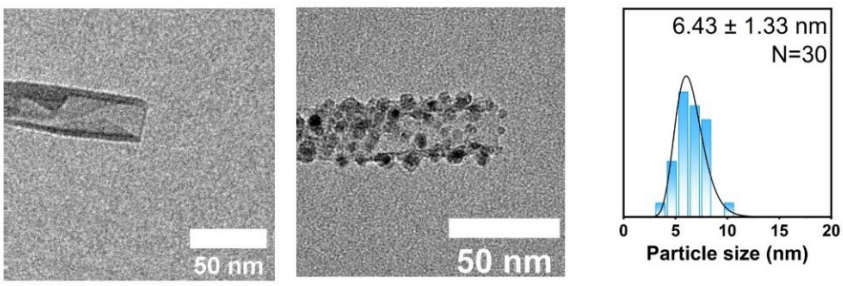

Figure 58: ILTEM NT 12

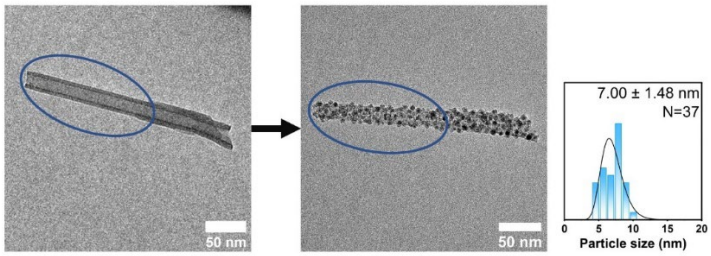

Figure 59: ILTEM NT 10

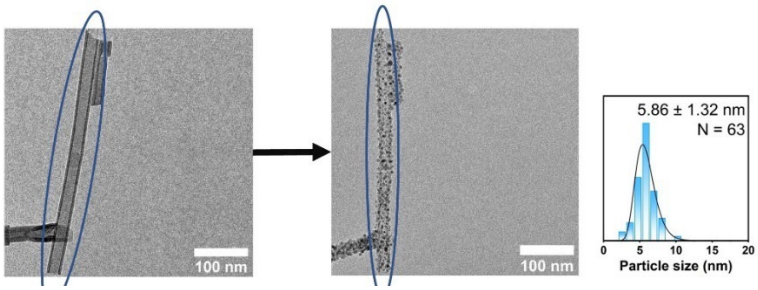

Figure 60: ILTEM NT 8

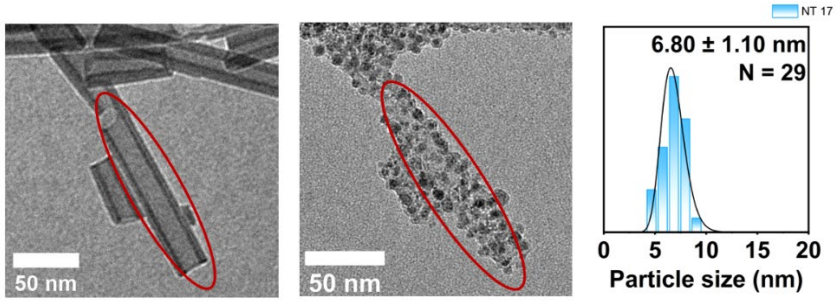

Figure 61: ILTEM NT 17

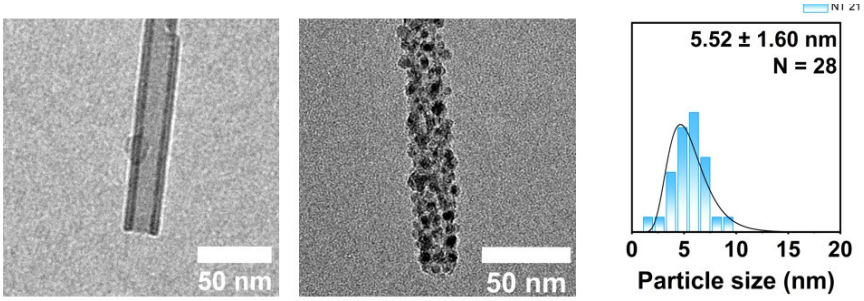

Figure 62: ILTEM NT 21

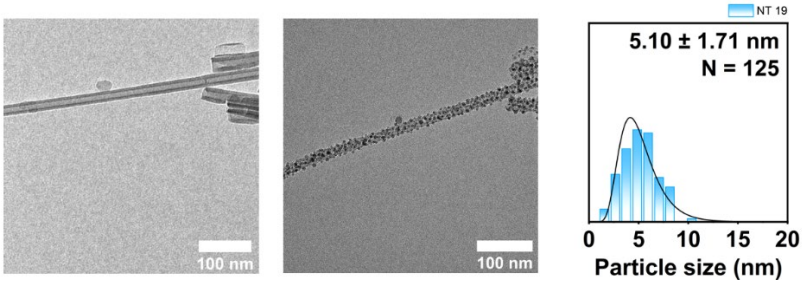

Figure 63: ILTEM NT 19

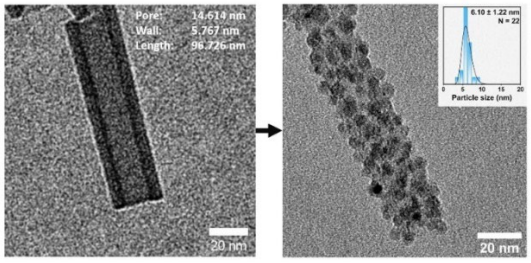

Figure 64: ILTEM NT 1

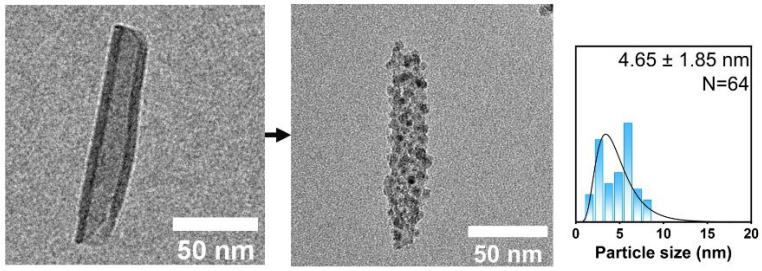

Figure 65: ILTEM NT 11

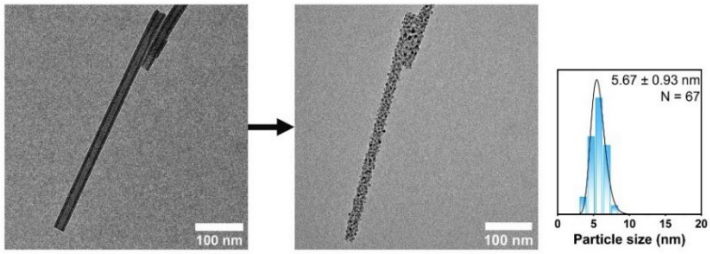

Figure 66: ILTEM NT 7

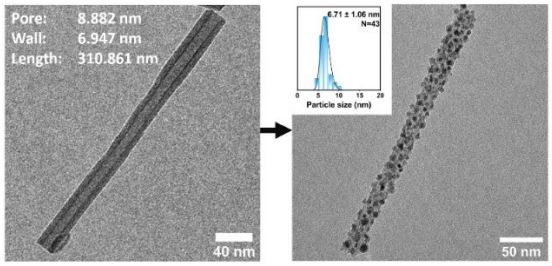

Figure 67: ILTEM NT 2

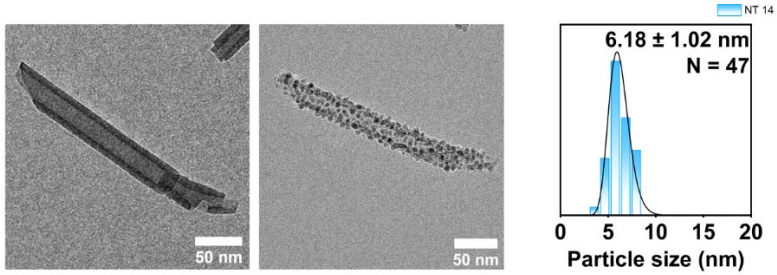

Figure 68: ILTEM NT 14

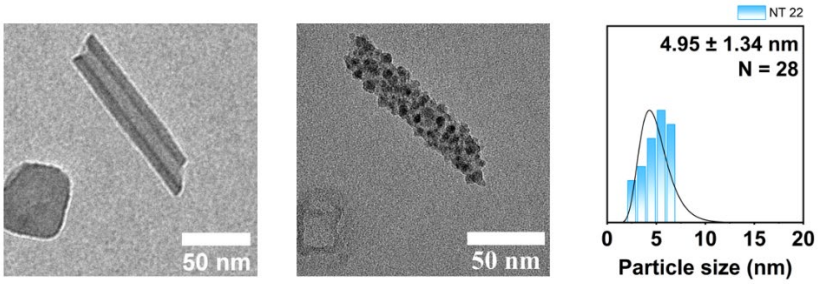

Figure 69: ILTEM NT 22

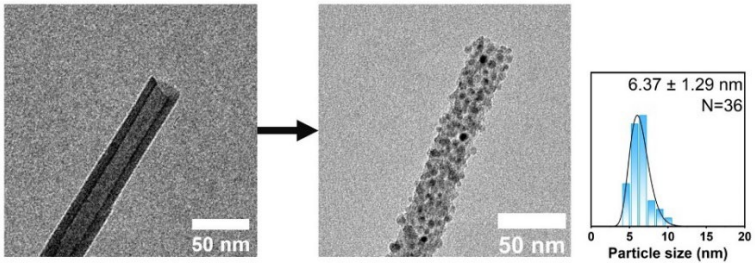

Figure 70: ILTEM NT 9

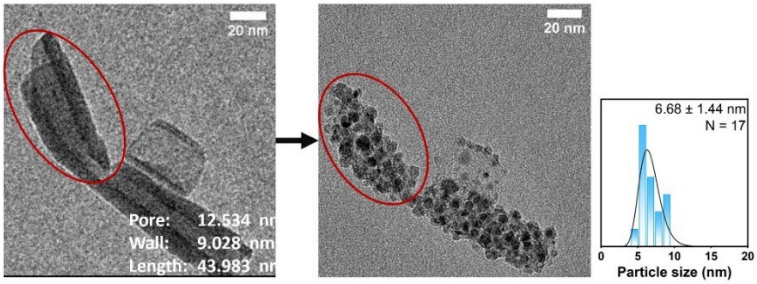

Figure 71: ILTEM NT 4

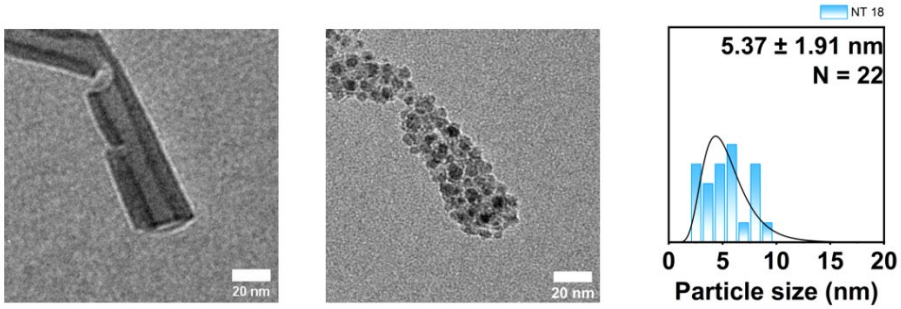

Figure 72: ILTEM NT 18

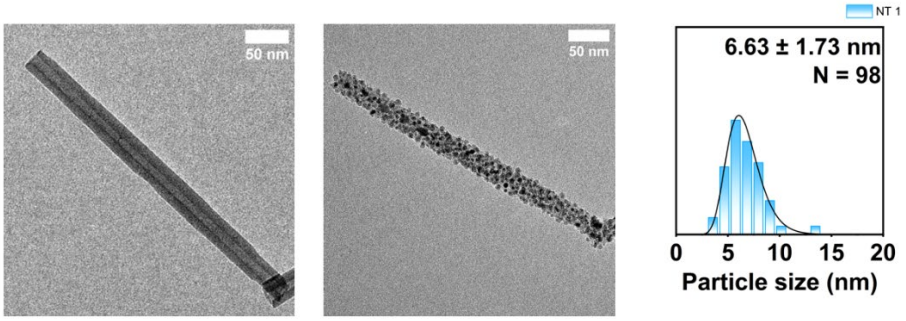

Figure 73: ILTEM NT 16

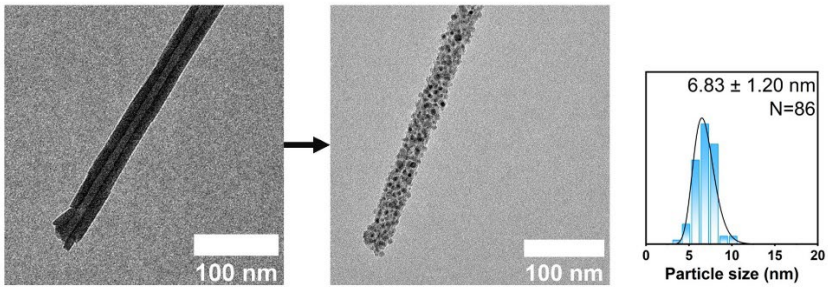

Figure 74: ILTEM NT 13

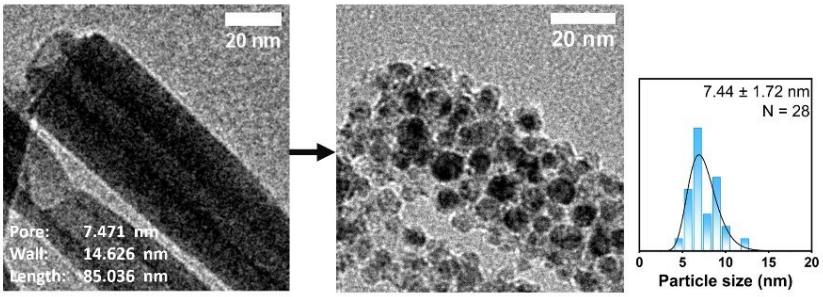

Figure 75: ILTEM NT 5

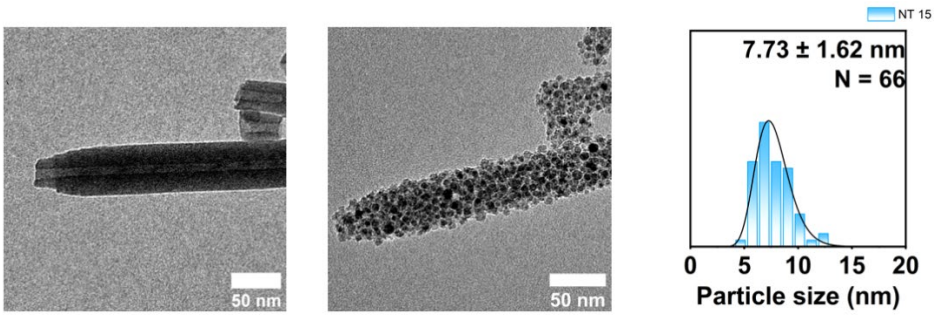

Figure 76: ILTEM NT 15

7.5 Ni hydroxide: TPR, XRD, EpH

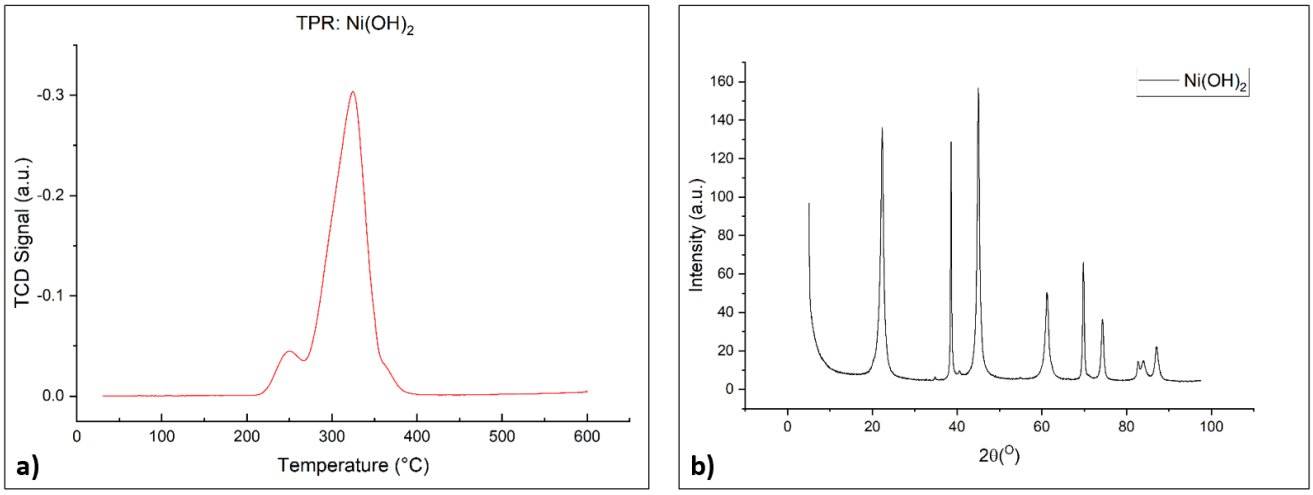

Figure 77: Nickel hydroxide was measured in TPR and XRD. $Ni(OH)_2$ specimen from Sigma-Aldrich, 60-70% Ni basis. (a) blanco $Ni(OH)_2$ TPR measurement. (b) blanco XRD $Ni(OH)_2$

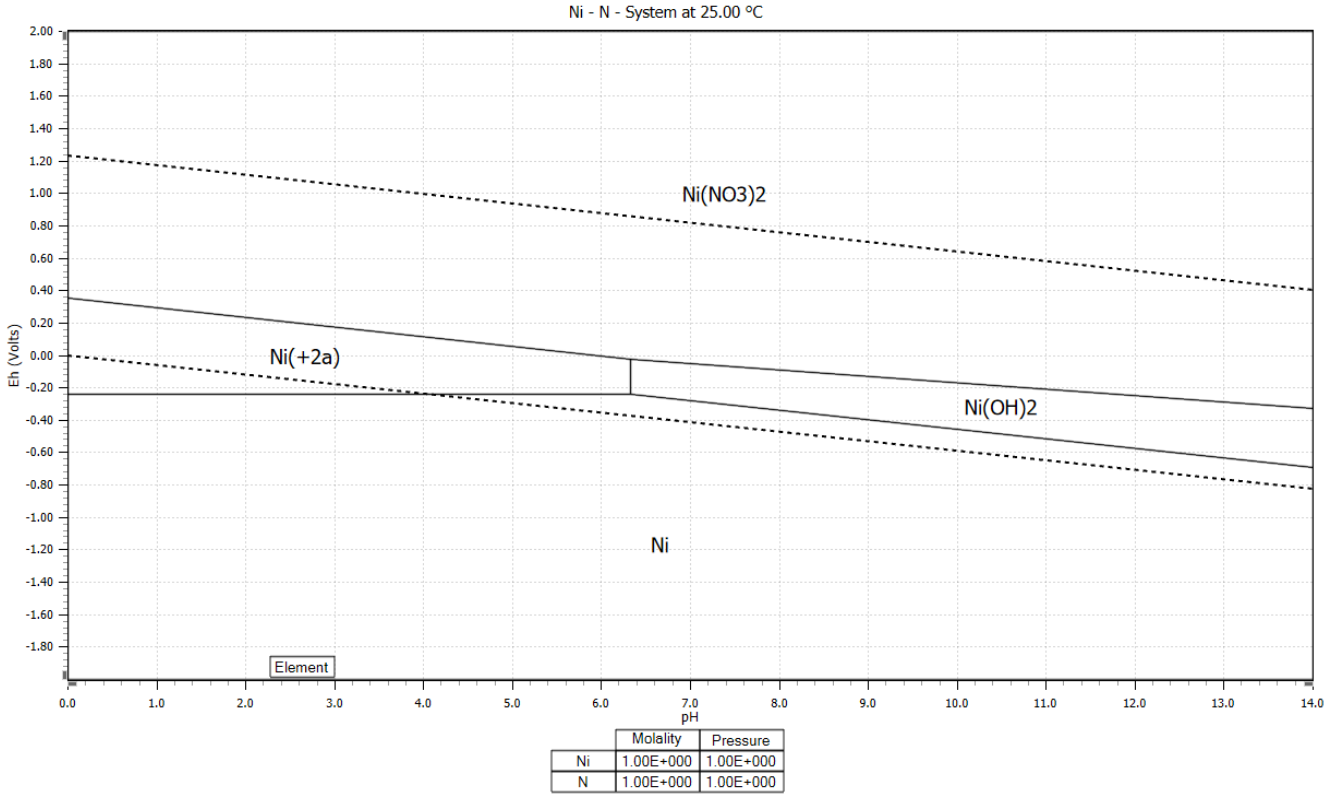

Figure 78: EpH diagram of Ni, $Ni(OH)_2$ and HNO3 species at 25 °C.

References

(1) de Jong, K. P. 1 General Aspects. In *Synthesis of Solid Catalysts*; de Jong, K. P., Ed.; Wiley-VCH, 2009.

(2) Hagen, J. Economic Importance of Catalysts. In *Industrial Catalysis: A practical Approach*; Hagen, J., Ed.; Wiley-VCH: Weinheim, Germany, 2015; pp 459–462.

(3) *Nickel Catalysts - Catalysts / Alfa Chemistry*. https://www.alfachemic.com/catalysts/products/nickel-catalysts.html (accessed 2021-09-29).

(4) *Processes - Nickel Catalysts in industry*. https://nickelcatalyst.weebly.com/processes.html (accessed 2021-09-29).

(5) de Jong, K. P.; Ngene, P. MSc Course Synthesis of Heterogeneous Catalysts and Related Materials, Utrecht University; 2021.

(6) Zhang, Y.; Liu, Q. Nickel Phyllosilicate Derived Ni/SiO2 Catalysts for CO2 Methanation: Identifying Effect of Silanol Group Concentration. *Journal of CO2 Utilization* **2021**, *50*, 101587.

(7) German Patent No. 740,634 to IG Farben, 1943.

(8) US Patent 3,668,148 to Lever Brothers Company, 1970.

(9) Netherlands Patent Application 68,16777 to Stamicarbon, 1970.

(10) Netherlands Patent Application 67,05259 to Stamicarbon, 1967.

(11) Burattin, P.; Che, M.; Louis, C. Metal Particle Size in Ni/SiO2 Materials Prepared by Deposition - Precipitation : Influence of the Nature of the Ni (II) Phase and of Its Interaction with the Support. *Journal of Physical Chemistry B* **1999**, *103* (30), 6171–6178.

(12) Burattin, P.; Che, M.; Louis, C. Ni/SiO2 Materials Prepared by Deposition-Precipitation: Influence of the Reduction Conditions and Mechanism of Formation of Metal Particles. *J. Phys. Chem. B* **2000**, *104*, 10482–10489.

(13) Burattin, P.; Che, M.; Louis, C. Molecular Approach to the Mechanism of Deposition - Precipitation of the Ni(II) Phase on Silica. *Journal of Physical Chemistry B* **1998**, *102* (15), 2722–2732.

(14) Burattin, P.; Che, M.; Louis, C. Characterization of the Ni(II) Phase Formed on Silica upon Deposition-Precipitation. *Journal of Physical Chemistry B* **1997**, *101* (36), 7060–7074.

(15) Che, M.; Cheng, Z. X.; Louis, C. Nucleation and Particle Growth Processes Involved in the Preparation of Silica-Supported Nickel Materials by a Two-Step Procedure. *J. Am. Chem. Soc.* **1995**, *117* (7), 2008–2018.

(16) Louis, C.; Cheng, Z. X.; Che, M. Characterization of Ni/SiO2 Catalysts during Impregnation and Further Thermal Activation Treatment Leading to Metal Particles. *J. Phys. Chem.* **1993**, *97* (21), 5703–5712.

(17) Hermans, L. A. M.; Geus, J. W. In. In *Preparation of Catalysts II*; Delmon, B., Grange, P., Jacobs, P. A., Poncelet, G., Eds.; Elsevier: Amsterdam, 1979; p 113.

(18) van Dillen, J. A.; Geus, J. W.; Hermans, L. A.; van der Meijden, J. In. In *Proceedings of the 6th International Congress on Catalysis, London, 1976*; Bond, G. C., Wells, P. B., Tompkins, F. C., Eds.; The Chemical Society: London, 1977; p 677.

(19) Geus, J. W. Dutch Patent Application 6813, 236, 1968.

(20) Geus, J. W. Dutch Patent Application 6705, 259, 1967.

(21) K.P. de Jong. Deposition Precipitation onto Pre-Shaped Carrier Bodies. Possibilities and Limitations. In *Preparation of Catalysts*; Poncelet, G., Jacobs, P. A., Grange, P., Delmon, B., Eds.; Elsevier Science Publishers B.V.: Amsterdam, 1991; Vol. V, pp 19–36.

(22) Bian, Z.; Kawi, S. Preparation, Characterization and Catalytic Application of Phyllosilicate: A Review. *Catal Today* **2020**, *339* (July 2018), 3–23.

(23) Bian, Z.; Kawi, S. Preparation, Characterization and Catalytic Application of Phyllosilicate: A Review. *Catal Today* **2020**, *339*, 3–23.

(24) White, R. D.; Bavykin, D. v.; Walsh, F. C. Morphological Control of Synthetic Ni3Si2O 5(OH)4 Nanotubes in an Alkaline Hydrothermal Environment. *J Mater Chem A Mater* **2013**, *1* (3), 548–556.

(25) Sivaiah, M. v; Petit, S.; Beaufort, M. F.; Eyidi, D.; Barrault, J.; Batiot-Dupeyrat, C.; Valange, S. Nickel Based Catalysts Derived from Hydrothermally Synthesized 1:1 and 2:1 Phyllosilicates as Precursors for Carbon Dioxide Reforming of Methane. *Microporous and Mesoporous Materials* **2011**, *140*, 69–80.

(26) McDonald, A.; Scott, B.; Villemure, G. Hydrothermal Preparation of Nanotubular Particles of a 1:1 Nickel Phyllosilicate. *Microporous and Mesoporous Materials* **2009**, *120* (3), 263–266.

(27) Li, H.; Chen, Y.; Liu, S.; Liu, Q. Enhancement of Hydrothermal Synthesis of FDU-12-Derived Nickel Phyllosilicate Using Double Accelerators of Ammonium Fluoride and Urea for CO2 Methanation. *Journal of CO2 Utilization* **2021**, *52*, 101677.

(28) Li, Z.; Wang, Z.; Jiang, B.; Kawi, S. Sintering Resistant Ni Nanoparticles Exclusively Confined within SiO2 Nanotubes for CH4 Dry Reforming. *Catal Sci Technol* **2018**, *8* (13), 3363–3371.

(29) van Haasterecht, T.; Swart, M.; de Jong, K. P.; Bitter, J. H. Effect of Initial Nickel Particle Size on Stability of Nickel Catalysts for Aqueous Phase Reforming. *Journal of Energy Chemistry* **2016**, *25* (2), 289–296.

(30) Kukovitsky, E. F.; L'vov, S. G.; Sainov, N. A.; Shustov, V. A.; Chernozatonskii, L. A. Correlation between Metal Catalyst Particle Size and Carbon Nanotube Growth. *Chem Phys Lett* **2002**, *355* (5–6), 497–503.

(31) van Haasterecht, T.; Ludding, C. C. I.; de Jong, K. P.; Bitter, J. H. Toward Stable Nickel Catalysts for Aqueous Phase Reforming of Biomass-Derived Feedstock under Reducing and Alkaline Conditions. *J Catal* **2014**, *319*, 27–35.

(32) Shabaker, J. W.; Simonetti, D. A.; Cortright, R. D.; Dumesic, J. A. Sn-Modified Ni Catalysts for Aqueous-Phase Reforming: Characterization and Deactivation Studies. *J Catal* **2005**, *231* (1), 67–76.

(33) Thompson, J.; Vasquez, A.; Hill, J. M.; Pereira-Almao, P. The Synthesis and Evaluation of Up-Scalable Molybdenum Based Ultra Dispersed Catalysts: Effect of Temperature on Particle Size. *Catal Letters* **2008**, *123* (1–2), 16–23.

(34) Gunter, P. L. J.; Niemantsverdriet, J. W.; Ribeiro, F. H.; Somorjai, G. A. Surface Science Approach to Modeling Supported Catalysts. *Catal Rev Sci Eng* **2006**, *39* (1–2), 77–168.

(35) Gao, F.; Goodman, D. W. Model Catalysts: Simulating the Complexities of Heterogeneous Catalysts. *Annu Rev Phys Chem* **2012**, *63*, 265–286.

(36) van den Berg, R.; Elkjaer, C. F.; Gommes, C. J.; Chorkendorff, I.; Sehested, J.; de Jongh, P. E.; de Jong, K. P.; Helveg, S. Revealing the Formation of Copper Nanoparticles from a Homogeneous Solid Precursor by Electron Microscopy. *J Am Chem Soc* **2016**, *138* (10), 3433–3442.

(37) Decarreau, A. Partitioning of Divalent Transition Elements between Octahedral Sheets of Trioct˜hedral Smectites and Water. *Geochim Cosmochim Acta 49*, 1537–1544.

(38) Decarreau, A. Cristallogenèse Expérimentale Des Smectites Magnésiennes : Hectorite, Stévensite. *Bulletin de Minéralogie* **1980**, *103* (6), 579–590.

(39) White, R. D. Metal Oxide and Silicate Nanotubes: Synthesis and Hydrogen Storage Applications. **2012**.

(40) Korytkova, E. N.; Pivovarova, L. N. Hydrothermal Synthesis of Nanotubes Based on (Mg,Fe,Co,Ni)3Si2O5(OH)4 Hydrosilicates. *Glass Physics and Chemistry 2010 36:1* **2010**, *36* (1), 53–60.

(41) Kijima, T. Introduction to Inorganic and Metallic Nanotubes. *Topics in Applied Physics* **2010**, *117*, 3–16.

(42) Krasilin, A. A.; Gusarov, V. v. Energy of Formation of Chrysotile Nanotubes. *Russ J Gen Chem* **2014**, *84* (12), 2359–2363.

(43) Krasilin, A. A. The Influence of Edge Specific Surface Energy on the Direction of Hydrosilicate Layers Scrolling. *Nanosystems: Physics, Chemistry, Mathematics* **2021**, *12* (5), 623–629.

(44) Krasilin, A. A.; Nevedomsky, V. N.; Gusarov, V. v. Comparative Energy Modeling of Multiwalled Mg3Si2O5(OH)4 and Ni3Si2O5(OH)4 Nanoscroll Growth. *Journal of Physical Chemistry C* **2017**, *121* (22), 12495–12502.

(45) Korytkova, E. N.; Maslov, A. v.; Pivovarova, L. N.; Polegotchenkova, Y. v.; Povinich, V. F.; Gusarov, V. v. Synthesis of Nanotubular Mg3Si2O5(OH)4-Ni3Si2O5(OH)4 Silicates at Elevated Temperatures and Pressures. *Inorganic Materials 2005 41:7* **2005**, *41* (7), 743–749.

(46) Yang, Y.; Liang, Q.; Li, J.; Zhuang, Y.; He, Y.; Bai, B.; Wang, X. Ni3Si2O5(OH)4 Multi-Walled Nanotubes with Tunable Magnetic Properties and Their Application as Anode Materials for Lithium Batteries. *Nano Research 2011 4:9* **2011**, *4* (9), 882–890.

(47) Ryu, K. W.; Jang, Y. N.; Chae, S. C. Hydrothermal Synthesis of Kaolinite and Its Formation Mechanism. *Clays Clay Miner* **2010**, *58* (1), 44–51.

(48) Maslennikova, T. P.; Korytkova, E. N. Influence of Synthesis of Physicochemical Parameters on Growth of Ni 3Si2O5(OH)4 Nanotubes and Their Filling with Solutions of Hydroxides and Chlorides of Alkaline Metals. *Glass Physics and Chemistry* **2013**, *39* (1), 67–72.

(49) Weller, M.; Overton, T.; Rourke, J.; Armstrong, F. *Inorganic Chemistry*, 5th ed.; Oxford University Press: Oxford, UK, 2010.

(50) Valange, S.; Sivaiah, M. v; Petit, S.; Barrault, J.; Batiot-Dupeyrat, C.; Valange, S. CO2 Reforming of CH4 over Ni-Containing Phyllosilicates as Catalyst Precursors CO 2 Reforming of CH 4 over Ni-Containing Phyllosilicates as Catalyst Precursors. *Catal Today* **2010**, *157*, 397–403.

(51) Bian, Z.; Kawi, S. Highly Carbon-Resistant Ni–Co/SiO2 Catalysts Derived from Phyllosilicates for Dry Reforming of Methane. *Journal of CO2 Utilization* **2017**, *18*, 345–352.

(52) Ye, R.-P.; Gong, W.; Sun, Z.; Sheng, Q.; Shi, X.; Wang, T.; Yao, Y.; Razink, J. J.; Lin, L.; Zhou, Z.; Adidharma, H.; Tang, J.; Fan, M.; Yao, Y.-G. Enhanced Stability of Ni/SiO 2 Catalyst for CO 2 Methanation: Derived from Nickel Phyllosilicate with Strong Metal-Support Interactions. **2019**.

(53) Dong, H.; Liu, Q. Three-Dimensional Networked Ni-Phyllosilicate Catalyst for CO2 Methanation: Achieving High Dispersion and Enhanced Stability at High Ni Loadings. *ACS Sustain Chem Eng* **2020**, *8* (17), 6753–6766.

(54) Zhao, Y.; Li, H.; Li, H. NiCo@SiO2 Core-Shell Catalyst with High Activity and Long Lifetime for CO2 Conversion through DRM Reaction. *Nano Energy* **2018**, *45*, 101–108.

(55) Li, M.; Lu, J. Cobalt in Lithium-Ion Batteries. *Science (1979)* **2020**, *367* (6481), 979–980.

(56) *Berghof digestec Pressure Vessel (DAB-3 XXL) - Team Medical & Scientific Sdn Bhd*. https://www.tms-lab.com/product/berghof-digestec-pressure-vessel-dab-3-xxl/ (accessed 2022-10-22).

(57) Williams, D. B.; Carter, C. B. *Transmission Electron Microscopy*; Springer: New York, USA, 1996.

(58) *The Transmission Electron Microscope (TEM)*. https://www.uni-augsburg.de/en/fakultaet/mntf/physik/groups/exp4/equipment/transmission-electron-microscope-tem/ (accessed 2022-07-24).

(59) *Energy Dispersive X-ray Spectroscopy - Clean Energy Institute*. http://www.cei.washington.edu/education/science-of-solar/energy-dispersive-x-ray-spectroscopy/ (accessed 2022-11-18).

(60) *Introduction to Energy Dispersive X-Ray Spectroscopy (EDX/EDS) - YouTube*. https://www.youtube.com/watch?v=vBu9Xzc1TgE (accessed 2022-11-18).

(61) Hammond, C. *The Basics of Crystallography and Diffraction*, 4th ed.; Oxford University Press: New York, USA, 2015.

(62) Thommes, M.; Kaneko, K.; Neimark, A. v.; Olivier, J. P.; Rodriguez-Reinoso, F.; Rouquerol, J.; Sing, K. S. W. Physisorption of Gases, with Special Reference to the Evaluation of Surface Area and Pore Size Distribution (IUPAC Technical Report). *Pure and Applied Chemistry* **2015**, *87* (9–10), 1051–1069.

(63) Kiani, M. A.; Mousavi, M. F.; Ghasemi, S. Size Effect Investigation on Battery Performance: Comparison between Micro- and Nano-Particles of β-Ni(OH)2 as Nickel Battery Cathode Material. *J Power Sources* **2010**, *195* (17), 5794–5800.

(64) Briggs, G. W. D.; Fleischmann, M. Oxidation and Reduction of Nickel Hydroxide at Constant Potential. *Transactions of the Faraday Society* **1971**, *67*, 2397–2407.

(65) Trafela, Š.; Zavašnik, J.; Šturm, S.; Rožman, K. Ž. Formation of a Ni(OH)2/NiOOH Active Redox Couple on Nickel Nanowires for Formaldehyde Detection in Alkaline Media. *Electrochim Acta* **2019**, *309*, 346–353.

(66) White, R. Electronic Supporting Information (ESI). *Journal of Materials Science A* **2012**, *1* (548).

(67) Wouterse, A.; Williams, S. R.; Philipse, A. P. Effect of Particle Shape on the Density and Microstructure of Random Packings. *Journal of Physics: Condensed Matter* **2007**, *19* (40), 406215.